Republic of Iraq
Ministry of Higher Education and Scientific Research
Babylon University
College of Engineering
Civil Engineering Department

Experimental and Analytical Investigation of Two Way Shear Behaviour of Fiber Reinforced Concrete Slabs

A Research

Submitted to the College of Engineering / University of Babylon in Partial Fulfillment of the Requirements for the Degree of Master in Engineering / Civil Engineering/ Structural

By

Ban Alaa Salman Ali

Supervised By

Prof. Dr. Rafea Flaih Hassan

Rajab
1445

January
2024

بِسْمِ اللَّهِ الرَّحْمَٰنِ الرَّحِيمِ

هُوَ الَّذي جَعَلَ الشَّمسَ ضِياءً وَالقَمَرَ نورًا وَقَدَّرَهُ مَنازِلَ لِتَعلَموا عَدَدَ السِّنينَ وَالحِسابَ ما خَلَقَ اللَّهُ ذٰلِكَ إِلّا بِالحَقِّ يُفَصِّلُ الآياتِ لِقَومٍ يَعلَمونَ ﴿٥﴾

صدق الله العلي العظيم

سورة يونس آية (٥)

Dedication

To my dad who left me physically, but whose soul still flutters in the sky of my life, to my tender mum... I can't find words that can give her due, and to my dear husband who is always with me, and all my family and friends…with all of My Love & Respect.

Ban Alaa Salman Ali

2024

Supervisor’s Certificate

I certify that the preparation of thesis entitled “Experimental **and Analytical Investigation of Two Way Shear Behavior of Fiber Reinforced Concrete Slabs**", was prepared by " **Ban Alaa Salman Ali** ", under my supervision at the Department of Civil Engineering in the University of Babylon in partial fulfillment of the requirements for the degree of Master in Structural Engineering

Signature:

Name: **Dr. Rafea Flaih Hassan**

Data: / /2024

Examination Committee's Certificate

We certify that we have read this thesis entitled (**Experimental and Analytical Prediction of Two Way Shear Behavior of Fiber Reinforced Concrete Slabs**) presented by (**Ban Alaa Salman Ali**) and as an examining committee, we examined the student in its content and in what is connected with it, and that in our opinion it meets standard of a thesis for the degree of Master in Civil Engineering / Structure Engineering.

Signature:

Name: **Prof. Dr. Haitham H. Muteb**

(Chairman)

Date: / / 2023

Signature:

Name: **Assist. Prof. Dr. Ali Ganim Abbas**

(Member)

Date: / / 2023

Signature:

Name: **Assist. Prof. Muna Hatim Jaber**

(Member)

Date: / / 2024

Signature:

Name: **Prof. Dr. Rafea Flaih Hassan**

(Supervisor and Member)

Date: / / 2024

Approved by the Head of the Civil Engineering Department

Signature:

Name: **Asst. Prof. Dr. Zaid H. Majeed Al-Hasson**

Date: / / 2024

Approved by the Dean of the College of Engineering

Signature:

Name: **Prof. Dr. Laith Ali. Abdul -Rahaim**

Date: / /2024

ACKNOWLEDGMENTS

In the name of **ALLAH**, the most compassionate, the most merciful. Praise be to **ALLAH**, and pray and peace be on his prophet Mohammed and his family.

First, I would like to express my appreciation and deepest gratitude to my supervisor **Dr. Rafea Flaih Hassan** for his remarkable suggestions, encouragement and guidance throughout the research. I am really indebted to him.

like to express my deepest feelings of my family for their care, patience and great support during the research period.

Thanks to all staff of Civil Engineering Department/College of Engineering / University of Babylon for their appreciable support.

Thanks also extended to staff of the Structures Laboratory at College of Engineering / Babylon University for their help in using the various facilities.

Ban Alaa Salman
2024

ABSTRACT

Researchers and engineers have developed an interest in using steel fiber reinforced concrete (SFRC) to enhance the performance of concrete structures in a variety of structural applications. However, there are few experimental test results regarding the effect of the parameters cross-section of the column, fiber dosage, and configuration on the shear punching behavior of SFRC slabs.

This research includes a practical and theoretical study of the effect of using two types of fibers (straight steel fibers of and hook steel fibers) and their dosages under the effect of punching shear for fiber reinforced concrete slabs. There were three different percentages of fiber used: 0.5%, 1% and 1.5% by volume. This investigation applied a concentrated load to fourteen cast slabs of every slab of 920 x920 x80mm (two each of non-fibrous concrete of square and circular column sections of the equivalent area while the other twelve slabs are made with steel fiber concrete). The mechanical properties of concrete mixtures (strength of compression , strength of tensile , flexural strength, and direct tensile strength) were tested and indicated that straight steel fibres are more effective than hook steel fibres.

Contrariwise, the slabs cast with hook steel fibres show higher load capacity than the slab casted with straight steel fibres. This behavior may be as a result of post crack stage in which the length of fibre gives better development length to increase bond strength. In general the failure was gradual in the fibre-reinforced slabs, while the failure was sudden in the non-fiber-reinforced slabs. The effect of column shapes (square and circular) fluctuated depending on the failure mode which varied from shear to complex shear and flexure. Therefore, it was inaccurate to adopt the equivalent area of circular columns as square columns in FRP slabs.

ABSTRACT

Adding of steel fibers in the concrete mix led to a reduction in the penetration area of the slabs, as the use of straight fibers at the ratios of 0.5%, 1.0% and 1.5% of the reduction was 59.51%, 49.05% and 70.15% for the circular column, while for the square column the percentage of reduction was 69.5%, 37.09% and 34.56%, respectively.

When using hook fibers at ratios of 0.5%, 1.0%, and 1.5%, the percentage of decrease was 72.81%, 49.99%, and 28.52% for the circular column, while for the square column, the percentage of decrease was 38.71%, 37.56% and 14.29%, respectively. This phenomena as the result of enhancing tensile strength that was changed failure mode from shear to compound shear and flexural. When comparing the experimental shear strength and the value obtained from the ACI cod coefficients, it gave varying and inaccurate percentages, as the error rate ranged from 40.04% to 62.71%, while when comparing the experimental shear strength and the value obtained from the proposed equations, the proposed equations gave acceptable predictions. The first proposed equation gave an error rate ranging from 3.38% to 39.48% and the second proposed equation gave an error rate ranging from 0.57% to 17.97% The comparison between experimental shear strength and the value obtained from suggested equations showed that the proposed equations provide accepted predictions for the shear strength of FRC slabs.

List of Contents

List of Contents

List of Contents

List of Contents

List of Figures

List of Figures

List of Figures

List of Plates

List of Plates

List of Tables

Abbreviations

Abbreviations	Descriptions
CFRP	Carbon Fiber Reinforced Polymer
CSCT	Critical shear crack theory
FE	Finite Element
GFRP	Glass fiber reinforced polymer
LWC	Light Weight Concrete
NC	Normal Concrete
NSC	Natural sand Concrete
RPC	Reactive Powder Concrete
SFRC	Steel Fiber Reinforced Concrete
SRC	Steel Reinforced Concrete
UHPFRC	Ultra High-Performance Fiber Reinforced Concrete

Notation

Most commonly used symbols are listed below, these and others are defined where they appear in the research;

Symbol	Description
A_b	Area of main deformed bar
As	Area of steel
A_v	Area of two legs of stirrups
b	Width of compression face of member, mm
b_o	Perimeter of the critical section for punching shear
d	Distance from extreme compression fiber to the centroid of the longitudinal reinforcement in tension.
d	Effective depth of the slab, mm
dg	Maximum diameter of the aggregate
dg_0	Reference aggregate size (16 mm (0.63 in))
f 'c	Specified compressive strength of concrete (cylinder)
f'_c	Nominal concrete compressive strength (cylinder test).
f'_{cu}	Compressive strengths of UHPC
k_{max}	Factors attained values of (1.725) and (1.80)
k_{sys}	Factors achieved values of 3.18 and 2.65 in the instance of CSCT theory-based mechanical models
Ø	Strength reduction factor (according to North-American practice, Ø = 0.75 for shear)
P	The highest stress at which the punching shear failure
PS	punching shear
τ_N	Punching-related nominal shear stress at failure
U_0	The length of the column periphery
Vc	The punching shear strength
V_f	Volume fraction of steel fibre
$V_{R.c}$	Normal punching shear strength
$V_{Rd,c}$	Design punching shear strength
Vu	The ultimate punching shear strength
ψd	Rotation of slab outside the column region due to factored shear force Vd
f_t	Concrete tensile strength of splitting test.
f_u	Ultimate stress of steel reinforcement.
f_y	Yield stress of steel reinforcement.

CHAPTER ONE

INTRODUCTION

CHAPTER ONE

INTRODUCTION

1.1 Overview

Reinforced concrete slabs are widely utilized as structural components; yet, despite their prevalence in design and construction, there is often a lack of comprehensive understanding and proper consideration of the elastic and plastic behavior of these slabs. This occurs at least in part due to the mathematical complexity of dealing with equations for plates that are elastic, Specifically, under conditions of support that approximate those of multi-panel floor slabs in buildings **[1].** According to the supporting system, the slab different kinds of systems include:

1. **One way Slabs:** As depicted in **Figure1.1**, slabs are only to have supports on two sides. In this case, structural effect of the slab is predominantly unidirectional, and loads are transferred in the perpendicular orientation to the supporting beams. As shown in **Figure 1.2**, intermediate beams are available. If the length-to-width ratio of a single slab exceeds approximately 2, Most of the load is transmitted to the supporting beams in the short direction, resulting in one-way action.**[2].**

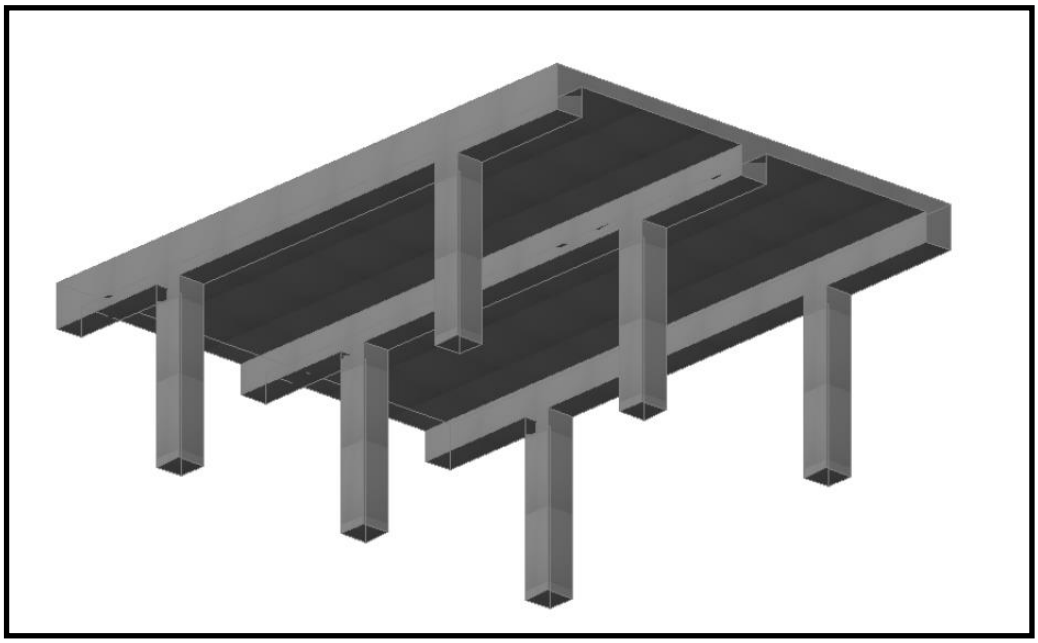

Figure(1.1) Slabs (only supported on two sides) [2]

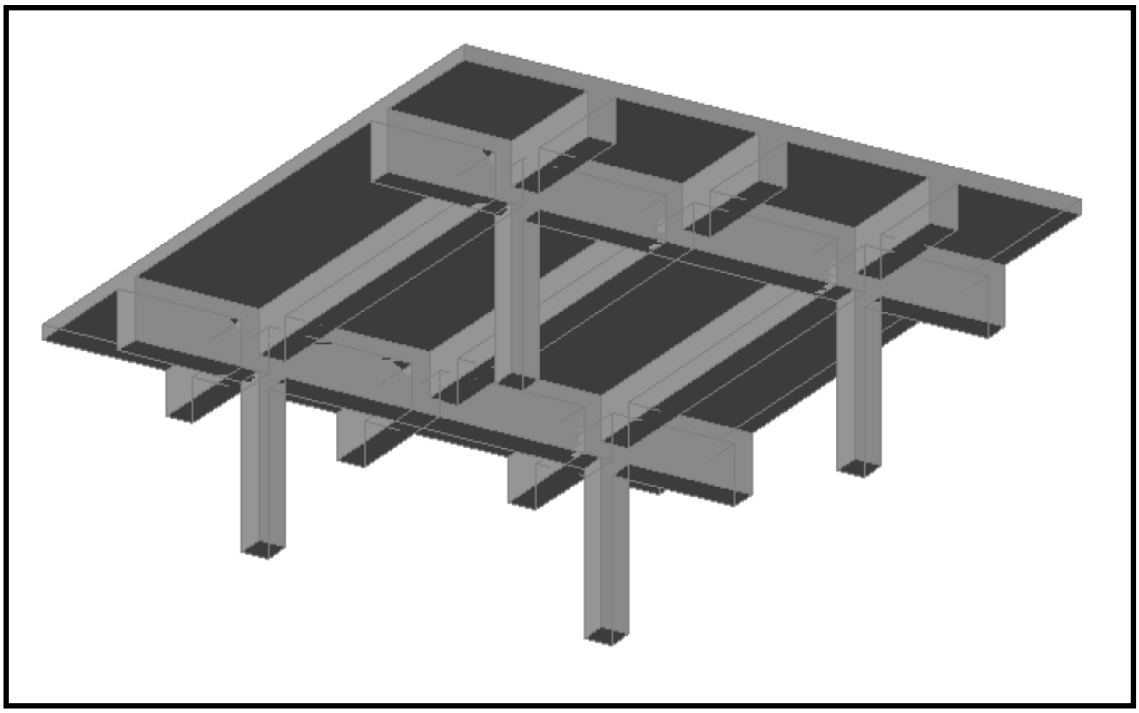

Figure(1.2) One-way slab(Supported on Four Sides). [2]

In addition, in Australia, banded slabs are a prevalent type of flat slab, As shown in **Figure 1.3**. The central section of the slab is designed as a one-way slab with spans equal to the clear span between the drop beams plus depth/2. **[3].**

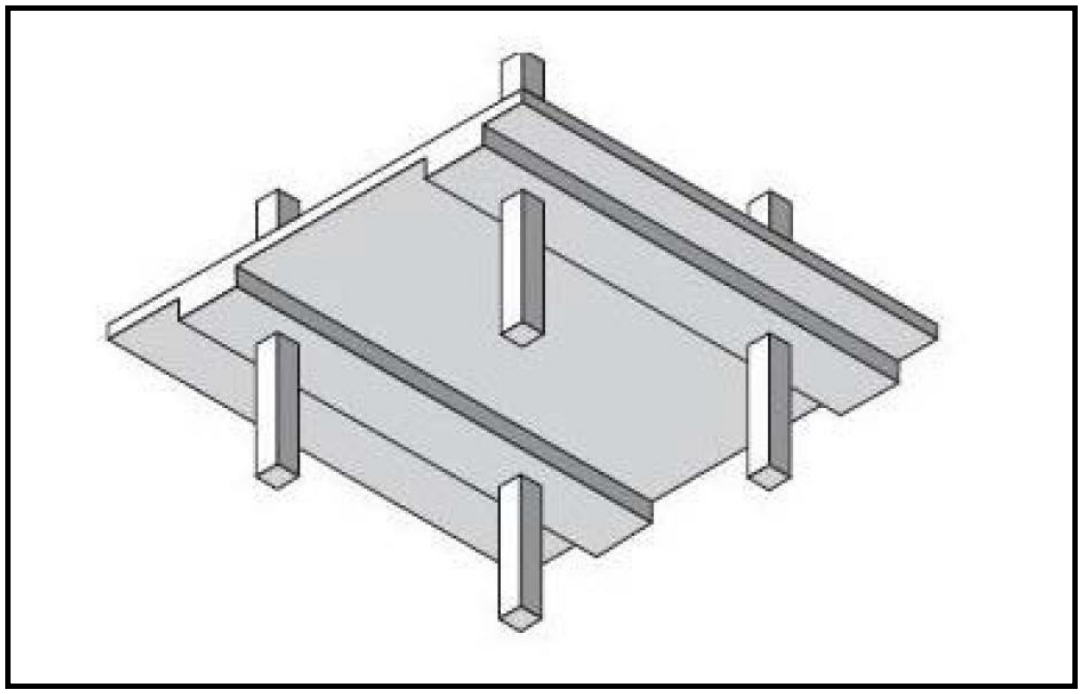

Figure (1.3) One-Way Slab (Banded Flat Slab) [3]

2- **Two-way Slabs on Supports:** Stiff or flexible supports on all four sides as illustrated in **Figure 1.4. [2].**

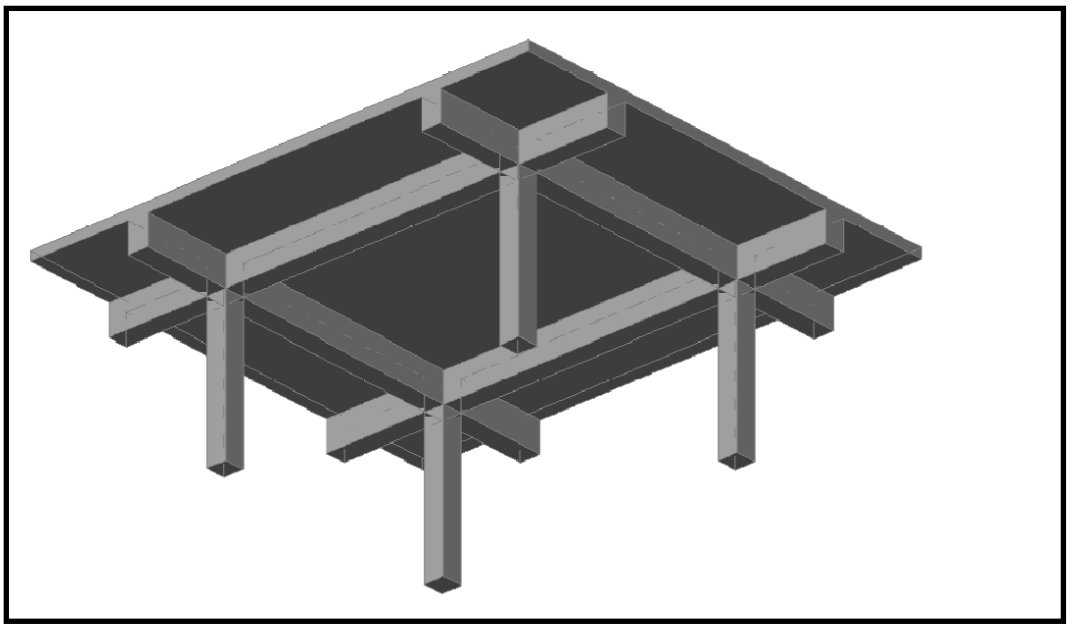

Figure (1.4) Two-Way Slab on Supports [2]

3- **Concrete Slabs Directly Supported by Columns:** As shown in **Figures 1.5** and **Figure 1.6**, these slab systems can be subdivided

into the Flat Plate System and the Flat Slab System, respectively [2].

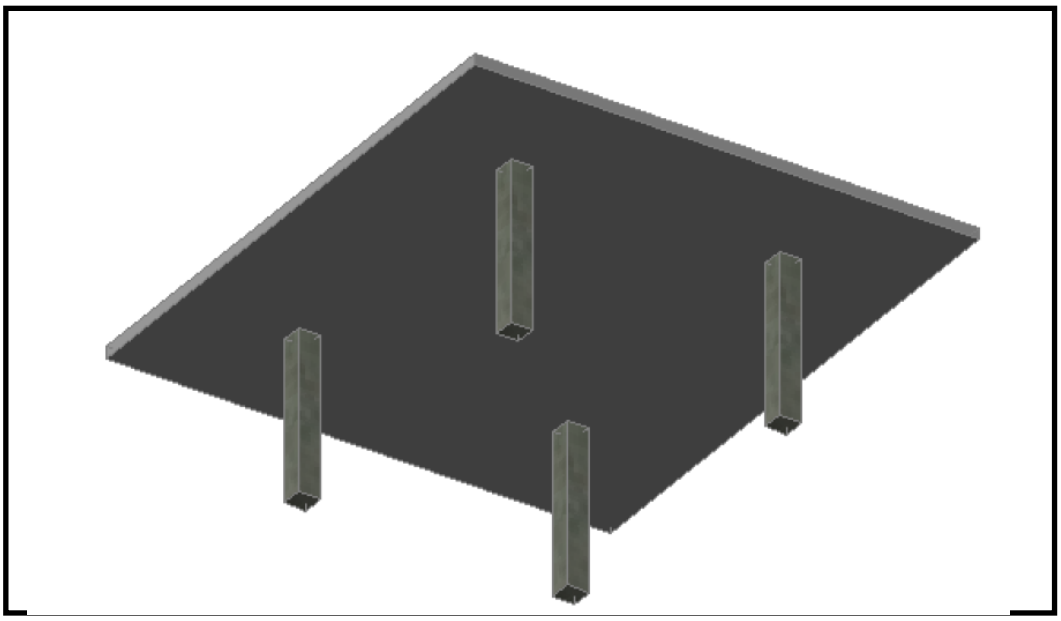

Figure (1.5) Flat Plate System [2]

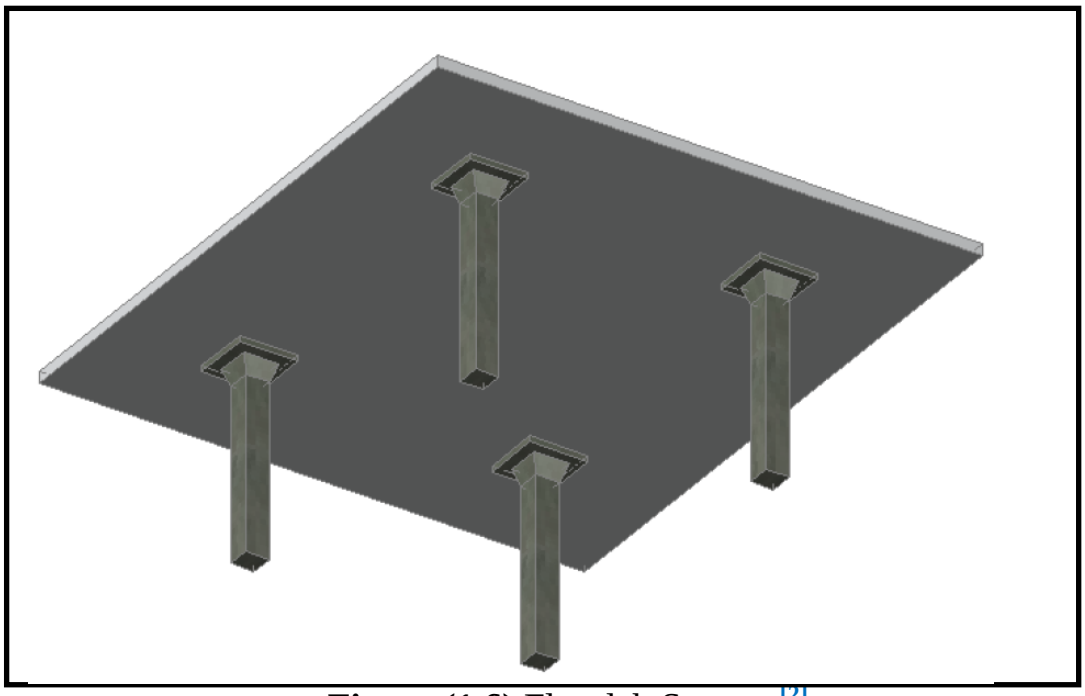

Figure (1.6) Flat slab System [2]

4- Waffle Slab: This type is used to reduce the dead load of solid slab construction by using metal or fiberglass form

inserts to create rectilinear cavities. Typically, by omitting inserts near columns, a solid slab can resist shearing and moments more effectively. The thickness of this slab system is usually 50mm to 100mm and is supported by ribs in two directions. The ribs are arranged in each direction at a spacing of about 500mm to 750mm. This type is shown in **Figure 1.7 [2].**

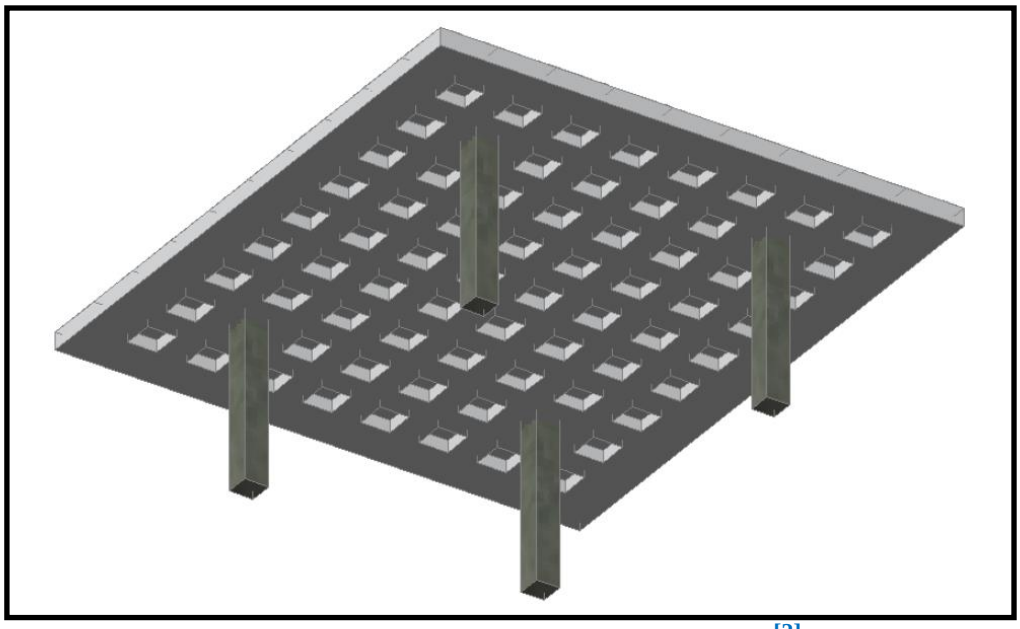

Figure(1.7) Waffle Slab System [2]

Also, flat slabs of reinforced concrete are frequently utilized within office buildings of medium height structures, and parking spot lots due to their construction and design advantages. The flat soffit allows for easier reduced overall storey heights due to proper positioning and installation, and greatly simplifies formwork and reinforcing. The punched shear capacity at the connectors between the slab and column typically determines the final strength of a concrete reinforcement for a flat slab. This type of failure was often brittle, and it can result in gradual collapses and the destruction of the entire structure.**[4],[5],[6],**and**[7]).**

Punching shear failure of slabs typically occurs suddenly and results in gradual failure of flat plate structures; as a result, care must be taken in

the design of such slabs and the sudden failure conditions must be avoided**. [8].**

Failure of the slab happens when the radial and diagonal tension cracks cross, creating a cone of failure as depicted in **Figure(1.8). [9].**

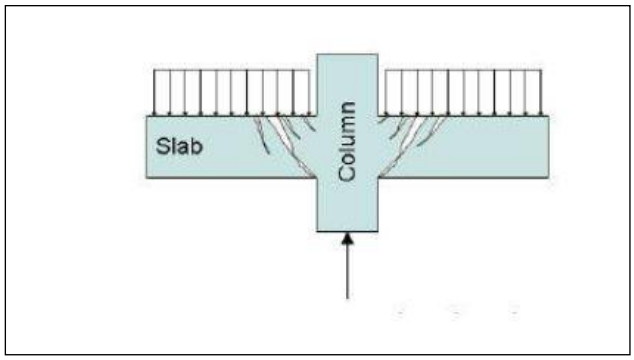

Figure(1.8): The punching shear failure [9]

Numerous studies were interested in the punching shear of rectangular (or square) shaped slabs.**[8]**and**[10].** Finding an appropriate material to be utilized in the building of any structure in order to satisfy these two aspects is extremely important. In structural design, two crucial points need to be taken into account, namely, the strength and serviceability considerations. Designers searched for the best building materials for their construction after long-ago realizing this truth. To acquire the benefits of sufficient strength and high serviceability, such studies led to the strengthening of weak materials with some strong ones**[11].**

1.2 Two-Way Shear (Punching Shear) Behavior

Numerous techniques have been utilized over the years to avoid and prevent this kind of failure, even though the shear process is not fully understood. Three steps are used to categorize punching shear failure. First is the spread of a crack as a result of bending and shear failures in the tension zone of the slab, which is close to the loaded sites' faces. Second is a slab tightening process that the steel reinforcement goes through in close proximity to the loaded places. A member's compression zone may be affected by flexure and shear cracks, which are represented by the third stage**[12].**

The concentration of shear stresses around the part connecting the slab with the column, which can result in abrupt punching shear failure at loads far below the slab, is a crucial design issue for reinforced concrete flat slabs. Flexural capability**[13].**

At half of the effective distance from the faces of the column, this crucial punching shear section is situated **Figure(1.9)**, Concrete's punched shear strength ought to exceed the shear stress at the crucial section **[14]**as follows:-

$$v_u = \emptyset\, v_c \qquad \textbf{(1-1)}$$

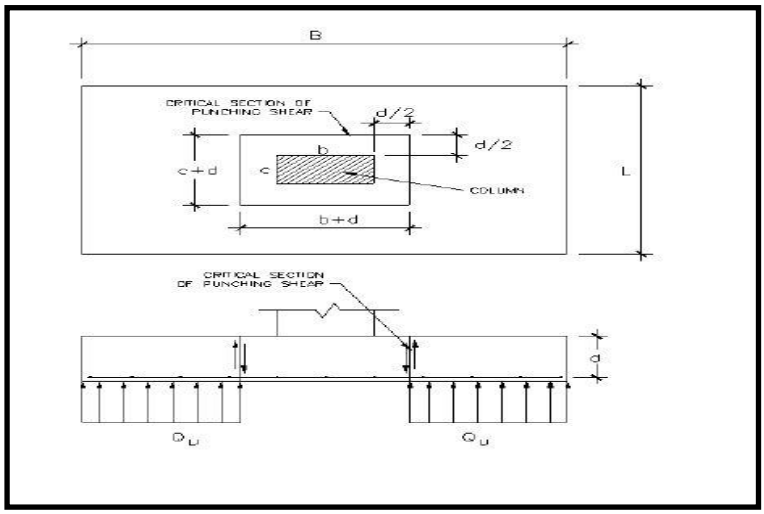

Figure (1.9): Critical Sections of Punching Shear [14]

There are several techniques that have been suggested to boost the flat slab's punching shear capacity, including :i)the use of stirrups, a conventional form of shear reinforcement, however this approach is not appropriate for shallow slabs (less than 150 mm in depth**).**(ACI Committee 318) **[15].** A novel approach utilizing headed studs, although it takes a long time to construct **[16].**

Muttoni presented a failure criterion for reinforced concrete slabs devoid of transverse reinforcement punching shear strength **[17]** as:-

$$\frac{V_{R.c}}{b_0 d\sqrt{f_c}} = \frac{3/4}{1 + 15\frac{\Psi d}{d_{g0} d_g}} \qquad \textbf{(1-2)}$$

where **Ψ** is the slab's maximum rotation; d is the effective depth of the slab; b0 is that control perimeter on the distance of d/2 from the face of column; fc is the strength of compression of concrete; dg is the size of aggregate, and dg_0 is maximum size of aggregate to (16 mm) as a reference the size of aggregate dg, by taking into consideration, criterion for failure in **Equation(1)** accounts for the effect of the strength of concrete and the texture of its cracks. It is necessary to understand the slab's load-rotation relationship in order to calculate the utmost shear puncturing strength and deformation capacity **[17].**

High stresses in the slab to column connections can cause pure punching failure or punching failure induced by bending **[18].** Steel fibers used in FRC slabs enhance tensile strength, ductility, and dissipation of energy, which improves performance of slab-column connections **[19].**

Increased rotations and wider cracks in the area of criticality of a slab surrounding a column as a result of higher loads reduce concrete's ability to transmit tensile forces transmitted from the slab to the column. Once again, a stress effect is involved here. As the result, The Critical Shear Crack Theory (CSCT) anticipates that, by Vanderbilt University's data, The penetration sheer force of unitary a slab-column connection's control perimeter falls with increasing column size **[20].**

Possible tension concentrations in the corner of the column are another factor that could lower the penetration strength large rectangular or square columns **[21]**. **Figure (1.10)** depicts the shear forces and distribution of stresses from shear in a slab d/2 from the margin of a column for various columns diameters and geometries. (calculated under the assumption of linear-elastic slab behavior). While the distribution can be considered to be uniform for both circular and small square columns (**Figure1.10(a) and 1.10(c)**), larger stresses can be seen in column corners when large square columns are included (**Figure 1.10 (b)**). To consider this effect, the Critical Shear Crack Theory (CSCT) advises making the assumption exclusively that the portions the containment perimeter adjacent to the corners of column (less than 1.5d distance) are effective for shear forces to carry **[22].**

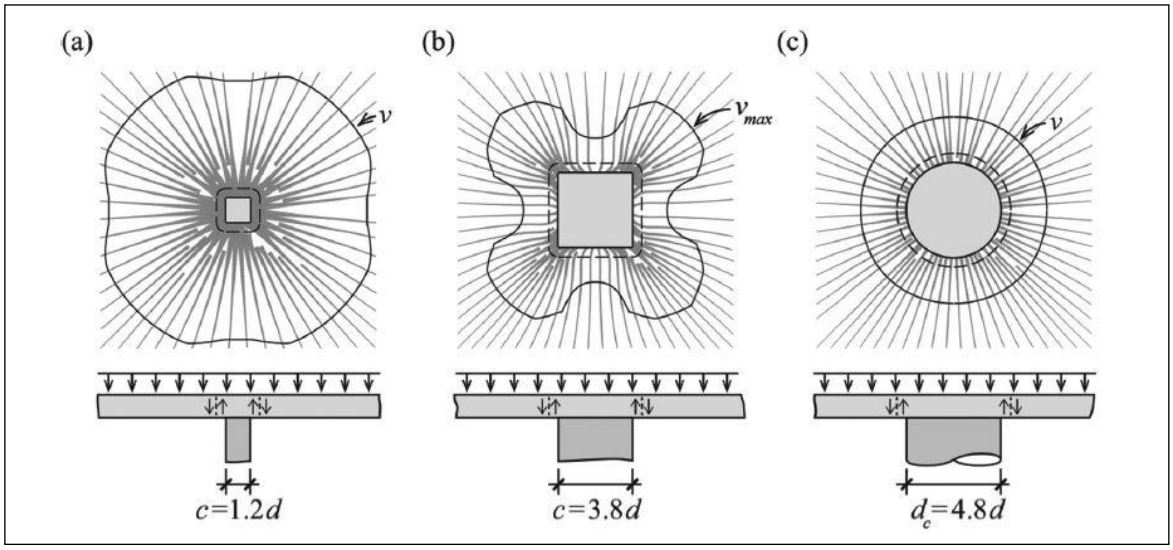

Figure (1.10): Fields of shear in the neighborhood of columns and distribution the stresses of shear at d/2 from the column's edge of the control perimeter: **(a)**Square column (small); **(b)** square column (large C/d>3); and **(c)** circular column (large). [22]

1.3 Steel fiber reinforcement

It takes into consideration the impact of fibers (steel kind) where fibers (steel kind) are added to achieve certain properties and that reinforced steel fibers are concrete according to (DS EN 206-1) **[23]**.

fibers will be enhanced, not simply in terms of strength, structural correctness, and post-crack state **[24]**. Short fibers that are randomly arranged serve as "ductility" reinforcement once cracks have formed by bridging over them. In the post-cracking state, the matrix can carry significant stresses over a relatively large strain capacity thanks to fibers that are sufficiently strong and attached to the material **[25]**. These features promote the usage of RPC in such a crucial area of punching shears. However, other aspects of RPC, such cost and density, limit its utility.

The tensile force conveyance properties of steel fibers could be employed to bridge cracks in the case of (SLS) and (ULS) stand for Serviceability Limit State and Ultimate Limit State, respectively., similar

to rebar strengthening. However, it should be noted that increased deformation typically results in a reduction in tensile strength remaining caused by the effect of steel fibers (opening cracks). Tensile force conduct of reinforced concrete with steel fibers is shown in **Figure (1.11)** in comparison with normal and traditional concrete reinforcement.

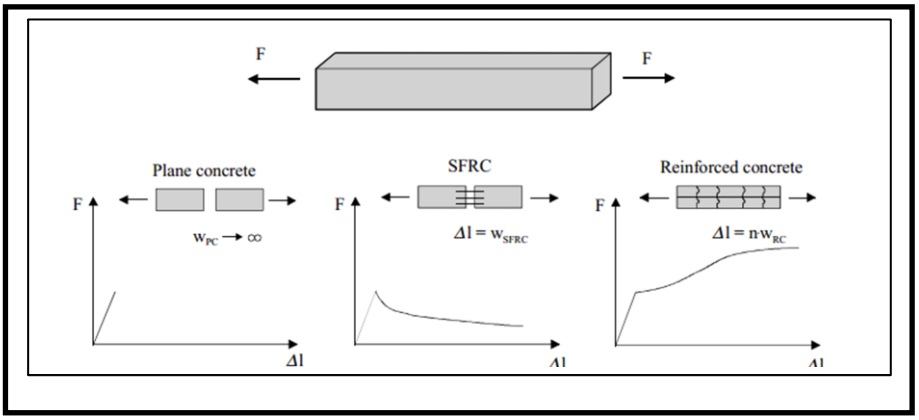

Figure (1.11): Tensile load vs displacement behavior of normal, steel fiber reinforcement and conventionally reinforced concrete [23]

Steel fibers are present in RPC, and there are no significant aggregates. Concrete with steel fiber reinforcement is essentially a less complex and more affordable version of reinforced concrete. Steel fibers help concrete become ductile, changing its brittle properties. Fibers' main function is to prevent cracks from forming and spreading by applying pinching stresses at the crack tips **[26]**.

Straight and hook steel fibers produced by the Chinese company Bekaert Corporation were employed in this test program.

1.4 The Research Objective.

The main objectives of the research include the experimental and theoretical aspects. The experimental aspect includes studying the mechanical properties of fresh and hardened concrete based on the fiber shape and fiber dosage, and studying the experimental investigation of the punching shear behavior of FRC based on the fiber dosage, fiber shape, and column shape.

The theoretical side includes comparing the experimental results with the different code equations and proposing new equations to calculate the shear strength in a way that is closer to reality based on the compressive strength and tensile strength of concrete and comparing them with the current study and previous studies.

1.5 Research Layout

The present research involves five chapters as follows:

The present chapter, **Chapter One** provides an overall introduction to the reinforcing element, punching shear, steel and hook fibers. **Chapter Two** reviews most of the previous investigation conducted in the field of this research. In **Chapter Three,** the program of experiments, the details of samples, characteristics of the material with test procedures will be presented. **Chapter Four** presents the analysis and comparison of empirical and theoretical results. Finally, **Chapter Five** examines the theoretical application of samples in accordance with international codes providing a comprehensive overview of the interpretation, analysis, discussion, presentation, and evaluation of theoretical research in comparison to experimental research on the performance and durability of models. The conclusions and recommendations for future studies are summarized in **Chapter Six**.

CHAPTER TWO

REVIEWI OF LITERATURE

CHAPTER TWO

REVIEW OF LITERATURE

2.1 Introduction

This chapter shows the experimental research that examined the behavior of slabs made of fiber-reinforced concrete under two-way shear. This chapter presents the details of the experimental study of concrete slabs reinforcement and compares the suggested model with the results of experimental.

2.2 Two Way Shear Behavior

Sagaseta et.al.,2014 [21] examined the behavior of the structural of RC flat slabs supported by rectangular columns in the interior and the effect of their strength depends on loading conditions (one- or two-way flexural) of shear punching. The strength of shear punching of slabs at rectangular columns could be less than that of slabs at equivalent columns of squares with a comparable control perimeter length. This is because of the potential shear force concentration along the control boundary. The presented theoretical models are validated by four punching shear experiments of slabs with one-way and two-way bending. For the examined experiments, accurate predictions of the strength and the capacity of deformation were obtained.

The decrease in strength of punching caused by the shear forces concentration close to the extremities of columns (rectangular and square) with (c/d > 3) is dependent on slab and column geometry bending deflections. However, in such situations, the majority of design protocols only consider the geometry of column. This simplification may lead to overly optimistic predictions of the impacting force utilizing EC2 in slabs

with one-way action along the length of an elongated column. In general situations of two-way acting in a slab, the suggested approach and the shear fields give identical estimates of the shear control perimeter resistance compared to the simplified MC2010 formulations. However, these two methods are more consistent among instances of (one and two)-way acting than simpler techniques based on the physical shape of the supporting area.

The tests conducted in this study revealed that the direction of the column relative to the primary orientation of spanning had a significant impact on the mode of failure, strength ultimate, and capacity of rotation. As anticipated, the forces reaction under the plate of bearing migrated towards the column's edges, particularly in experiments involving one-way action along the large axis of a column elongated. In comparison to slabs with equal rotations in both orientations, slabs with substantially larger rotations in one direction demonstrated greater residual capacity. This is because of a redistribution of shear that could be measured with the authors' previously devised model of non-axis-symmetrical punching in square columns. Although this repeated method provides more precise estimates of strength and deformation of capacity in such situations, the MC2010 simplified procedure based on maximum rotations seems more appropriate for the purpose of design.

Einpaul Jürgen, et. al.,2016[27] Compared experimental results from previous researches with the predictions of CSCT4 and a few main rules of practice (ACI 318, Eurocode 2, and Model Code 2010) were analyzed for their suitability and precision. It was tested on 13 slabs. Two prior punching tests that were conducted in the lab with comparable settings ($PL7^{10}$ $PV1^{24}$) round up the test series.

A diagonal crack failure was discovered after the samples have been saw-cut as shown in **(Figure 2-1)**, The image of a crack in **Figure (2-**

2(a)) state how the crack failure was uneven, with a typical angle between the slab surface and the failure fracture of about 45° or less is typically the case. On various column sides in certain samples, the crack failure had various angles and forms. On the seeing-cuts sloped to column angles and forms, there were multiple flexural cracks, addition to the crack failure.

All slabs' saw-cuts have cracking patterns that are sheared. The failure zone was significantly reinforced, as evidenced by the. cracked as well as having flexural and shear damage according to **Figure (2-2(b))**, in the shear stud anchorage zones.

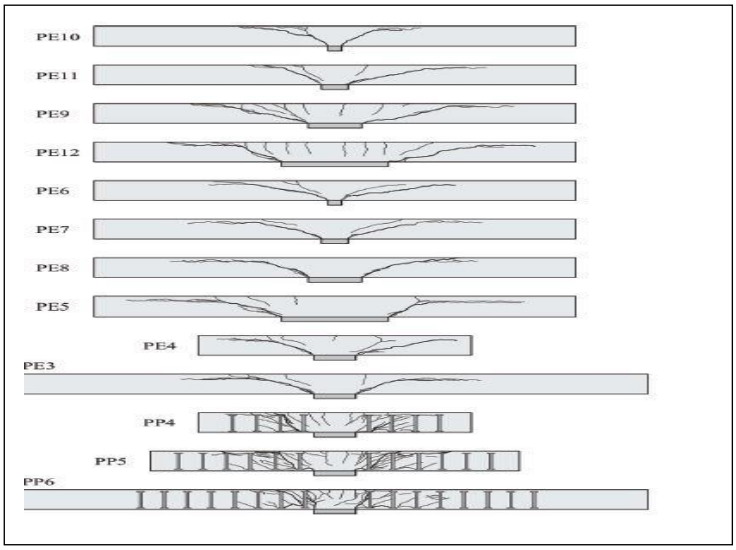

Figure (2-1) Cuts in slabs along a weak axis [27]

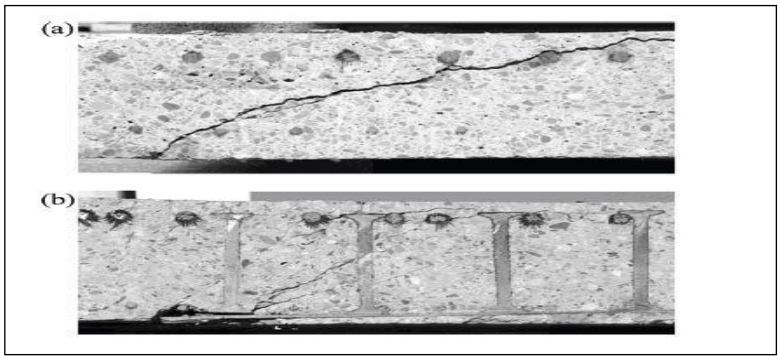

Figure (2-2) Photographs of common puncturing fractures on see-cut slabs: (a) slab without reinforced shear (PE7) and (b) slab with reinforced shear (PP4)[27]

Research demonstrates that a specimen's slenderness has an impact on the load-rotation response's rigidity. It has an impact on both the crack widths and the punch's strength. This impact, particularly, is notable in the slabs reinforced for shear and must be taken into account when designing punching tests, considering the specimen size, which is the opposite of experimental data. This criterion is not taken into account in punching regulations of (ACI 318) and (Eurocode2).

According to two-way shear experiments of slabs with various supports, the nominal unitary strength for shear at d/2 from the column face on a control perimeter falls as the size of the column increases. That result is also explicable by the impact of cracks appearing close to the supported region.

When reinforcement ratios are decreased and slabs are increased in thickness, the drop in, specifically, the ACI 318 unitary nominal shear strength for big columns could cause an overestimation of punching strength. However, the strength of punching of very small columns is exaggerated if the circumference is placed as per (Eurocode2) at 2d.

The Model Code's punching provisions and the CSCT 2010 consistently take into consideration the impact of the size of the column and slab thinness. The (CSCT) offers the most accurate means covariance coefficient of experimental to the models that were compared for anticipated punching load.

Simões,et.al.,2016[28] used a total of eight 550 mm-thick reinforced concrete footings were used in this experiment, The effects of the size of the column, element slenderness, compression and shear reinforcement were all present examined in these studies. compared samples with and without shear reinforcement, those with shear strengthening showed a greater ductile failure.

Reinforcement for shear, the surface of failure of footings, it seems to be reliant on the slimness of the shear, with surfaces of steeper shown slabs that are more compact, it is also crucial to notice from **Figure (2.3)**

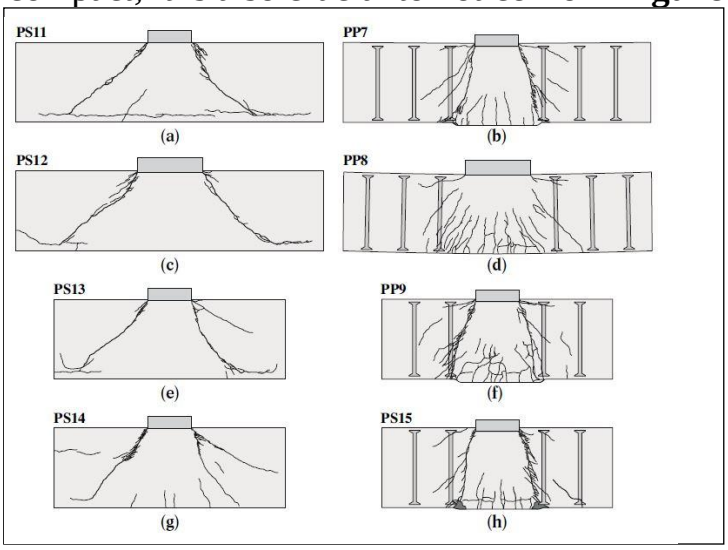

Figure (2.3) Saw cuts depicted schematically [28]

The nominal thickness (550 mm) and bottom flexural reinforcement (0.75%) were held invariable during the effects of the size of the column, slenderness, both shear reinforcement and horizontal reinforcement at the top of the structure were analyzed. The experimental testing produced precise data in the shear-critical zone. It is demonstrated that as the shear slenderness decreases, the ability to punch through shear-reinforced concrete footings increases. Furthermore, ratios of span to effective depth that are low, it appears that the critical shear crack's inclination is steeper.

Double headed shear studs can greatly improve resistance to punches exhibited by reinforced concrete footings. It has been demonstrated experimentally that the shear slenderness affects this reinforcement's effectiveness, with low ratio of effective span to depth resulting in lower effectiveness. The phenomena that cause failure, according to a comprehensive measurements analysis taken critical region of shear, is The destruction of the concrete diagonal support near the column. This

zone contains pulverized concrete is confirmed by observances concerning saw-cuts following the experiment.

Jaroslav and Lucia,2018[29] investigated the findings of a test operation performed on flat slab samples with transverse reinforcements created in a manner that any failure caused by the crushing of the struts. The test samples were section of flat slab with an octagonal shape and a thickness of 250 mm; see **Figure (2.4)**. To shorten the column perimeter's length and maintain a ratio of (u_0/d = 2.83), the specimens were held aloft by 180 mm-diameter columns. A (20/100) mm flexural reinforcing composed of (B500B) steel was added to the slabs for reinforcement. The typical effective depth was 200 millimeters, and the average the ratio of reinforcement was 1.57 percent, and two specimens (S1-1 and S2-1) exhibited reinforcement transverse made of Peikko PSB double-studs of headed made of (B500B) steel with a 10 mm diameter as shown in **Figure (2.5)**.

.

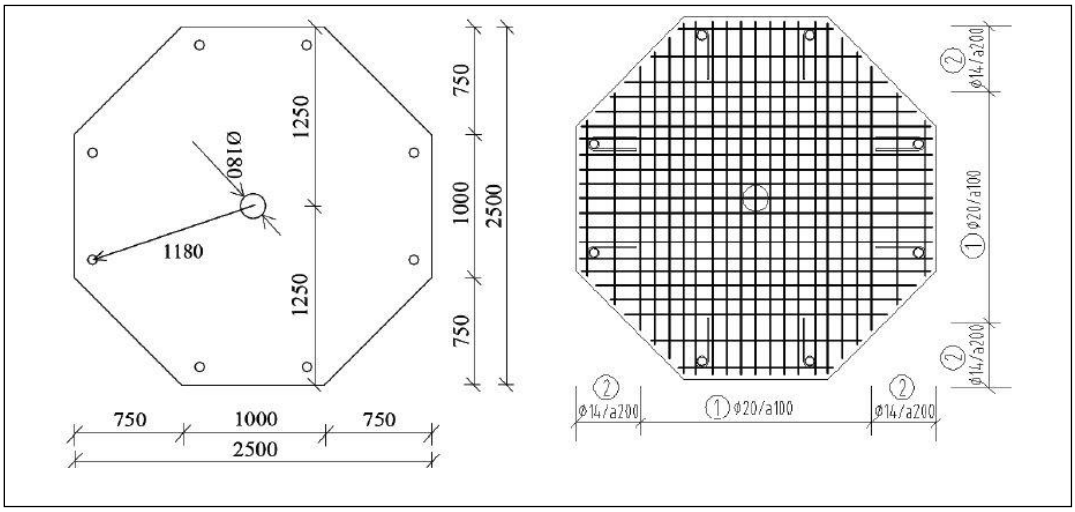

Figure (2.4) Test specimen – view of the plan [29]

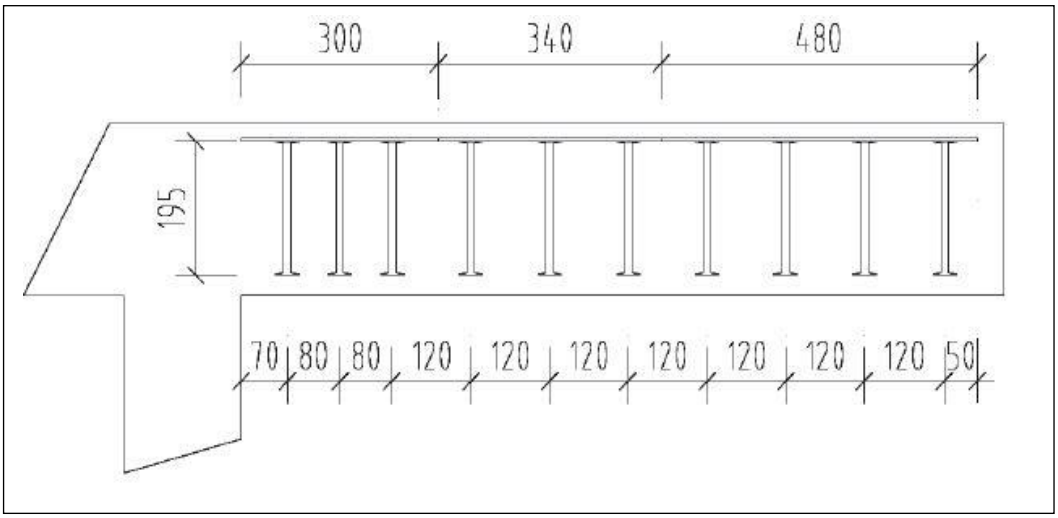

Figure (2.5) Peikko PSB fasteners - shear reinforcement configuration [29]

The slabs that lacked any reinforcement of shear collapsed in a typical cone-shaped failure mechanism. For specimen S1-2, a critical shear fracture had a slant at around 25° angle (**Figure 2.6**). The shear-reinforced specimens failed differently. In contrast to the situations of the samples lacking any reinforcement for shear, the critical fracture was extremely sharp and the punching cone was considerably smaller **(see Figure 2.7).**

Figure(2.6) Section S1-2, specimen without transverse reinforcement, saw-cut[29]

Figure(2-7) Section S2-1, specimen without transverse reinforcement, saw-cut[29]

According to the German NA, the k_{max} factor suggested based on the existing EC2 model, 1.5 is suitable for samples and individuals alike. permits the elimination control of the capacity of strut in the event of punching. The model offers conservative answers, such as the need for thicker slabs or more bending reinforcement. In the instance of flat slabs where the strut of concrete crushing is not the dominant mechanism of punching failure. If the capacity of the strut is directly controlled, larger values of the k_{max} factor greater than 1.6 in the case of flat slabs reinforced with double-headed rivets are transverse reinforcements were permissible. If we take into account that the evaluation of the capacity of strut is absent from the model, the value of the k_{max} factor in the instance of the ETA 13/0151 model is very high at 1.96.

ZoranBrujić,et.al.,2018[30] analyzed the moment transmission effects at the inner-column flat-slab connection as well as the impact of the strength of concrete on slab resistance of punching. Experimental and numerical investigations are conducted on seven full-scale specimens.

The findings are provided as load-rotation curves and contrasted with various equivalent formulations in addition to the shear critical fracture theory (CSCT) failure criterion.

To ensure better agreement between the numerically determined load rotation relationship and the experimental findings, a thorough nonlinear FEM study that involves model calibration using experimental data is carried out.

Eccentricities of applied force that have been calculated as well as force amounts that result in punching failure are shown. The eccentricities found on the y-axis were less than 5mm. After plastic deformations in the slab's top reinforcement developed, all seven specimens broke down owing to brittle punching.

In this article, the parameters of load eccentricity and concrete strength are analyzed. The range of this study is constrained by the use of experimental specimens that have flat slabs with uniform geometry (the size of the column, span of the slab, and the depth of the slab), vertical load at constant eccentricity, and constant ratio of reinforcement and layout.

Joao Tiago,2018[31] Checked according to the established refined mechanical example, the theoretical CSCT principles for the failure of shear punching of prestressed slabs and footing of the reinforced concrete

To better comprehend the parallels and distinctions among the behaviors of slim and squat members, the program of experimental regarding the punching behavior of foundations is shown. The measurements reveal that the shear strains, in addition to the slab's rotation, have a considerable impact on the condition of deformations at failure of squat members. Utilizing the limit analysis upper bound theorem, a theoretical work is created. It demonstrates the presence the

influence of shear-flexural interaction in compact footings, which affects their resistance and establishes a seamless transition between the pure bending and punched shear systems. To accurately anticipate Limit analysis is used to determine the strength of punching for compact footings, strain- and size-effects need to be taken into account, according to a comparison between theoretical and experimental results.

This design is used to analyze the situation of thin slabs and confirm using experimental findings, which demonstrates a good level of consistency. The CSCT's analytical failure criteria as well as its primary presumptions can both be theoretically validated by a boundary investigation according to the refined criterion for failure

As its opening disturbs shear-carrying compression structures, the evolution of a critical shear fracture controls the strength of punching of flat slabs. Failure may result from localized strains in this fracture or by the initiation of a new one (crack failure) as a result of transverse tensile stresses (Splitting) stresses generated close to the area of support. This is also consistent with **Einpaul et.al.(2017)**[32] measurement results based on interior cracking results in punching experiments.

According to the experimental findings of **Clément,2012**[33]**,** the kinematics of a sector of the slab at failure is administered by both the slab rotations and the shear deformations that evolve in the shear crack critical.

When compared to a record of previously tested samples and single test chains where just a single parameter is changed, the model's findings demonstrate good agreement with experimental findings. Finally, the first outcomes of the use of the mechanical design to analyze slabs prestressed and foundation demonstrate that the CSCT concepts were equally applicable to the analysis of those scenarios.

2.3 Two Way Shear Behavior for Fiber Concrete

Abdulhameed Abdullah Yaseen,2006[34] The objective of this investigation was to determine how reinforced by steel fiber affected the characteristics of strength and deformation of connections between high strength of concrete slabs and columns reinforced without reinforced for shear. It was also done to determine how well fiber concrete resisted punching shear.

Fourteen 800 x 800 x 60 mm slabs of tests were conducted on concrete reinforced with steel fibers by merely supporting them around four edges and loading them by the column central. The compressive strength of the concrete is (35 to 65 Mpa), column dimension is (75, 100, and 150 mm), volume fraction is (0.0, 0.25, 0.5, 0.75, and 1.0%), and aspect ratio of the steel fibers is (50, 67, 83, 100, and 133).

The research is based on examinations of isolated, solitary, simply supported specimens that are thought to mimic a section pertaining to a plate floor system close to a head of the column. The compressive strength, steel fiber volume portion, fiber aspect ratio for steel, and column size were among the factors examined

Figure (2.8) depict the slabs in series one's failure pattern.

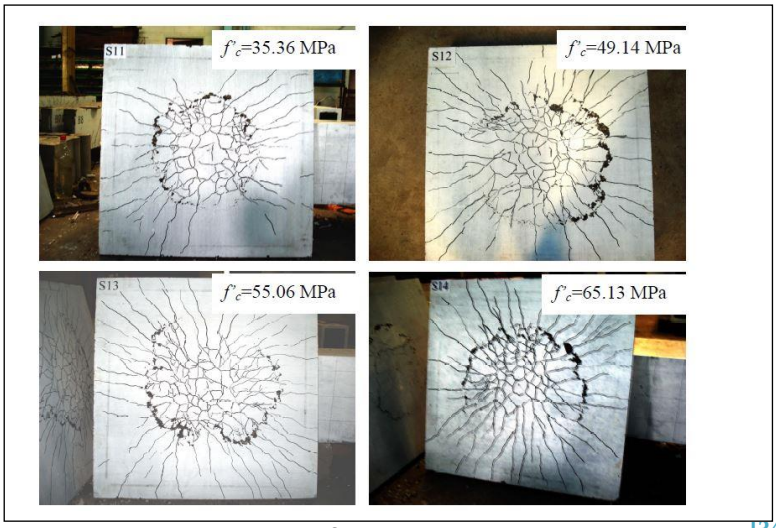

Figure (2.8) Failure modes for slab-column connections[34]

The surface of failure is pushed away from the face of the column by about 2.62 to 2.96 when fibers are present, which is lower than the distance for concrete slabs with a lot of strength devoid of steel fibers. Angles of failure that have been observed also progressively grew from (18.6) degrees to (20.9) degrees by lowering the fiber factor. At greater levels of fiber content, the introduction of fibers modified the converting failure shape of punching to a more shape of circular. Increases in compressive strength (f'c) for high strength concrete slabs result in increases in the slab's load-carrying capacity, stiffness, and, as a result, a decrease in its ductility.

Since doubling the size of the column enhanced the slabs' punching shear strength by roughly 50%, the influence of the size of the column could be regarded as a significant parameter. Additionally, the ductility rose by around 50% with a 100% increase in column size.

The form of the shear perimeter was not significantly changed by increasing the column size in slabs, but the failure surface was pushed around 44% farther away from the column face. The tested slabs' observed cracking load (shear or flexure) always at a minimum (83 to 88) % below the ultimate load. The punching shear strength that is created by HSFRC slabs is satisfactorily predicted by the proposed equation.

L. NGUYEN-MINH et.al.,2011[35]conducted an experimental investigation consisting of twelve small-scale planar slabs of various dimensions that were tested to determine the impact of the effects of the resistance of steel fibers on the shear punching and fracture conductance of SFRC slabs were evaluated. Additionally, according to the data from authors and additional researchers, the report assesses the precision of using existing formulas to forecast the capacity of punching shear for (SFCR) flat slabs.

Twelve modest-sized flat slabs were tested, nine of which were made of SFRC and three of which were control slabs made of steel reinforced concrete (SRC).

In **Figure (2.9)**, the typical slab's crack patterns are depicted. Punching shear (PS) tests on all slabs are negative. The fibreless slabs broke down in a very brittle way, causing the concrete covering on the bottom surface to crumble. The fiber-filled slabs cracked more readily. Due to the effect of bridging of the steel-fibers, cracks in these slabs formed consistently and with lesser widths. The ductility and integrity of the concrete around the connections of slab-column are considerably improved by presence of steel fibers.

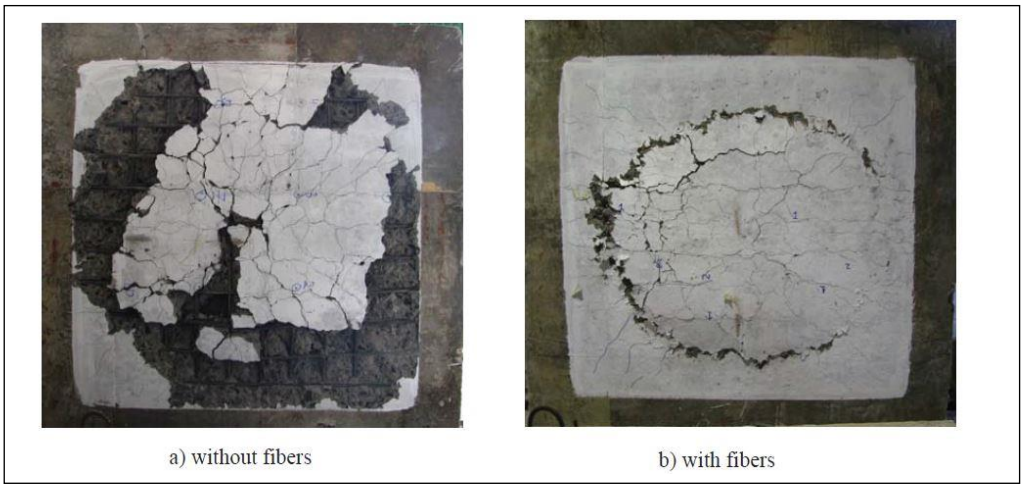

Figure (2.9): Failure pattern typical for testing slabs – bottom face[35]

The average breadth of a crack is 0.241mm is visible in the slabs free of fibers. There was a considerable reduction in the average width of crack for (SFRC) slabs (about 70.8%) at the same quantity of loading, with the average crack width measured at 0.141 mm. The reduction rises sharply and varies between 41.5% and 89.5% at greater load levels.

The evaluation findings showed that, while compared to the trial results, the equations produced erroneous results with a significant amount of scatter (COV of about 24%). For a more precise calculation of the resistance of punched shear for (SFRC) slabs, a new formula should

be developed, in which the impact of fiber shape, length, and ratio to diameter as well as the contributed to the tensile reinforcement dowel action should be taken into account.

Maya, et.al.,2012[36] discovered that adding fibers to concrete increases the reinforced concrete slabs' deformation capacity as well as their shear behavior. In this study, a model of mechanical is presented for forecasting the punching resistance and performance of reinforced concrete slab with steel fibers, in addition to reinforcement traditional.

The principal hypothesis of the theory of shear critical crack (CSCT), which states that the crack opening for critical shear relates to the production of the slab's rotating and the member's effective depth, takes into consideration both the contribution of concrete and fibers as shown in

Figure (2.10).

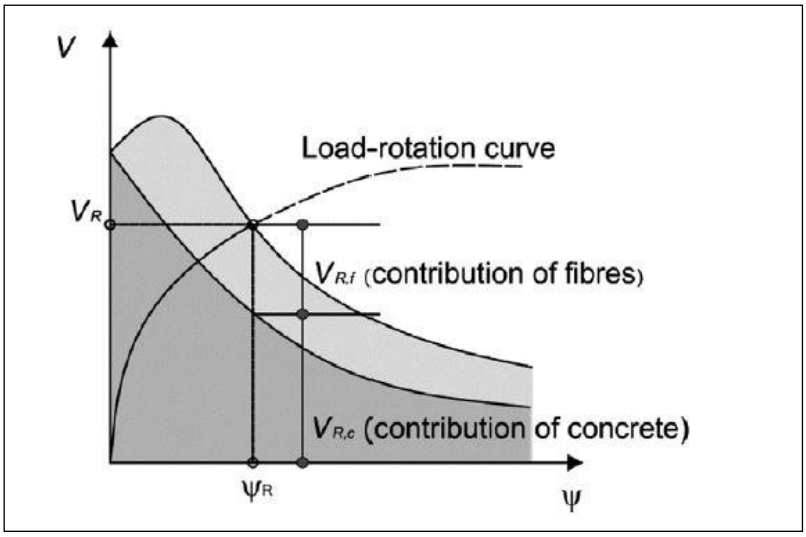

Figure (2.10) Capacity of Punching shear [36]

An opening of crack-fiber stress of bridging connection is necessary for assessment of the fiber's participation in the strength of punched shear. The Calibration of material property values must be based on the results of test findings, by the strategy for fiber reinforced concretes used in the majority of current design codes. As an alternative, Voo and

Foster's Variable Engagement Model could be utilized to evaluate the tensile behavior of fiber concretes reinforcement that shown in **Figure (2.11)**:-

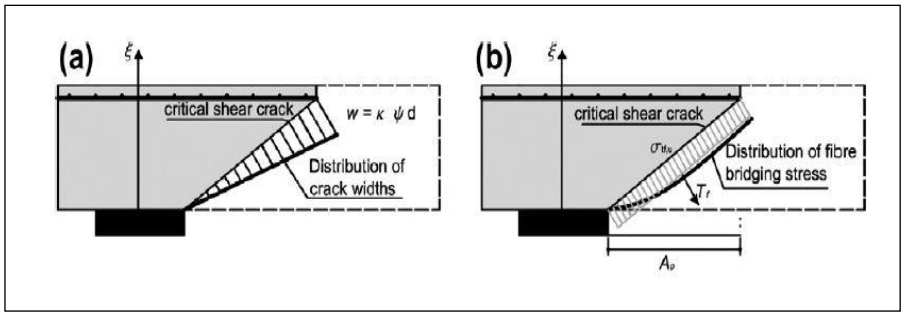

Figure (2.11) :(a) Hypothesized distribution of fracture widths along the surface of failure and **(b)** Fiber bridge tension along the surface of failure[36]

The suggested Model of prognosis accurately depicts the impact of the fibers on the impact resistance of FRC slab-column connections and shows excellent concordance with the test data and it is suggested to use a more straightforward method that produces accurate predictions of the strength of punching shear and adequate safety for ordinary designs. When compared to test findings, there are several experimental design formulas exhibit a scatter of noticeable, which could result in predictions of the strength of punching shear that is dangerous.

Hassan, et.al.,2015[37] stated the capacity of concrete to withstand the Shear of punching was attempted to be measured using a novel testing method. Detailed Experiential research on (UHPFRC) failure of slabs subjected to puncturing shear was conducted using the proposed test setup. From the findings, the value of the critical of the fundamental control boundary, the mode of the failure, and the relationship between the punched load for shear and the shear plane angle were explored. This experimental investigation offers important new information about the strength of UHPFRC for punching shear slabs. Because of additional strength provided by compression supports within the concrete, it was

discovered that the ultimate load of the punching shear increased with increasing the angle of punching shear. The practice is referred to as shear support improvement. At an angle of punching shear of 28.2, the load of punching shear was found to be the lowest (basic perimeter control about 2d) which is largely consistent with reports for regular concrete BS EN, Euro code 2 2004 **[38].**

All of the slabs collapsed with a sectioned cone form on the side of the supported and a punching stub on the loaded side, according to an analysis of the test failure patterns. This failure mechanism verifies the test's reliability procedure used in the research and is comparable to the typical failure of punching shear described for regular concrete **Mosley et.al.,2012 [39].**

Similar to the typical punching shear failure behavior for regular concrete, the failure behavior for UHPFRC slab sample with angles of punching shear equal to and larger than 62 (basic perimeter control of 0.53d or less) was shown to be fragile **Mosley et.al.,2012[39].** However, for samples with angles of punched shear equal to or less than 45 (perimeter of basic control exceeding 1.02and more), the failure behavior changed to a ductile mode, mimicking its characteristic flexural failure described in the literature **Mahmud et.al.,2013[40]**. The effect of bridging fibers along the concrete planes of shear contributed to the test's increased ductility. As a result, once maximum load capacity was obtained, the slab samples were capable of more deflection. The ideal mechanism of slab failure in concrete designs is a ductile behavior. The results on the conduct of UHPFRC slabs without reinforcement for shear during punching shear failure are significant. Comparing the results to what is stipulated in EC2 for normal concrete, the results show a decrease in the fundamental control perimeter for UHPFRC slabs of the half. When necessary, the high strength of tension and enhanced ductility of

the concrete can be used to limit the reinforcement of shear in UHPFRC slab members to 1d. When designing structures with thin UHPFRC decks of highway bridges, when significant shear reinforcing is not a possibility and punched shear failure is imminent, this behavior is advantageous.

I. Siva Kishore, and Mallika C.,2015[18] obtained a notable improvement in the cracking behavior, a large increase in punching shear capacity, and satisfactory reliability of the connection of column-slab of the fiber-reinforced slabs. The slabs reinforced with fibers collapsed in a more ductile manner than the slabs without fibers, and it was found that as specimen size grows, failure shear stress reduces. 12 flat slabs (small-scale) altogether, consisting of nine SFRC and three conventional slabs, were tested in this experiment. Punching-related nominal shear stress at failure may be stated as:

$$\tau_N = \frac{P}{\pi b d}$$

which P is the highest stress at which the punching shear failure occurred b is the punching diameter at the section of critical, and d is the slab thickness.

When the ultimate punched shear load is large, the slabs with a higher fiber volume percentage can withstand more deflection. The present investigation punched shear experiments on geometrically identical concrete slabs of various sizes show that the size effect is no longer existent, meaning that as the size grows, the nominal stress at failure reduces.

Steel fibers also make the slabs more rigid and enhance the concrete's ductility and structural stability near the slab-column connections. The strength is reduced since there is no interlink connection between the fiber and the concrete in this area. In comparison to the experimental

results, the evaluation's findings showed that the formulas produced erroneous results with a significant amount of scatter.

If 10mm aggregate is utilized, and the concrete and aggregate are properly interconnected when the aggregate is placed in the column, the column may not fail. The size of the circular slabs must be raised because the minimum size of aggregate that is often considered is 20 mm. If the size is raised, the outcomes will be favorable since the strength will increase.

Tamara Adnan Qasim Al-Shaikhli,2016[41] investigated reactive powder concrete slabs with square and triangular shapes were tested punched for shear and flexural strengths. Three slab specimens of the same size but with varying constituent qualities made up each of the two test slab groups that were cast and tested. slabs in the square shape with dimensions of 450 × 450 mm and with a thickness of (50mm). While being triangular in design and measuring 500 mm in width, 810 mm in height, and (50mm).

Each group consists of three specimens with different amounts of steel fiber (0, 0.5, and 1%) about the overall volume. The test results are shown in **Figure (2.12).**

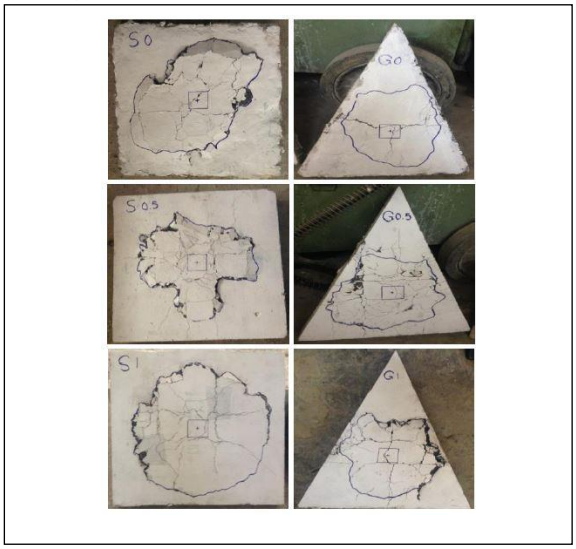

Figure (2.12) The test specimens [41]

As the percentage of steel fiber grew, the maximum capacity also increased. In square specimens that contain steel fiber in amounts of 0.5% and 1% of the volume total, respectively, the ultimate load rose by about 37% and 100%, whereas this proportion is about 59% and 100% in triangular slabs that contain steel fiber in amounts of 0.5 and 1%, respectively. Steel fiber usage enhances punching shear resistance and permits the transfer of greater pressures via the connection of slab-column. As a result, both the amount of steel fiber and the slab's shape affect the final capacity. The inclusion of steel fibers significantly increases the deflection (Δ_o) at ultimate load. In comparison to the nonferrous RPC slab, the addition of steel fibers to RPC square slabs at volume fractions of 0.5% and 1.0% is (19.5 and 99%), while these percentages are (3.4 and 13%) in triangular slabs. The steel fibers addition also enhanced the ductility ratio. When the percentage of steel fibers was expanded from 0.5 to 1%, the ductility ratio in square slabs increased from 8.1 to 16.6, and in triangular slabs, it increased from 3.75 to 6.1. This is to be expected because fibers enhance deflection at ultimate force while decreasing deflection at cracking load. The conclusion is that triangle slabs are less ductile than square slabs.

Dr. Layth Al-Jaberi, et.al.,2016[42] investigated how the volume of fibers (Vf) affects the shear of punching behavior of a hybrid flat slab system consisting of reactive powder concrete and lightweight concrete (RPC).

Five slab specimens measuring (900x900x80) mm were put to the test. NSC and LWC, two instances, were entirely constructed using one type of concrete. The other three specimens, on the other hand, were produced as hybrid slabs made of two different types of concrete. The whole slab was composed of LWC, with the exception of the key punching shear

zone. The factors are the slab's critical punching shear zone's concrete type and the value of V_f in the RPC mix.

Simply supported at all sides, all slabs. At the center of the slab, a single point load is used.

The crack patterns for the slabs are depicted in photos in **figure (2.13)**. (S1, S2, S3, S4 and S5). All of the slabs broke as a result of punching shear, and for S1, S2, and S3, cracks can be seen around the connection area between the column and the slab, but for S4 and S5, the failure occurred in the area that LWC occupied away from the column face. The type of failure and the separation between the column face and the cracks are not the same and vary from slab to slab.

Figure (2.13) Cracks Patterns and Failure Mode for the Tested Slabs [42]

The values of (f_{cu}), (P_c), and (P_u) for S2 are the lowest among all the values in this table, as can be observed. The values of S1 are around 69%, 29%, and 42% greater than the values of S2. While the same properties' values for S3 are around (622%, 128%, and 144%) greater than those for S2 and about (326%, 78%, and 71%) higher than those for S1, respectively.

All of the examined slabs' load deflection curves react first linearly, then nonlinearly till failure. Up until the failure occurs via punching shear, the slabs made entirely of NSC or LWC develop cracks all around the column. RPC matrix, which comprises fibrous materials, exhibits high levels of structural strength and ductility, which increases the ability of the hybrid flat slab system, which contains LWC and RPC, to handle higher levels of the cracking load and ultimate load

2-4 Two Way Shear Behavior (Numerical study)

Jae Ho Lee, and Busan (KR),2012[43] stated a reinforced concrete structure may use a device of truss-type reinforcement shear with twice functions of upper and lower anchorage portions of the increase resistance of structure to failure of shear. The device of truss-type shear reinforcement consists of a truss with a top chord element, a bottom chord element, and one or more connection members for connecting the top chord element and the bottom chord element; one or more top anchor element; and one or more bottom anchor elements.

Double heads of anchor are installed on the bottom and top of a truss (20) that is constructed by joining an upper member (24) to a lower member (26) via connection members (21). These connecting members may be either vertical or inclined. The truss-type tensile reinforcement material is constructed with double anchorage functions at both its top and bottom (23). Upper anchor heads (34) and the upper member (24) perform a dual function of anchorage at the top, while lower anchor heads (44) and the lower member (26) perform a dual function of anchorage at the bottom. Additionally, it enhances construction quality as the process of concrete structure building becomes more suitable.

Gerd Ginther, and Bad Orb (DE), 2014[44] The present disclosure refers to a concrete component including a minimum of one upper and lower longitudinal reinforcement layer and one transverse reinforcement layer extending above the uppermost and lowermost longitudinal reinforcement layers. At the lower 20 structural components of steel L-shaped sheet metal with attached of stirrups are used to generate the required transverse force as shown in **Figure (2.15).**

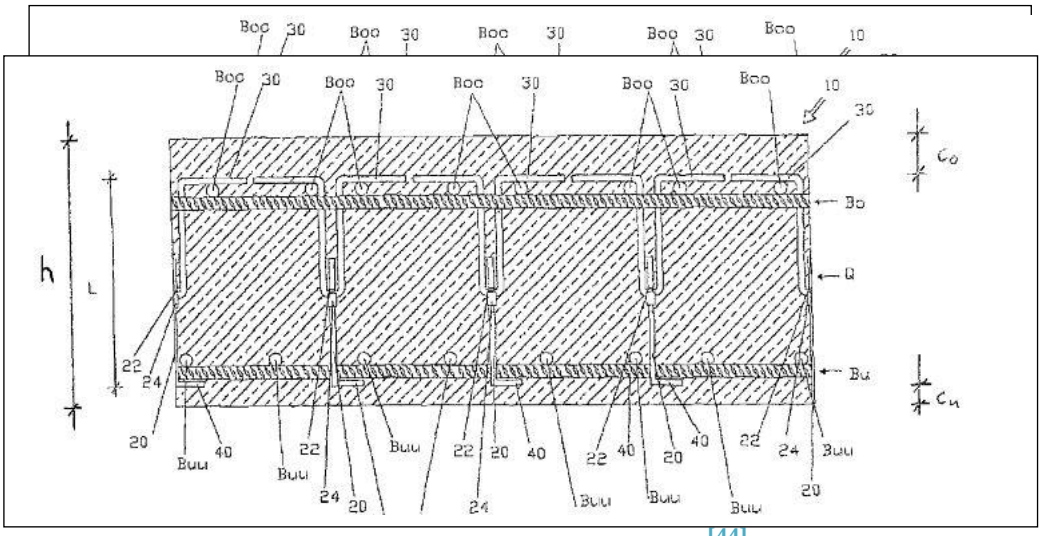

Figure (2.14) Drawing Sheets[44]

The current disclosure relates to a concrete component with a transverse force reinforcement whose extension passes across the topmost and lowermost longitudinal reinforcement layers and minimum upper and lower longitudinal reinforcement layers.

A piece of reinforced concrete that has a transverse force reinforcement that extends above both the highest and the lowermost longitudinal reinforcement layers, as well as at minimum one upper and one lowest layer longitudinal of reinforcement. The uppermost or lowermost longitudinal reinforcement receives the chamfer, appropriately.

Majid M.A. Kadhim, et.al.,2021[45] The findings demonstrate that the slabs' punching shear capability rises as the UHPC zone's area grows. Furthermore, the ratio of UHPC's strength of concrete compressive to NC's had a major impact on how the hybrid slabs behave and should be taken into account in future design guidelines. Additionally other elements like the plate of loading and the frame test were modeled using 8-node masonry elements with reduced integration (C3D8R). **Figure(2.17)** compares the patterns of crack of the tests with the FE model in terms of the crack pattern. According to the original investigations, the tested specimens experienced two different failure modes: A combination of flexural and punching failure for samples with the ratio of reinforcement 1.8% and 0.6%, and failure of punching shear for samples with the ratio of reinforcement 1.8% and 0.6%. As evidenced by **Figure(2.18)**, the FE model was reasonably accurate in capturing both failure scenarios that occurred in the trials.

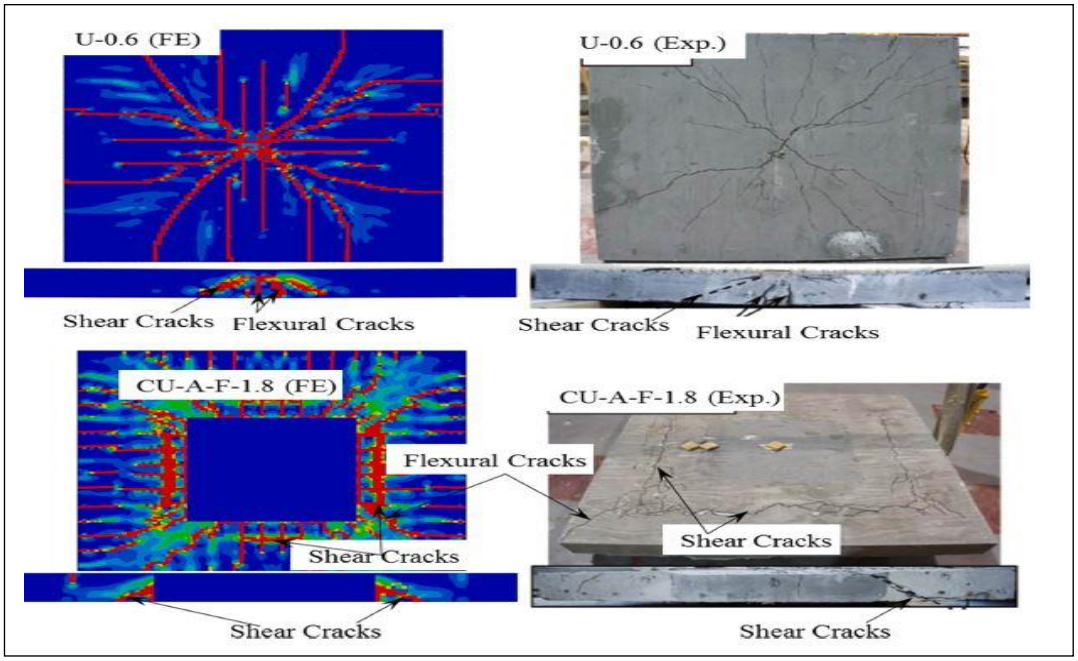

Fig.(2.15) Comparative analysis of computational and experimental fracture patterns originating from **Zohrev.et.al,2015[30]**. as part of a validation study[45]

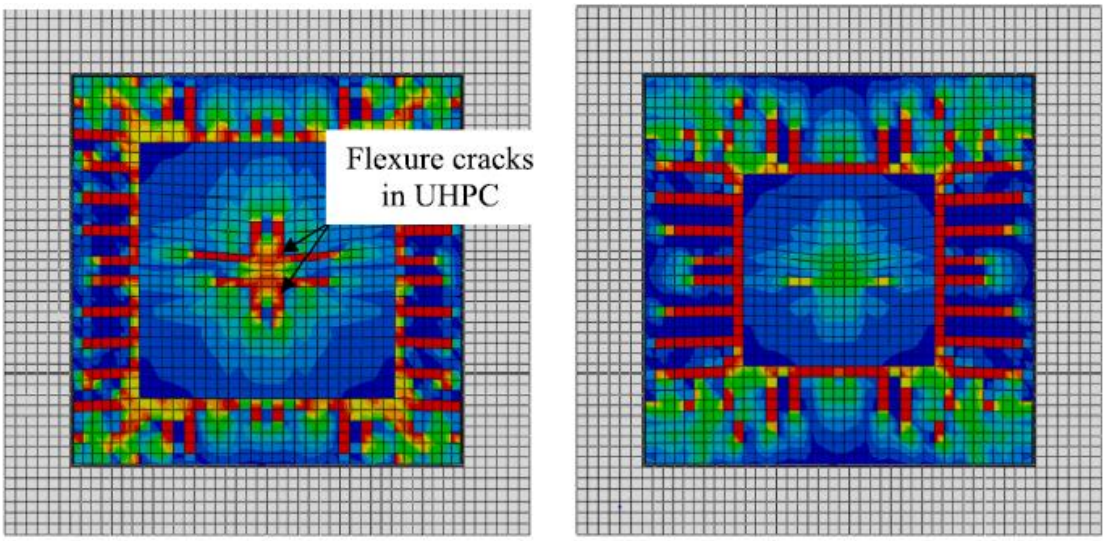

Fig.(2.16): Failure mode for slabs with different UHPC zone dimensions for 1.8% reinforcement ratio[45]

When applied in the parametric investigation, the (FE) modeling approach correctly predicted the reaction of (UHPC) slabs and (NC/UHPC) hybrid slabs in contrast to the empirical behavior, demonstrating its validity and dependability. The increased of ultimate load as the UHPC perimeter of the zone was increased from 0.325 to 3 times the thickness of slab from the face of the column. Due to the punching shear failure, the increase was, however, more noticeable when a UHPC perimeter of zone of more than 1.6 times the thickness of slab was utilized. Future design guidelines should take into account the apparent significant impact of the ratio of (f'_u /f'_c)on the behavior of the hybrid slabs. As the column diameters and hybrid thickness of slab grew, the ultimate loads followed suit. These two variables also alter the threshold among punching and failures of flexural, proving the effect of the size. Accordance with the findings, code models such as ACI 318-14, Eurocode 2, and Model Code 2010 are unable to predict the capacity of punched shear of reinforced UHPC slabs and hybrid NC/UHPC slabs with any degree of accuracy. It is suggested to alter the current ACI

equation to produce precise estimates for reinforced UHPC and hybrid slabs.

Minkwan Ju, et.al.,2021[46] suggested a novel strength of punching shear formula that may be used for concrete slabs reinforced with fiberglass-reinforced plastic or steel rods. The ratio of test to prediction and the chance of exceeding for overestimating strength of punched shear to the strength of design serve to validate the forecasting capacity. The proposed strength of punching shear formula's predicting ability is improved by this study new probabilistic method. This approach can limit the danger of overestimating punching shear strength, which is typically vulnerable to brittle failure, while yet ensuring more reliable validation. According to the ratio of test to forecast, the suggested strength of punching shear formula offers the most precise prediction and conservative characteristic. The proposed new formula has the lowest probability of exceeding between the formulas for calculating strength of punching shear that were chosen, according to the probabilistic method presented in this study. As a result, it is thought to be the most secure prediction formula in terms of the possibility that the predicted strength of punching shear will exceed the nominal strength of punching shear.

As a result, coming from the possible approach, it is demonstrated how the new formula being proposed can result in the more forecasts for punching shear that are precise, safer, and trustworthy strengths of concrete slabs strengthened with steel or FRP.

2.5 Two Way Shear Behavior Strengthened

Hadi Al-Maliki, et.al.,2021[47] got Flexural strength, ductility, and hardness are all improved as a result of strengthening using CFRP and GFRP in addition to punching shear resistance in both directions. In comparison to other expensive and challenging methods like increasing the cross-sectional area of columns, they are better suited for practical use. As a result, at the points where they contact with columns, they experience a shear failure, which causes a bigger portion of the structure to collapse. Shear failure happens for several reasons. The facility's functions altering, technical mistakes in the design and execution processes, a growth in the load, material deterioration ,and poor quality among other factors.

When there is a structural flaw, a composite section made of sheets and segments of carbon fiber reinforced polymer (CFRP) and glass fiber reinforced concrete polymer (GFRP) are two types of fiber-reinforced polymers. is utilized.

The two most popular methods for using CFRP strips or sheets to strengthen the area adjacent to the column involve screwing CFRP to the surface of the concrete surrounding the column on the slab's side of the tension. The alternative, however, entails mounting CFRP strips or sheets vertically using a variety of techniques to ensure an improvement in the resistance to shear.. In addition, numerous factors impact of the evolution of the capacity of the load, such as how the CFRP strips are placed in relation to the column support area and mooring points, as well as the area and number of CFRP sheets and strips, and the anchorage points.

According to ACI-318, the ability to endure punching shear stresses is not linked with the flexural steel reinforcement. While the CSA and Euro code 2 as well as other international codes and standards attest to

the fact that steel reinforcement for flexural aids in the growth of punched the resistance to shear.

2.6 Summary.

Previous studies dealt with the effect of adding fiber to concrete to increase the resistance to punching shear, as well as the use of other techniques. The result, when comparing the experimental results with the international code equations, gave a dispersed prediction of the resistance to punching shear. Therefore, they proposed modifying these formulas to be more accurate and capable of prediction.

In this research, study the effect of adding two types of fiber (straight, hook) and study the effect of column shape and different percentages of fiber on the punching shear of the slab used, in addition to proposing a new formula to predict the punching shear resistance of fiber-reinforced concrete to give more accurate results.

CHAPTER THRRE
EXPERIMENTAL WORK

CHAPTER THREE

EXPERIMENTAL WORK

3.1 Introduction

This chapter provides a comprehensive description of the experimental method used in this study to examine the behavior and punching shear strength of flat slabs. Cast and examined were fourteen samples of flat plate. Several variables were considered about the system efficacy. The design of the column and the tensile reinforcement were among these elements. In addition to the testing apparatus, additional information is provided regarding the samples, materials, and blending characteristics. The experiments were conducted in the Civil Engineering Department at the Babylon University of Babylon Structural Lab.

3.2 Description of Specimens

To examine the impact of punching shear for reinforced concrete slabs with different varieties of fibers, fourteen reinforced concrete flat slabs were manufactured. **(920x920x80)mm** is the measure of the slabs that were tested. All flat slabs in the tensile district were reinforced longitudinally and transversely with **10Ø8-mm** bars. The column is available in two configurations: a (**110x110)mm** square column and a **120mm** diameter circular column with the same equivalent area. The main reinforcement for both types of columns was 4Ø8mm , with a stirrup added around the main reinforcement every 90mm to avoid failure at the edges of the column. The geometric slab of the test sample is depicted in **Figure 3.1**, and its design are detailed in **Appendix A**.

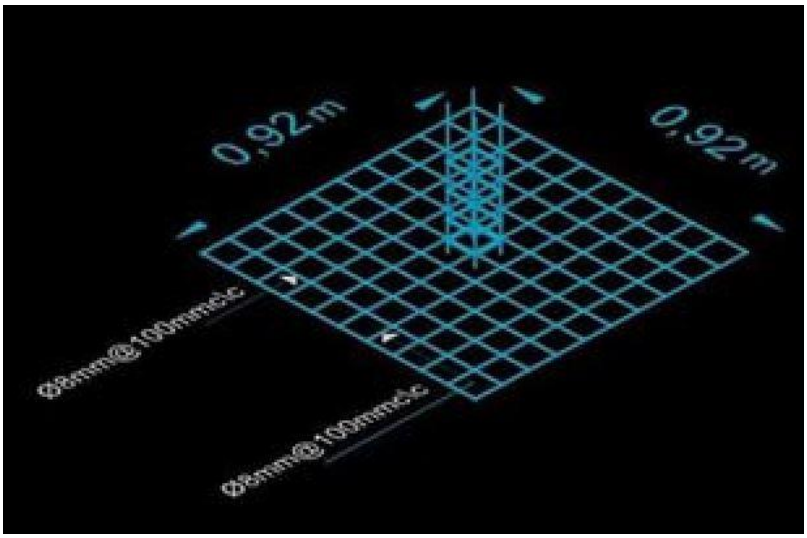

a

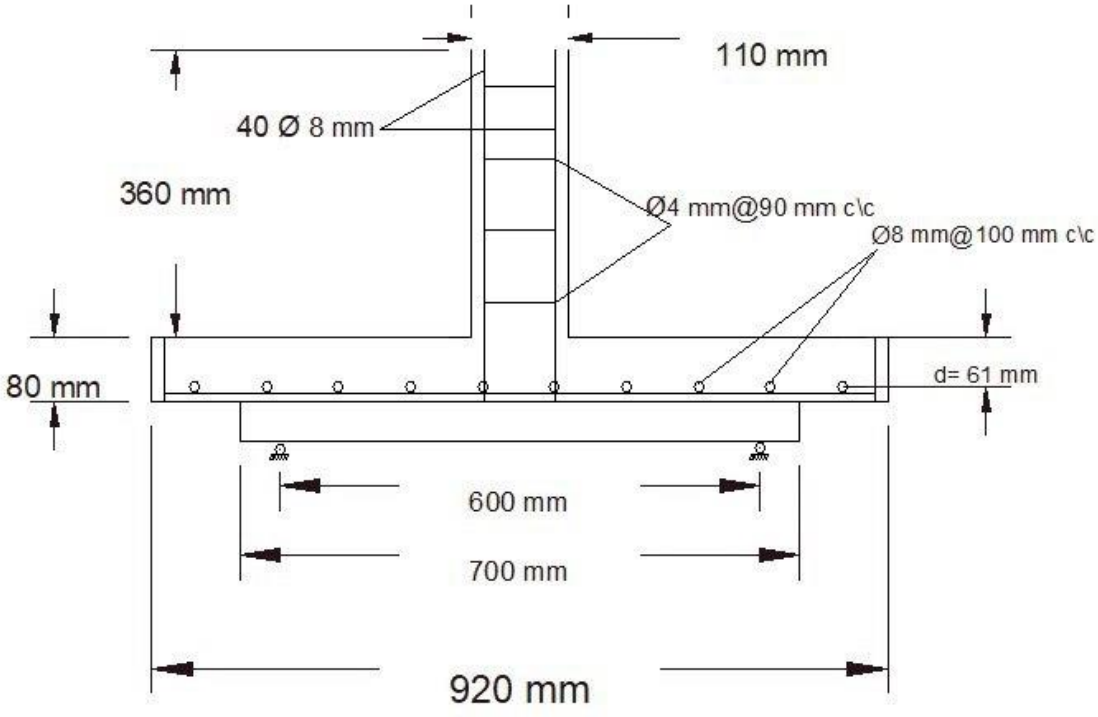

b

Figure (3.1): Details of specimens Cross-section a- reinforcement three dimension view and b- Section in slab.

3.3 Identification of Samples

To prevent column failure at its ends, ties rods measuring 4 mm by 90 mm were added to the tested column. **Table 3.1** depicts the determination system of sample. **Figure 3.2** consists of the first part, which represents the column's shape, the second part which represents the fiber shape, and the third part represents the fiber percentage.

- **N**: Described by non-fibrous control slab.
- **C**: Described by slab with circular column.
- **S**: Refer to slab with square column .
- **M**: Refer to straight fiber.
- **H**: Refer to hook fiber.

Table (3.1): Details of tested slabs with column.

Specimen identification	Description
CN	Concrete slab with circular column reinforced non-fibrous
SN	Concrete slab with square column reinforced non-fibrous.
$CM_{0.5}$	Concrete slab with circular column fibrous with straight steel fiber 0.5%
$SM_{0.5}$	Concrete slab with square column fibrous with straight steel fiber 0.5%
$CH_{0.5}$	Concrete slab with circular column fibrous with hook steel fiber 0.5%
$SH_{0.5}$	Concrete slab with square column fibrous with hook steel fiber 0.5%
$CM_{1.0}$	Concrete slab with circular column fibrous with straight steel fiber 1.0%
$SM_{1.0}$	Concrete slab with square column fibrous with straight steel fiber 1.0%
$CH_{1.0}$	Concrete slab with circular column fibrous with hook steel fiber 1.0%
$SH_{1.0}$	Concrete slab with square column fibrous with hook steel fiber 1.0%
$CS_{1.5}$	Concrete slab with circular column fibrous with straight steel fiber 1.5%
$SM_{1.5}$	Concrete slab with square column fibrous with straight steel fiber 1.5%
$CH_{1.5}$	Concrete slab with circular column fibrous with hook steel fiber 1.5%
$SH_{1.5}$	Concrete slab with square column fibrous with hook steel fiber 1.5%

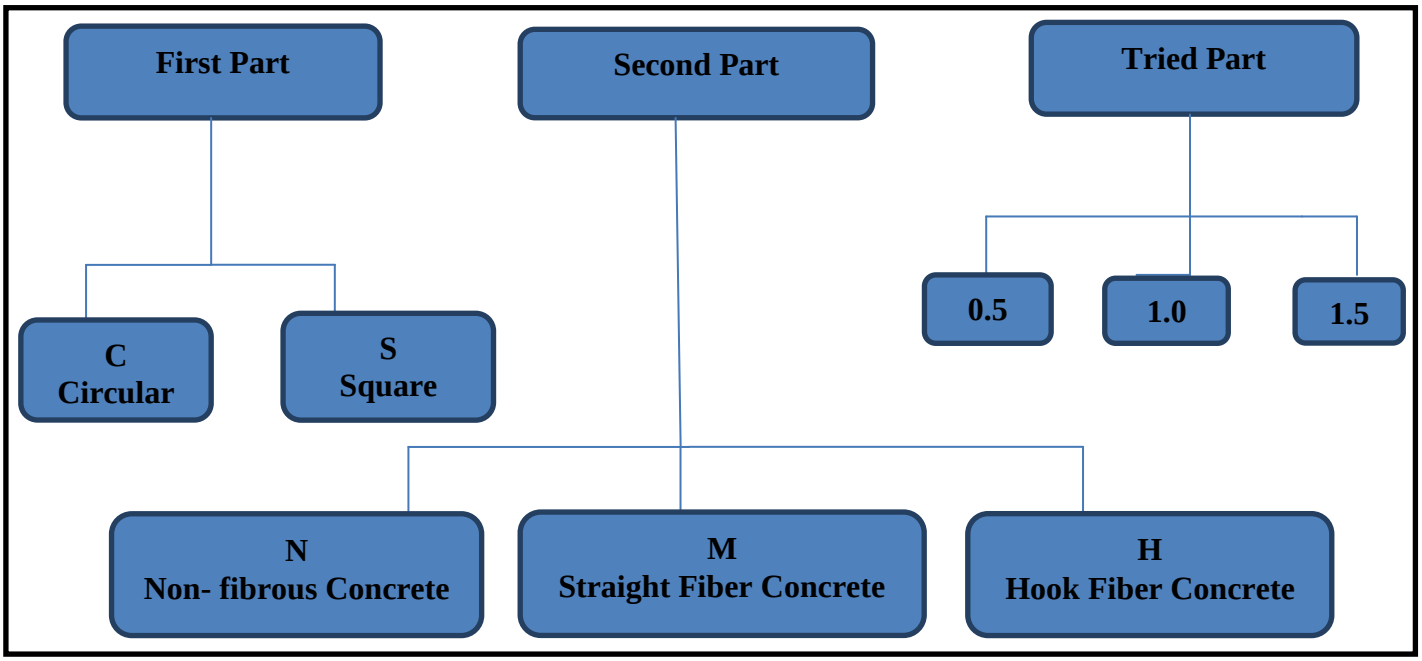

Figure (3.2): The determination system of the sample.

3.4 Materials

To ascertain the material qualities (IQS), standardized evaluations were conducted according to the Iraq Specification and ASTM stands for the American Society for Testing and Materials.

3.4.1 cement

At the construction facility of the engineering faculty at University of Babylon, the test was conducted. All research samples were fabricated with Type V cement, which is resistant to sulfate. **Appendix B** and **Tables B.1** and **B.2** detail the cement's chemical analysis and physical characteristics, respectively which agree with the requirements of Iraqi Specification No. 5/1984 **[36].**

3.4.2 Fine-aggregate

Regarding this investigation, standard grit was used to mix concrete. After being repeatedly cleansed and washed with water, the sand was spread out and permitted to dry in the air prior to use. The outcomes attained are depicted in **Table B.3** of **Appendix B**'s estimation results. Iraqi Specification No.45/1984**[49]** was met in terms of overall precision. In **Table B.4**, the specific gravity, sulfate concentration, and sediment absorption are detailed. This test was conducted in the structure's facility of the University of Babylon department of Civil Engineering.

3.4.3 Coarse Aggregate

This investigation utilized a greatest quantity of crushed gravel (14 mm) available. Before the gravel was used, it was washed and cleansed multiple times with water, stretched out, and left to dry in the open air. The categories of coarse aggregates are listed in **Table B.5** of **Appendix B**. The obtained results demonstrated that the crude classes met IQS No.

45/1984[50] specifications. The coarse aggregate absorption, sulfate concentration, and specific gravity are shown in **Table B.6** of **Appendix B**.

3.4.4 Water of Mixing

Regarding this experiment, the use of potable water casting and treatment the samples.

3.4.5 Steel Reinforcing Bars

All concrete sections are reinforced with the same size deformed steel reinforcing rods. For the longitudinal and transverse reinforcement of the tensile zone, (Ø8) mm bars were utilized. As closed stirrups, bars of dimension Ø4mm are also used for shaft sections (round and square). Materials Laboratory Tensile Test Approved ASTM A615-86 [51], based on the University of Babylon Faculty of Engineering

Table (3.2): A description of the qualities of steel reinforcing**.**

Bar Size	Existing diameter (mm)	Stress of Yield (MPa)	Ultimate strength (MPa)
8	7.64	468	582
4	4.25	513	608

3.4.6 Super-Plasticizers

The super plasticizers utilized in this investigation appear to have been a commercially available third-generation superplasticizer to make mortar and concrete referred to as PC200 Hyperplastic. This is composed of polycarboxylic Long-chained polymers, is free of chlorides and meets ASTM C494/2001 [52], which is an industry standard intended to get the concrete's moisture content function more efficiently. This differentiates it from conventional super plasticizer." **plate 3.1** depicts the Hyperplast PC200 utilized in the study.

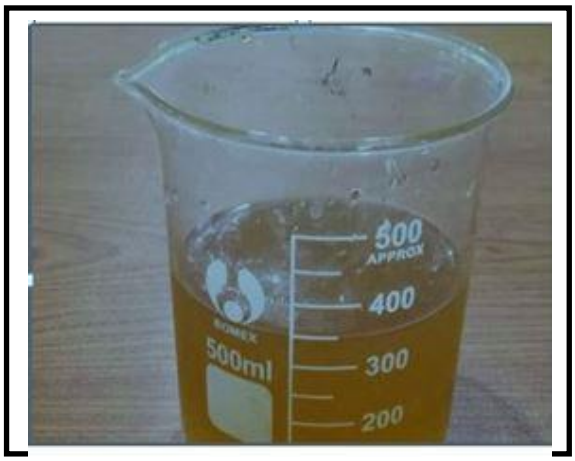

Plate (3.1): Super-Plasticizers

3.2.7 Steel Fiber

As shown in **Plate (3.2)** steel fiber was utilized in this experiment to reinforce slabs. The microfibers have a density of approximately 7800 kg/m3 as described in **Table (3.3).**

Plate (3.2): Types of steel fiber

Table (3.3): Micro and hook fibers of steel Characteristics.

Product	Lengths, L (mm)	Diameters, D (mm)	Aspect proportion, L/D	Tensile strengths (MPa)
Micro steel fiber (WSF0213)	13	0.2	65	2200
Hooked fiber (KF 65/35)	35	0.55	64	900 ~ 2,200

3.5 Concrete Mix Design

Numerous experimental compositions' ability to attain the requisite compressive strengths was evaluated ACI 211.1-95 **[53]**. The quantity of cement was (500 kg/m3), and the ratio of water to cement was (0.38), where the sag was (8 cm). After 28 days of treatment, the weight blending ratios for typical concrete slabs with 40MPa for compressive strength of (1:1.55:1.65) were established.

Table (3.4): concrete mixture's Details.

Material	Quantity
Cements (kg/m^3)	**500**
Sand (kg/m^3)	**775**
Gravel (kg/m^3)	**825**
Water (kg/m^3)	**190**
Super plasticizer (1.0/100 kg cement)	**5**
Fibre amount (%) by volume	**0.5**
Fibre amount (%) by volume	**1.0**
Fibre amount (%) by volume	**1.5**

3.6 Mixing and Casting Procedure Spacemen.

Fourteen wooden blocks with dimensions of **(920 x 920 x 80) mm** and eighteen cubes for compressive strength testing (three of them are regular concrete and the other is fiber-reinforced with dimensions of **(150 x 150 x 150) mm** and cylinders with **(100 x 200) mm** dimensions and prism with dimensions **(100x100x400)mm**, respectively, as well as the direct tensile test samples shown in the figure, used to evaluate the cleavage strength, bending strength, and strength of direct tensile and the concrete mixing steps as follows:-

1- All of the dry materials, beginning with the heaviest gravel ,sand ,and cement, have been weighed, and the contents of the mixer have been thoroughly mixed.

2- The super plasticizer is incorporated into water, after that the mixed during the mixing process, liquid is introduced to the powdery mixture. The process of mixing is then resumed for four minutes.

3- Lastly, small amounts of steel filament are introduced while the mixing device continues to spin for three minutes.

The steps of casting specimens are shown in **Plate (3.3).**

Preparation

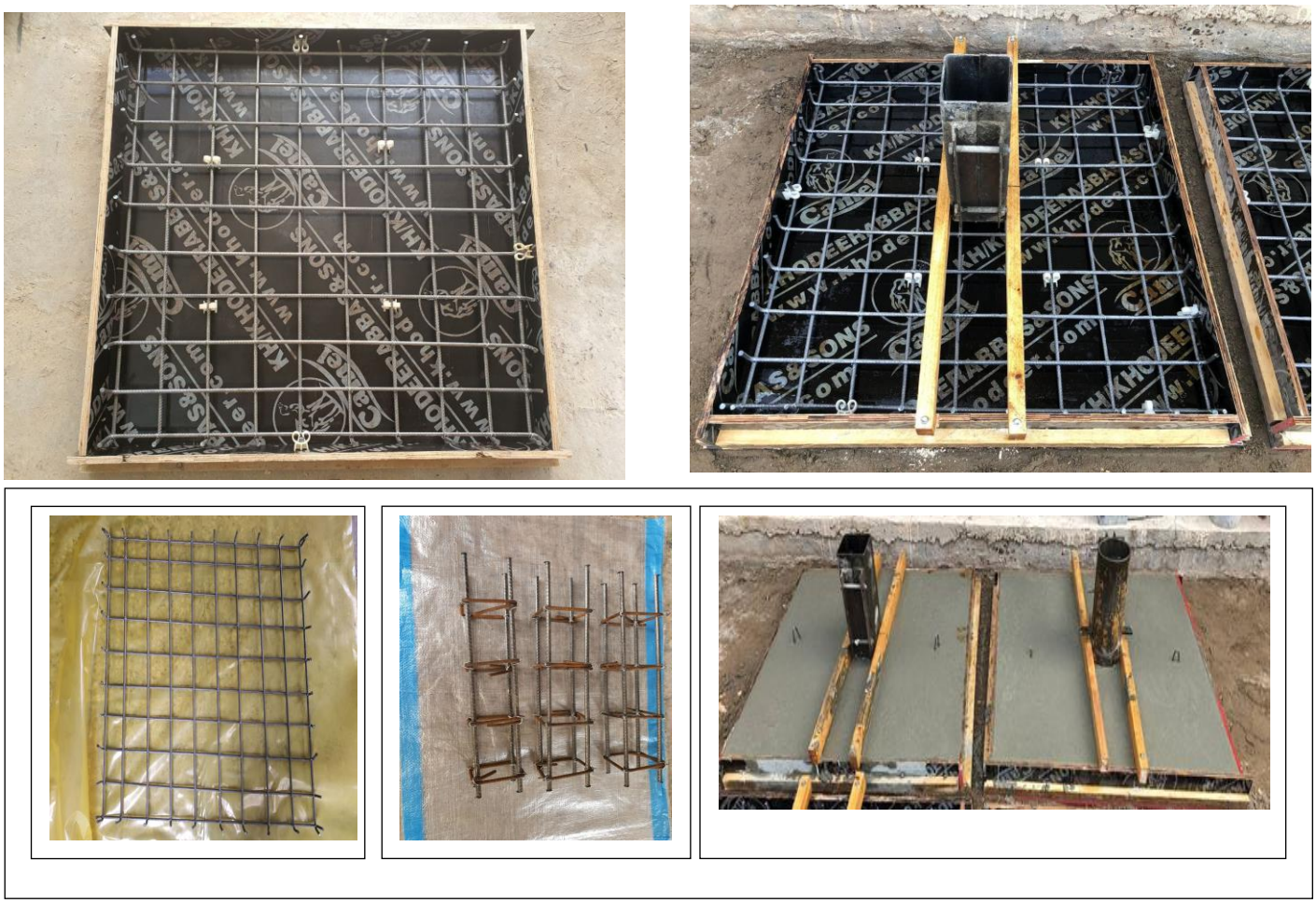

Plate (3.3): Casting specimens steps.

Using the table of flow test per ASTM C1437-01 [54], the workability of all classes of FRC mixtures is evaluated. For all mixtures, the table of flow dispersion was the value (105 ± 5 %). This test was conducted immediately subsequent to the combining procedure has been completed by the table of dropping containing the FRC mixture 25 times in fifteen seconds in the **plate (3.4).** The flow is expressed as a percentage of the inside base diameter of the original test cone.

$$\textbf{Flow}=\frac{Dave-Do}{Do}\textbf{x100\%.....(3.1)}$$

Where:

$\mathbf{D_{avg}}$:Average Diameter of the concrete spread (mm)measured in 4 directions.

D_o: Inside base of original, Diameter of the cone test (mm).

Slump flow testing is widely used for non- fibrous nowadays. This analysis yields helpful data on the concrete and uniformity of the concrete **[55],[56],**and**[57].** Slump flow testing was utilized to evaluate self-consolidating concrete due to smoothness. This strategy is extensively employed in labs and on construction sites to assess the cohesiveness of concrete. Concrete's workability and consistency can be gauged by averaging the diameters of two cones placed at right angles to one another after the material has flowed out of the slump cone. The concrete results are displayed in **Table (3.5)**, confirming the predictions made by the literature **[58]**and**[59].** Using both types of steel fibers (micro and hook) in varying percentages (0.5 , 1.0, and 1.5%) raised the diameter while decreasing it by (6.04%, 10.77%, 16.45%) and (4.85%, 11.83%, 18.11%) respectively

(compared to the mixture without fiber, with a time of (5.8, 6.1, 6.8) sec and (5.7, 6.2, 7.2) sec, respectively).

Plate (3.4) Slump Flow Test

Table (3.5) Slump flow test.

Index of Mixes	Slump flow Test	
	D(mm)	Final (sec)
N	845	5.6
M $_{0.5\%}$	794	5.8
M $_{1.0\%}$	754	6.1
M $_{1.5\%}$	706	6.8
H $_{0.5\%}$	804	5.7
H $_{1.0\%}$	745	6.2
H $_{1.5\%}$	692	7.2

Depending on The European Guidelines for Concrete Specification, Production and Use ,Slump-Flow (760 to 850)mm. The mix classified in Slump- Flow in class SF3 **[60].**

3.7 Casting and Curing Procedure

To prevent cement concrete from adhering to the molds, all templates were cleansed, and their inner surfaces were lubricated with engine oil.

Before pouring concrete into the template, then reinforcement was positioned in the base mold. The mold was filled with concrete in two equal layers. In addition, The surface of the concrete was leveled well with a steel trowel, and the surface of the slab was covered with polyethylene sheets to avoid loss of moisture. After pouring it for 48 hours, it was extracted from the wooden mold and placed in water basins for treatment. It was extracted after completing the curing period for 28 days.

3.8 Characteristics of Mechanical Hardened Concrete

3.8.1 Test of Compressive Strength

The compressible strength of cube (f_{cu}) was evaluated in accordance BS (1881–116**[61]**. The compression resistance of FRC mixtures was established by performing compressive strength experiments on standard 150-mm cube samples using a compression machine with a capacity of 2000kN, **plate (3.5)** and **Table (3.6)** state the tested results . An average of three examples was utilized to calculate the compressive strength.

Table(3.6): The outcome of testing on concrete cubes**.**

Cubes (150x150x150)mm	Compression strength (f_{cu}) (MPa)
N	49.5
$M_{0.5\%}$	50.2
$M_{1\%}$	55.2
$M_{1.5\%}$	59.8
$H_{0.5\%}$	53.1
$H_{1\%}$	59.4
$H_{1.5\%}$	60.1

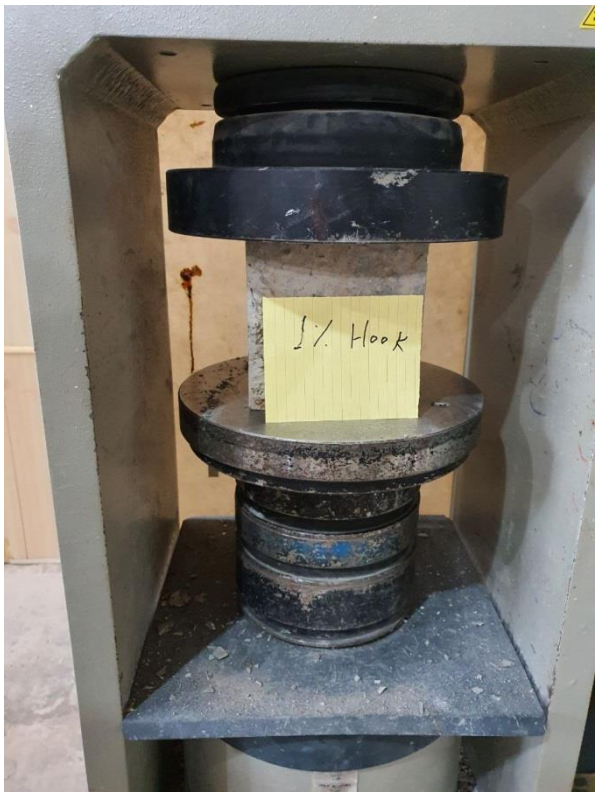

Plate (3.5): Test of compression for Cubes

3.8.2 Splitting Tensile Strength

According to ASTM C496-2004[62], an average of two cylindrical concrete specimens (100 x 200 mm) have been subjected to a tearing tensile force. **Plate 3.6**, and **Table 3.7,** show the testing data for the strength of tensile splitting.

Table(3.7): The result of tensile strength test.

Cylinder (100* 200)mm	Splitting tensile (f_t) (MPa)
N	3.6
$M_{0.5\%}$	5.5
$M_{1\%}$	6.1
$M_{1.5\%}$	8.0
$H_{0.5\%}$	5.2
$H_{1\%}$	5.9
$H_{1.5\%}$	7.0

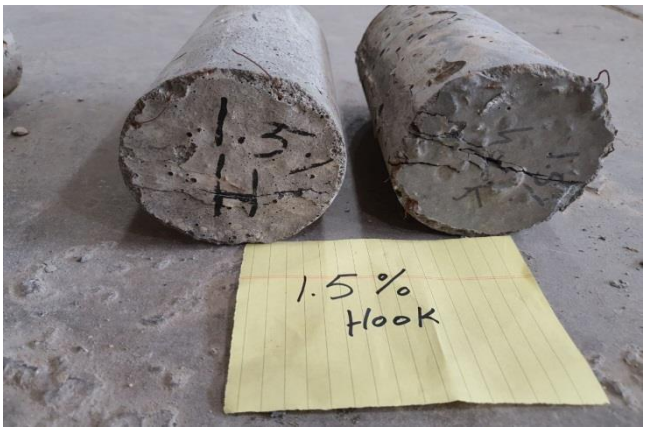

Plate (3.6): The test of splitting tensile strength.

3.8.3 Direct tensile Strength test

Based on ASTM D2936-08[63], an average of two concrete specimens with dimension shown in **Figure (3.3)** were subjected to device of tensile strength test. **Plate (3.7)**, and **Table (3.8)** show the testing data for the direct tensile strength of samples.

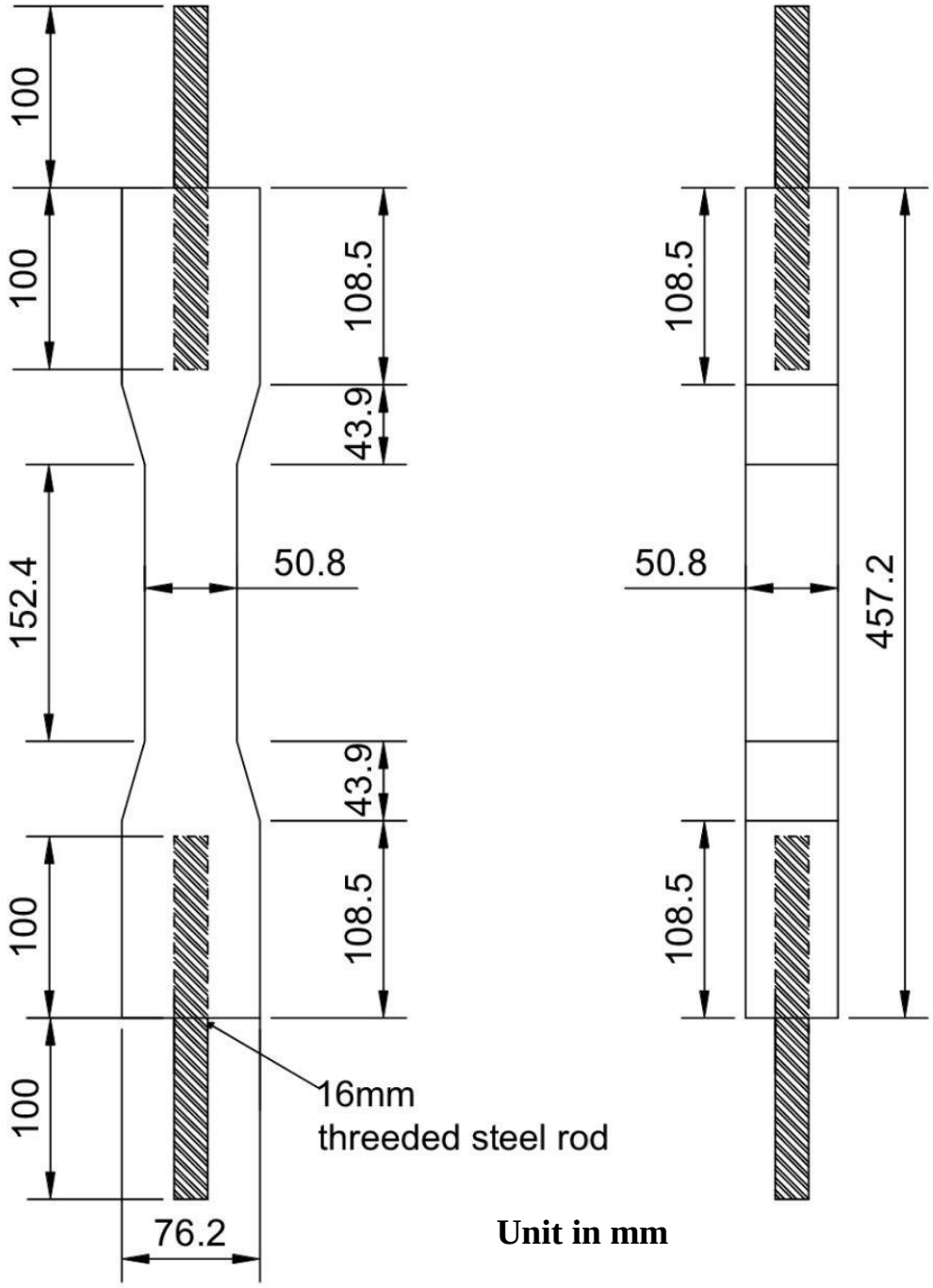

Figure (3.3) Dimension of the direct tensile test sample

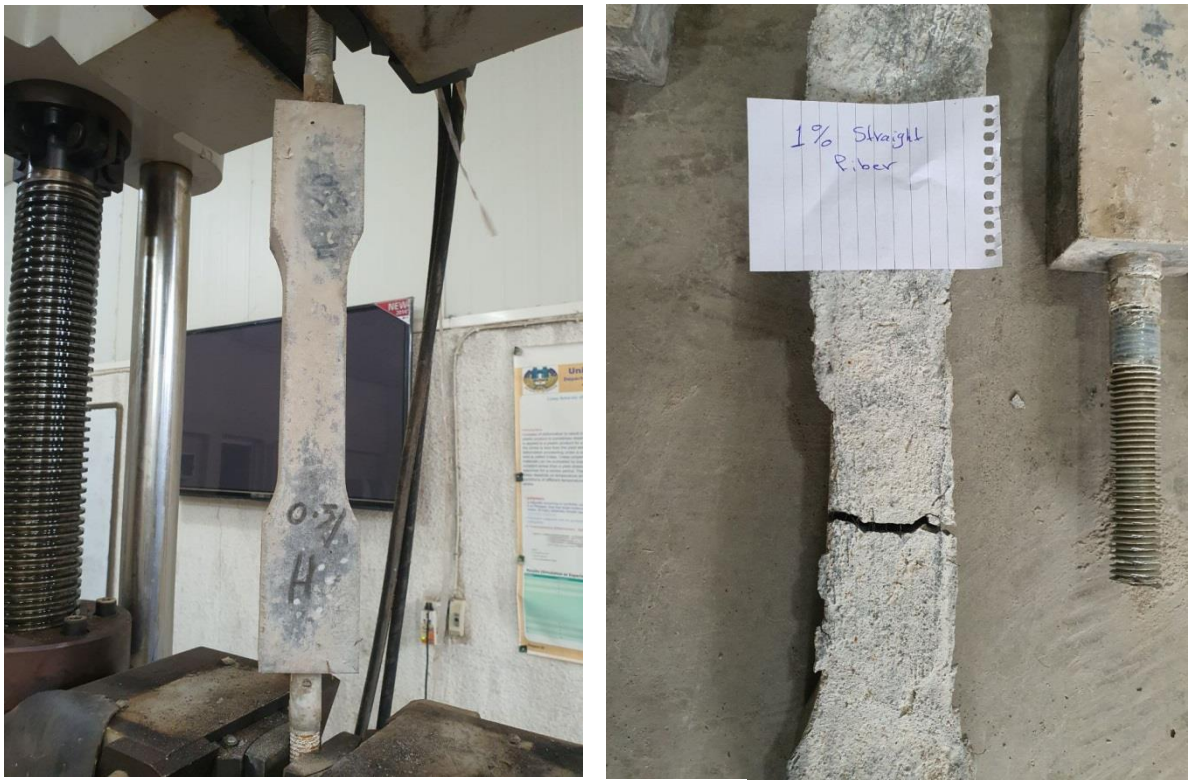

Plate (3.7) Direct tensile test

Table (3.8): The result of direct tensile strength test.

Samples	Direct tensile (f'_t) (MPa)
N	2.4
$M_{0.5\%}$	3.7
$M_{1\%}$	4.5
$M_{1.5\%}$	6.3
$H_{0.5\%}$	3.5
$H_{1\%}$	4.2
$H_{1.5\%}$	6.0

3.8.4 Modulus of rupture

On FRC specimens, modulus of rupture f_r experiments were conducted in accordance with ASTM C293-02[64]. The rupture modulus was tested utilizing an equipment with a testing capacity of 2,000kN. Using the center-point loading shown in **plates (3.8)** and **Table (3.9)**, (100x100x400) mm prisms were tested, and the average of two specimens' test results was used for each test.

Plate (3.8) flexural test of prism

Table (3.9): The result of the Modulus of rupture test.

Samples	Modulus of rupture f_r (MPa)	ACI code $f_r = 0.62\sqrt{f_{cu}}$	% Decrease Of f_r (MPa)
N	5.2	4.36	16.15
$M_{0.5\%}$	7.5	4.39	41.47
$M_{1\%}$	8.4	4.61	45.12
$M_{1.5\%}$	9.7	4.79	50.62
$H_{0.5\%}$	5.8	4.52	22.07
$H_{1\%}$	6.7	4.78	28.66
$H_{1.5\%}$	8.1	4.81	40.62

3.9 Measuring Instruments

3.9.1 Load Measurement

All slabs have been tested by employing hydraulic testing equipment with a maximum range capacity of (480kN) as depicted in **plate (3.9).**

Plate (3.9): Universal Testing Machine

3.9.2 Deflection Measurement

At each load stage, the vertical deflection of specimens was measured at the slab's center using a dial gauge with a precision of 0.01 mm. The gauge is positioned beneath the lower face of the stone being tested.

3.9.3 Column Penetration Measurement

At each loading stage, the penetration of the samples was measured at the center of the slab using a contact gauge with an accuracy of 0.01 mm. The gauge is placed in the area of contact between the column and the slab being tested.

3.10 Test Procedure

At the age of 28 days, all slab samples were removed from processing. To illustrate fracture propagation, slab specimens are cleaned and sprayed white before the test day, and each slab specimen is marked. In addition, load locations have been identified. The locations of gauges, were the first on the surface of the slab. The second is in the contact area between the column and the slab, and the specimen slabs have been loaded onto the machine. As depicted in **plates (3.10)** and **(3.11)**, steel frames measuring 700mm x700mm (length x width) were placed over the load locations to prevent tension concentration on the top surface of the slabs at loading as shown in **Figure (3.4).**

All slabs were loaded to failure in a concentrated load test on the center of the column. The failure occurred when the slab collapsed suddenly at the same time that the dial gauge in the area where the column contacts the slab stopped reading. The ultimate load has been recorded. The main objective was to evaluate the ultimate load of the slabs, to know the type of failure for each sample, and

to compare the non-fibrous samples with the reinforced samples using fibers.

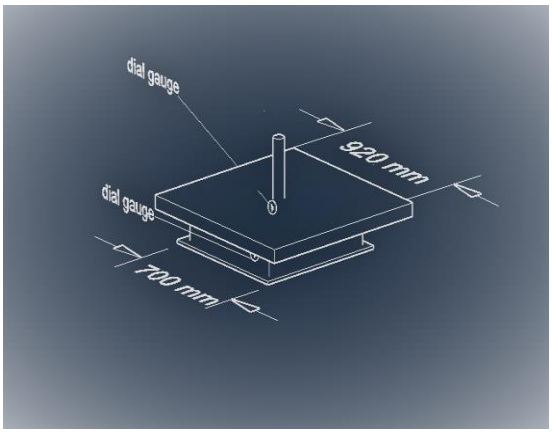

a

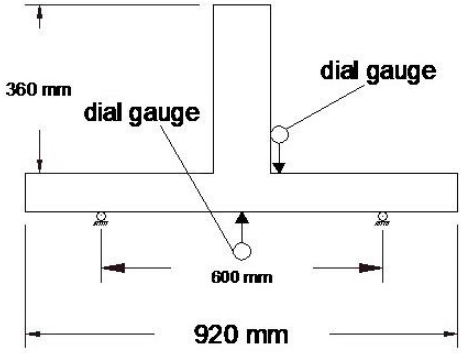

b

Figure (3.4) : Details of slab with frame a- Slab with frame three dimension view. b- The dial gauge position.

plate (3.10) Slab under Testing

A:Upper dial gauge B:Lower dial gauge

Plate (3.11) position of dial gauges

CHAPTER FOUR

RESULT AND DISCUTION

CHAPTER FOUR

RESULT AND DISCUTION

4.1 Introduction

This study details the outcomes of the empirical plan run through the course of this study. The experimental program included the testing of fourteen slabs with square and circular columns, twelve of which were reinforced with steel fibers (straight and hook) and other of which was non-fibrous sample.

4.2 Result of the test

4.2.1 Mechanical Properties for Non- Fibrous Concrete

To ascertain the concrete's mechanical properties, control samples were blended and poured. Three 150*150*150 mm cubes were examined of each mix in accordance with BS 1881[65], three 100x100x400 mm prisms were examined in accordance with ASTM C293-02[64], and three 100 x 200 mm cylinders were examined for compressive strength, flexural modulus, and tensile test, respectively. In addition to three direct tensile test samples. The findings are outlined in **Table (4.1),** which illustrates the average value obtained from the samples of non-fibrous concrete.

Table 4.1 Mechanical properties of Non- Fibrous Concrete

Strength of compression (f_{cu})(MPa)	Splitting tensile (f_t) (MPa)	rupture Modulus f_r (MPa)	Direct tensile (f'_t) (MPa)
49.5	3.6	5.2	2.4

4.2.2 Mechanical Properties for fibrous Concrete Mixes

In the beginning, cubes, cylinders, prisms, and direct tensile samples were examined to determine the strength of compression, tensile, flexural, and direct tensile, respectively, of six concrete formulations for each model in the three groups. This provided an initial sign of the evolution of the concrete's resistance to tensile, compression, flexion, and direct tension resulting from the addition of steel-fibers, flexure of whether the fibers used were straight or hooked. The outcomes are shown in **Table (4.2)**.

Table 4.2 Mechanical features of fibrous concrete at the age of 28 days for 7 mixes.

Mix symbol	Vol. fraction of fibers V.f (%)	Compressive Strength Mpa	Percentage increase w.r.t. Nc %	Tensile strength Mpa	Percentage increase w.r.t. Nc %	Direct tensile strength Mpa	Percentage increase w.r.t. Nc %	Flexural strength Mpa	Percentage increase w.r.t. Nc %
0.5M	0.5	50.2	1.41	5.5	52.78	3.7	54.17	7.5	44.23
1.0M	1	55.2	11.52	6.1	69.44	4.5	87.5	8.4	61.54
1.5M	1.5	59.8	20.81	8.0	122.22	6.3	162.5	9.7	86.54
0.5H	0.5	53.1	7.27	5.2	44.44	3.5	45.83	5.8	11.54
1.0H	1	59.4	20.00	5.9	62.88	4.2	75.00	6.7	28.85
1.5H	1.5	60.1	21.41	7.0	94.44	6.0	150.00	8.1	55.77

4.2.3 Impact on the compressive strength by the fiber parameters

Figure 4.1 shows the average compressive strength of three cubic samples for all groups of fiber ratios (0.5%, 1%, and 1.5%) after twenty-eight days. Increasing the percentage of fibers helps to enhance the strength of compression for concrete. The use of straight steel fibers increases the strength when compressing the cube progressively by 1.41%, 11.52%, and 20.81% of the fiber content.

It was discovered that using hook fibers produces better results in developing compressive strength in SFRC compared to using straight steel fibers, which increased by 7.27%,20%, and 21.41% for the same

percentages of fibers used in both types (0.5%, 1%, 1.5%)because the hook fibers are longer than the straight fiber (this increases the compressive strength at a slower rate). Based on the steel fibers and mixture bonding strength, the maximum strength of compression of the concrete increased. Thus, crack growth stops. The steel fibers can cross the micro-cracks developing at the gravel-mortar interface, which increases the concrete's tensile strength. The failure was gradual in the fiber-reinforced samples, while it was sudden in the conventional concrete samples. **Plate 4.1** shows the samples after failure.

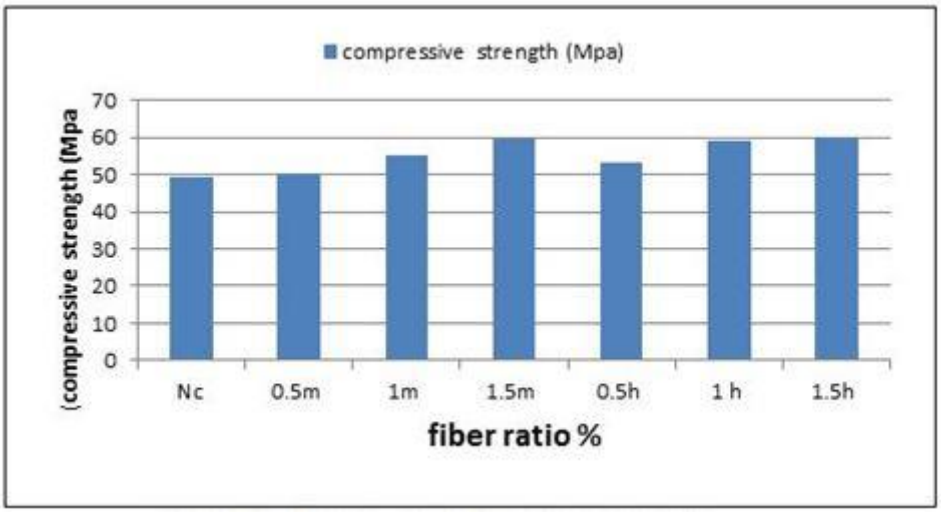

Figure 4.1 Average compressive strength of the three cube specimens

Plate 4.1 Cubes after failure

4.2.4 Impact on the tensile strength by the fiber parameters.

Figure 4.2 depicts the impact of steel fiber type on the tensile fracture strengths of SFRC. Upon examination, the failure of the fiber-reinforced samples was gradual, whereas the failure of the non-fibrous

concrete samples was sudden. Due to the bond strength among fiber and concrete components, SFRC is less likely to fracture than conventional concrete. In comparison to the control sample of concrete, the strength of tensile of reinforced concrete with micro-straight fiber is better because it gives a good distribution in the mix. When using two different types of fibers (straight and hook), the increases are approximately (52.78%, 69.44%, and 122.22%) and (44,44%, 62.82%,and 94.44%), respectively, for the same steel fibers percentages (0.5%,1.0%, and 1.5%). This is due to the frictional bond between the fibers and the mixture, as the steel yield is drawn rather than split under tensile stress. One of the possible explanations for the apparent superiority of microfibers over hook steel fibers is their greater tensile strength and thus the improved reinforcing effect of steel fibers on concrete and SFRC strength**. Plate 4.2** shows the samples after failure.

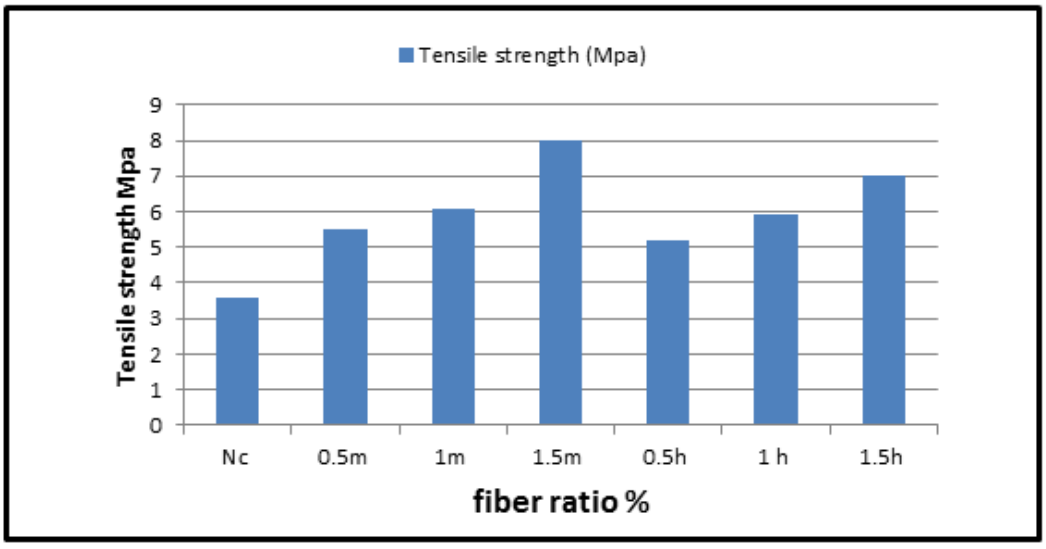

Figure 4.2 splitting tensile strength of the three cylinder

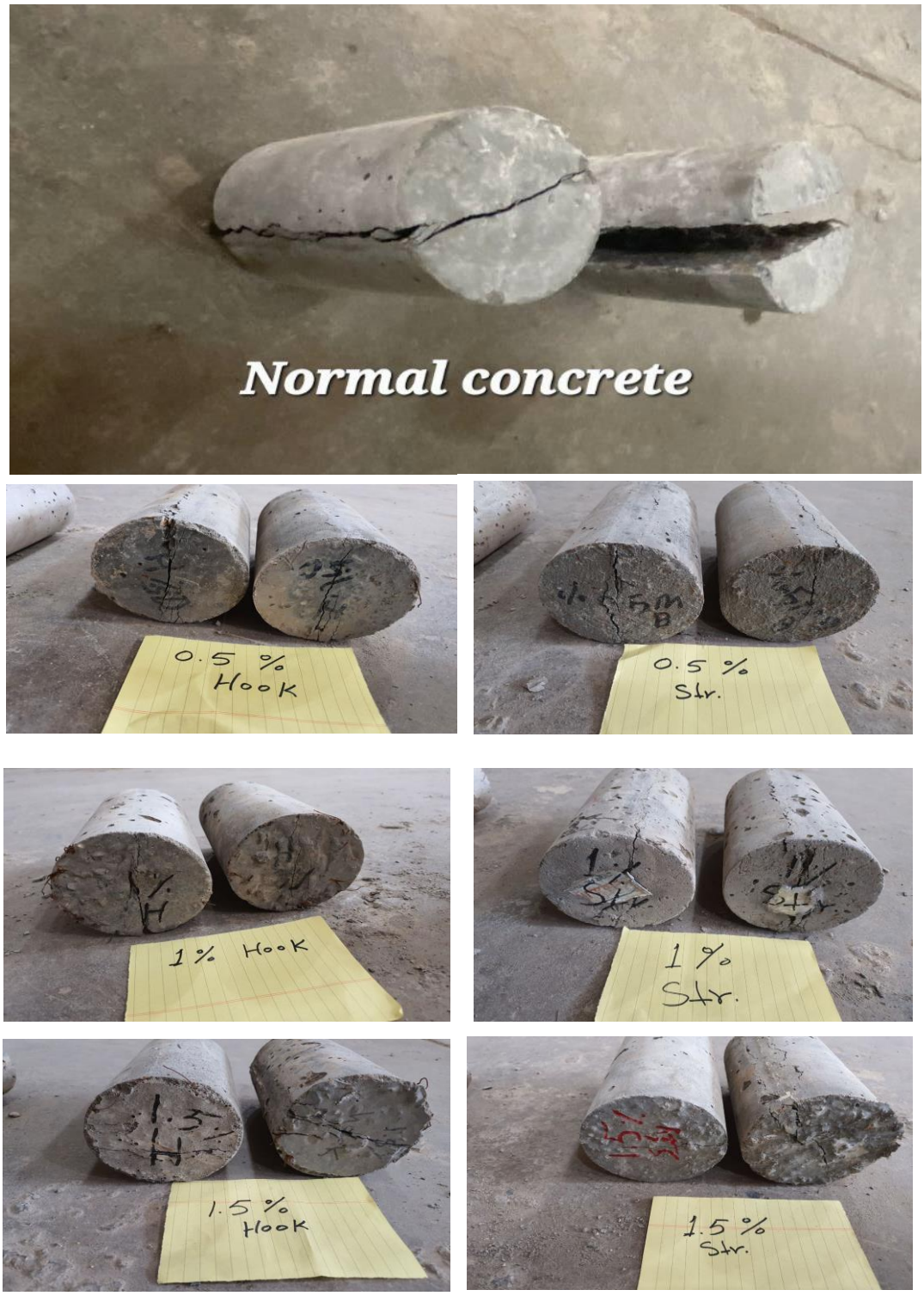

Plate 4.2 Cylinder after failure

4.2.5 The influence of fibers on direct strength of tensile

The direct strength of tensile test is indicative of how concrete may behave in a real-world environment, such as a bridge. However, indirect testing methods may not always be able to determine concrete's tensile strength precisely. **Figure 4.3** demonstrates that, depending on the type of steel fibers used, the strength of direct tensile of steel-fiber reinforced concrete (SFRC) can range from extremely low to extremely high. Non-fibrous concrete was reinforced with steel fiber to increase its tensile strength along a straight line. Microfibers increase the direct tensile strength of a control concrete sample by 54.17, 87.5%, and 162.5%, whereas hook fibers increase the strength by 45.83, 75%, and 150.0%. Non-fibrous concrete samples failed abruptly, whereas fiber-reinforced concrete samples failed gradually upon examination. **Plate 4.3** shows the samples after failure.

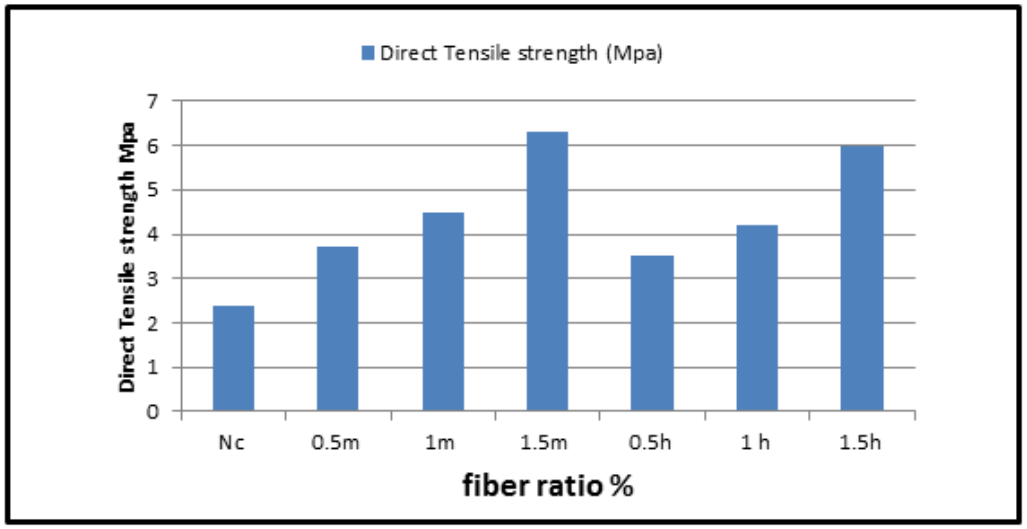

Figure 4.3 Direct tensile strength of the three specimens

Plate 4.3 Samples after failure

4.2.6 Impact on the flexural strength by the fiber parameters

Increasing fiber length decreases the likelihood that steel fibers will disseminate through the concrete. When the length of the steel fibers increases, the overall amount of steel fibers added to the mixture may decrease, as well as the randomness of fiber distribution in that region of the sample. Compared to the control sample, the flexural strength of fine steel fibers increased by (44.23%, 61.54%, 86.54%) and the flexural strength of hook steel fibers increased by (11.54%, 28.85%, 55.77%). **Plate 4.4** shows the samples after failure. The flexural strength of concrete can be increased by loading the fibers before matrix fracture and the loss of matrix-fiber interfacial contact. Using straight and hook-type steel fibers, prism testing was conducted. As shown in **Figure 4.4**, steel has a much higher tensile strength than concrete, so it is conceivable that the steel fibers were able to be driven out during the prism's breakage without causing the concrete to fracture. When the percentage of steel fibers in concrete is increased, the material tends to become more resilient and flexible. **Plate 4.5** illustrates the effect of steel fiber type on SFRC bending strength. When the test prism reinforced with steel fibers was subjected to a bending force, it did not completely separate into two parts

because the steel fiber was pulled out without breaking. This may be because of the high steel fiber's tensile strength, which is inherently greater than the weak the concrete's tensile strength, whose behavior differs from that of the prism without reinforcement.

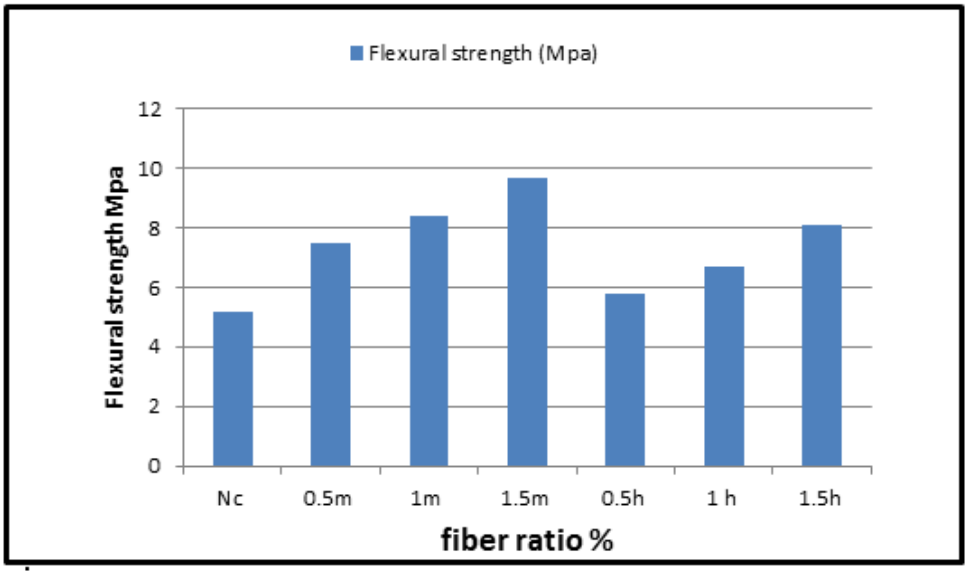

Figure 4.4 The impacts of steel fibers type on flexural strength of SFRC

Plate 4.4 Samples after failure

Plate (4.5): Fiber pullout in concrete

4.3 Results of examined for slabs

All the examined slabs showed elastic behavior under the applied load and at low load levels, and the mid- span deflection was small and proportional to the applied load. When the load rises, the first crack appears on the tensile face of the slab around the sides of the column, and additional cracks form in the middle area of the slab. These cracks grow larger and multiply as the load increases. In the event of final stress, shear perforation failure occurs differently for each type of slab used.

Table (4.3) Test Results of Slabs Samples

Designation of Slab	Ultimate Load (Pu)(KN)	Max lower Deflection (mm)	Max column Penetration (mm)	Mode of Failure
CN	144.14	7.25	1.01	Punching sudden
SN	144.5	6.3	0.6	Punching sudden
$CM_{0.5\%}$	147.84	6.49	1.1	punching somewhat gradual
$CM_{1.0\%}$	148.16	9.95	1.58	Punching & flexural
$CM_{1.5\%}$	193.6	9.82	1.4	Punching & flexural
$SM_{0.5\%}$	161.32	7.1	0.59	punching somewhat gradual
$SM_{1.0\%}$	179.52	8.74	0.74	Punching somewhat gradual & flexural
$SM_{1.5\%}$	191.04	12.8	2.16	Punching somewhat gradual & flexural
$CH_{0.5\%}$	151.2	6.87	1.0	punching somewhat gradual
$CH_{1.0\%}$	164.8	6.75	1.07	Punching gradually & flexural
$CH_{1.5\%}$	212.94	13.27	3.64	Punching gradual & flexural
$SH_{0.5\%}$	165.23	7.65	0.34	Punching gradual
$SH_{1.0\%}$	195.33	7.6	0.84	Punching gradual
$SH_{1.5\%}$	197.9	10	1.33	Punching gradually & flexural

4.4 Crack Pattern For Slabs

4.4.1 Non- fibrous concrete slab with a circular and square column with (CN) and (SN)

This sample consisted of a compacted concrete slab with a circular column of non-strengthening concrete. The slab has been subjected to monotonic and incremental load testing until failure. In this sample, shear fractures appeared around the column on the slab's tension face, as well as cracks around the column on the pressure face of the slab, and the column penetrated the slab, resulting in failure due to punching shear. whereas the failure zone pattern was circular around the column area from the tensile side. **Plate 4.6** and **Plate 4.7** depicts the shape of the failed sample

Plate 4.6: The sample of non- fibrous concrete slab with circular column (CN)

Plate 4.7: The sample of non- fibrous concrete slab with square column (SN)

4.4.2 Fibrous Concrete Slab with a Circular Column (CM0.5%),(CM1.0%) and (CM1.5%)

This sample consisted of a compacted concrete slab with a circular column of strengthening with the ratio of straight steel fiber 0.5% concrete. The slab has been subjected to monotonic and incremental load testing until failure. In this sample, shear fractures appeared around the column on the slab's tension face, as well as cracks around the column on the pressure face of the slab, and the column penetrated the slab, resulting in failure due to punching shear. Whereas, the failure zone pattern was circular around one-fourth of the column area from the tensile side. **Plate 4.8** and **Plate 4.9** and **Plate 4.10** depicts the shape of the failed sample.

Plate 4.8: The sample of fibrous concrete slab with circular column(CM0.5%)

Plate 4.9: The sample of fibrous concrete slab with circular column (CM1.0%)

Plate 4.10: The sample of fibrous concrete slab with circular column(CM1.5%)

4.4.3 Fibrous concrete slab with a circular column ($CH_{0.5\%}$),($CH_{1.0\%}$) and ($CH_{1.5\%}$)

This sample consisted of a compacted concrete slab with a circular column of strengthening with the ratio of hook steel fiber 0.5% concrete. The slab has been subjected to monotonic and incremental load testing until failure. In this sample, shear fractures appeared around the column on the slab's tension face, as well as cracks around the column on the pressure face of the slab, and the column penetrated the slab, resulting in failure due to punching shear. Where it was more toughness, and the failure was a few cracks on the tensile area around the column. **Plate 4.11** ,**Plate 4.12** and **Plate 4.13** depicts the shape of the failed sample.

Plate 4.11: The sample of fibrous concrete slab with circular column ($CH_{0.5\%}$)

Plate 4.12: The sample of fibrous concrete slab with circular column ($CH_{1.0\%}$)

Plate 4.13: The sample of fibrous concrete slab with circular column ($CH_{1.5\%}$)

4.4.4 Fibrous concrete slab with a square column ($SM_{0.5\%}$), ($SM_{1.0\%}$) and ($SM_{1.5\%}$)

This sample consisted of a compacted concrete slab with a square column of strengthening with the ratio of straight steel fiber 0.5% concrete. The slab has been subjected to monotonic and incremental load testing until failure. In this sample, shear fractures appeared around the column on the slab's tension face, as well as cracks around column on tension of slab face, and the column penetrated the slab, resulting in failure due to punching shear. Where it was more toughness, the failure zone pattern was circular around one-fourth of the column area from the tensile side. **Plate 4.14** , **Plate 4.15** and **Plate 4.16** depicts the shape of the failed sample.

Plate 4.14: The sample of fibrous concrete slab with square column ($SM_{0.5\%}$)

Plate 4.15: The sample of fibrous concrete slab with square column ($SM_{1.0\%}$)

Plate 4.16: The sample of fibrous concrete slab with square column ($SM_{1.5\%}$)

4.4.5 Fibrous concrete slab with a square column ($SH_{0.5\%}$),($SH_{1.0\%}$) and ($SH_{1.5\%}$)

This sample consisted of a compacted concrete slab with a square column of strengthening with the ratio of hook steel fiber 0.5% concrete. The slab has been subjected to monotonic and incremental load testing until failure. In this sample, shear fractures appeared around the column on the tension slab face, as well as cracks around the column on the slab's tension face, and the column penetrated the slab, resulting in failure due to punching shear. Whereas the failure zone pattern was circular around one-fourth of the column area from the tensile side. **Plate 4.17** and **Plate 4.18** and **Plate 4.19** depicts the shape of the failed sample.

Plate 4.17: The sample of fibrous concrete slab with square column ($SH_{0.5\%}$)

Plate 4.18: The sample of fibrous concrete slab with square column ($SH_{1.0\%}$)

Plate 4.19: The sample of fibrous concrete slab with square column ($SH_{1.5\%}$)

4.5 Effect of steel fiber dosage on deflection.

Figures (4.5) and (4.6), (4.7),and (4.8) explain the connection among load and deflection for all slab specimens submitted to monotonous loading conditions. The load versus displacement curves commences as linear forms with constant slopes at moderate loading levels. After increasing the applied load, a first fracture initiates at the tension face of the slab, followed by an abrupt change in the slab's curvature. As load increases, additional fractures were started, and the relationship between load and deflection is nonlinear with an incline that varies. When the deflection varies rapidly with a small increase in applied load up to the failure load maximum, the third stage commences. The load versus deflection curves appeared to depend on the column's size, shape, and steel fiber types and quantities. The following can be deduced:

1- The shear deflection of the plates reinforced with straight fibers with a circular cross-section of the column increased by approximately 37.24% and 35.45% for steel dosages of 1.0% and 1.5%, respectively, whereas it decreased by 0.5% for the fibers. About 10.48% in comparison to standard plates.

2- The shear deflection of the plates reinforced with straight fibers with a square cross-section of the column increased by approximately 12.69%,38.73%, and 103.17% for steel dosages of 0.5%,1.0%, and 1.5%, respectively in comparison to standard plates.

3- The shear deflection of the plates reinforced with hooked fibers with a circular cross-section of the column decreased by approximately 5.24% and 6.89% for steel dosages of 0.5% and 1.0%, respectively, whereas it increased by 1.5% for the fibers. About 83.03% in comparison to standard plates.

4- The shear deflection of the plates reinforced with hooked fibers with a square cross-section of the column increased by approximately 21.43%,20.63%, and 58.73% in comparison to standard plates, for steel ratio of (0.5%), (1%), and (1.5%).

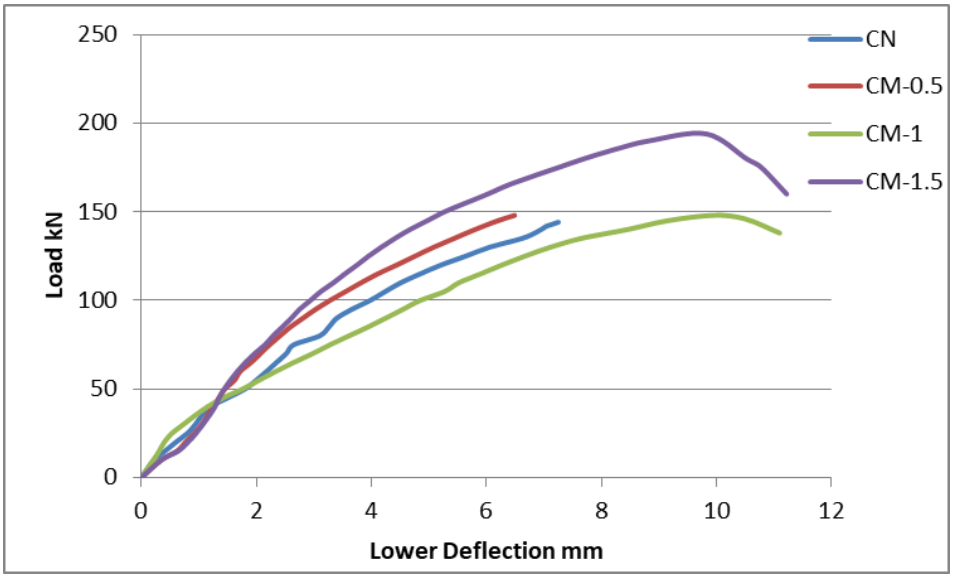

Figure (4.5): load - deflection of slabs reinforced of straight fiber with circular column sections

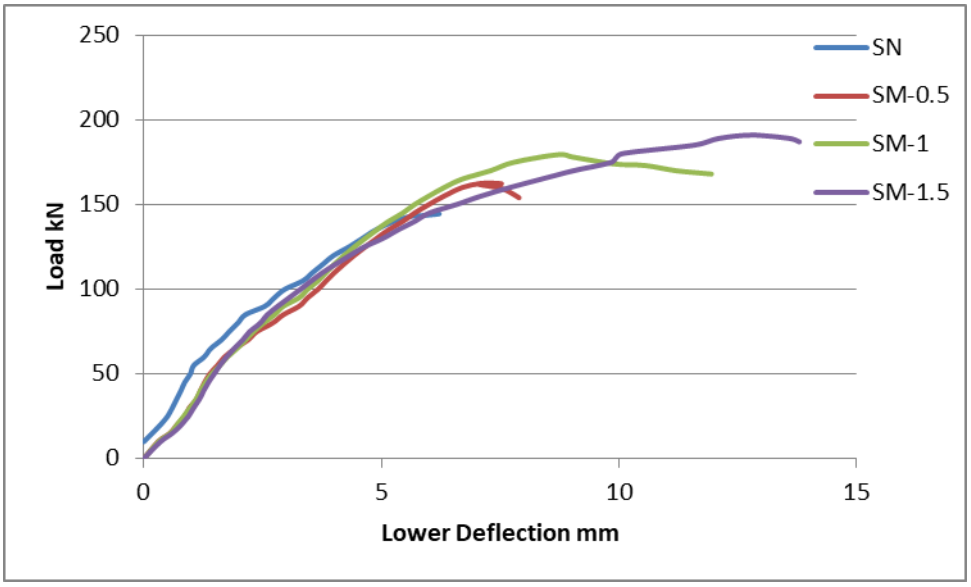

Figure (4.6): load - deflection of slabs reinforced of straight fiber with square column sections.

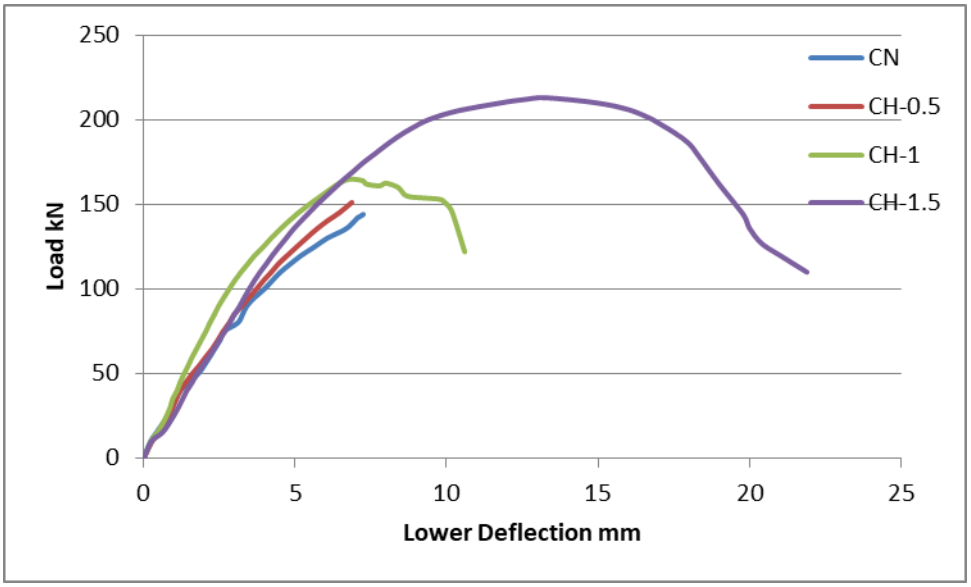

Figure (4.7): load - deflection of slabs reinforced of hooked fiber with circular column sections.

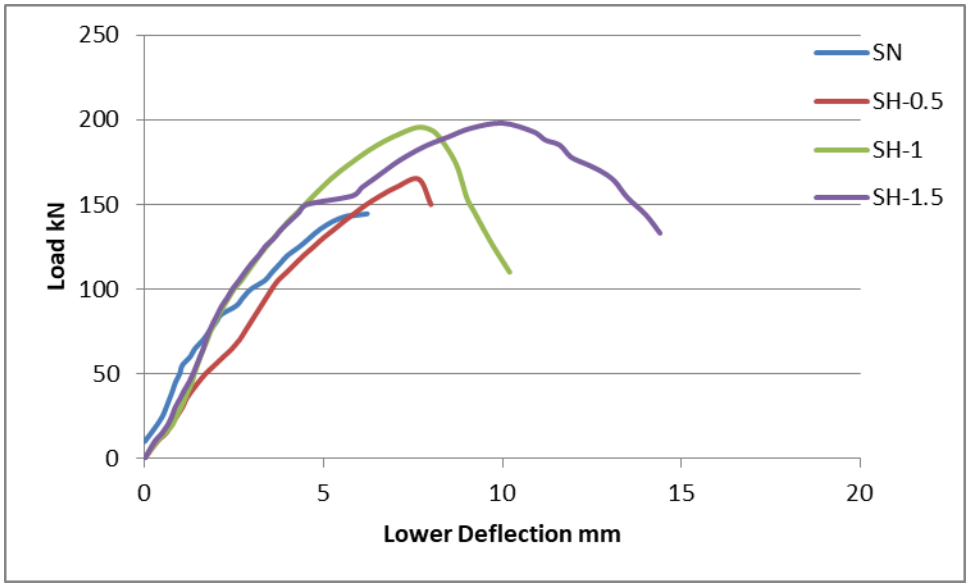

Figure (4.8): load – deflection of slabs reinforced of hooked fiber with square column sections

It was found that the use of steel-fibers in the concrete reduces the deflection of slabs reinforced with hook and straight steel fibers with circular columns and low percentages of steel-fibers. However, performance of the slabs reinforced with hooked fibers was better. The reason for this is attributed to the right angles of the square column, which make it more deflected than the circular column, and the higher the percentage of fibers, the greater the deflection of the columns when compared to non-fibrous concrete. In addition, the hooked ends of the fibers make the concrete more resistant to deflection, but this resistance decreases as the percentage of fibers increases because their distribution becomes irregular and more random.

4.6 Effect of types and dosages of steel fiber on column penetration.

Column penetration, the area of contact between the column and the slab, is shown in **Figures 4.9, 4.10, 4.11, and 4.12.** The load against column penetration is initially linear with constant slopes, when the applied load is increased. As the load increases, the column begins to penetrate the slab, and the relationship between load and column penetration assumes a variable-slope nonlinear form. The third stage begins when the penetration changes rapidly in response to a slight increase in the applied load leading up to the ultimate load at failure. The relationship between load and column penetration appears to depend on the column's form and types and quantities of steel fibers. The following can be extrapolated:

1- The column penetration of the slabs reinforced with straight fibers with a square cross-section of the column increased by approximately 26.67% and 260% for steel dosages of 1.0%,1.5%

respectively, whereas it decreased by 0.5% for the fibers. About 1.67% in comparison to standard plates.

2- The column penetration of the plates reinforced with straight fibers with a circular cross-section of the column increased by approximately 8.91%, 56.44%,and 38.61% for steel dosages of 0.5%, 1.0%, and 1.5%, respectively in comparison to standard plates.

3- The column penetration of the plates reinforced with hooked fibers with a square cross-section of the column increased by approximately 40% and 121.67% for steel dosages of 1.0%, and 1.5% respectively, whereas it decreased by 0.5% for the fibers about 43.33% in comparison to standard plates.

4- The column penetration of the plates reinforced with hooked fibers with a circular cross-section of the column increased by approximately 5.94% and 121.67% for steel dosages of 1.0%, and 1.5% respectively, whereas it decreased by 0.5% for the fibers about 0.99% in comparison to standard plates.

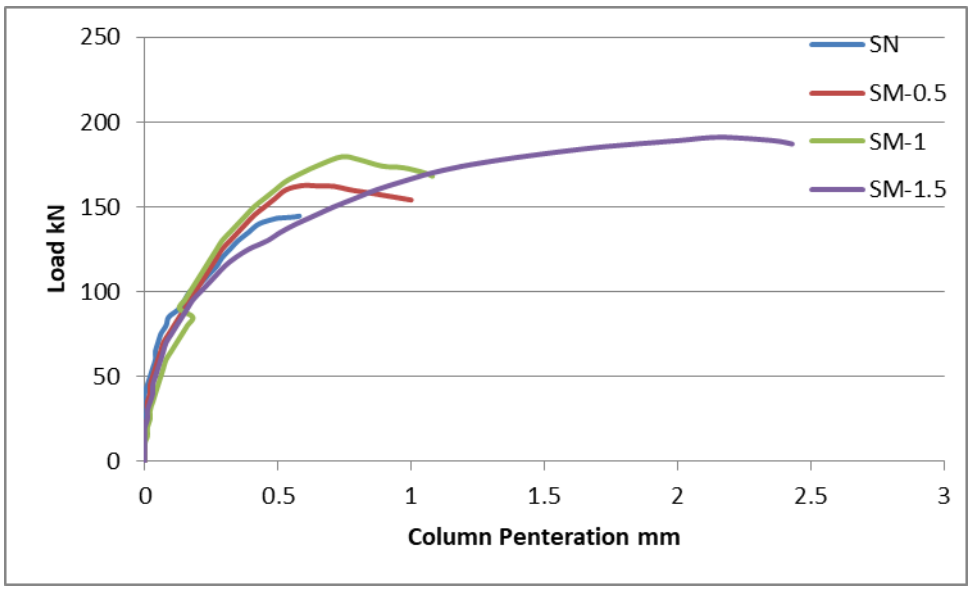

Figure (4.9): load – Column penetration slabs reinforced of straight fiber with square column sections.

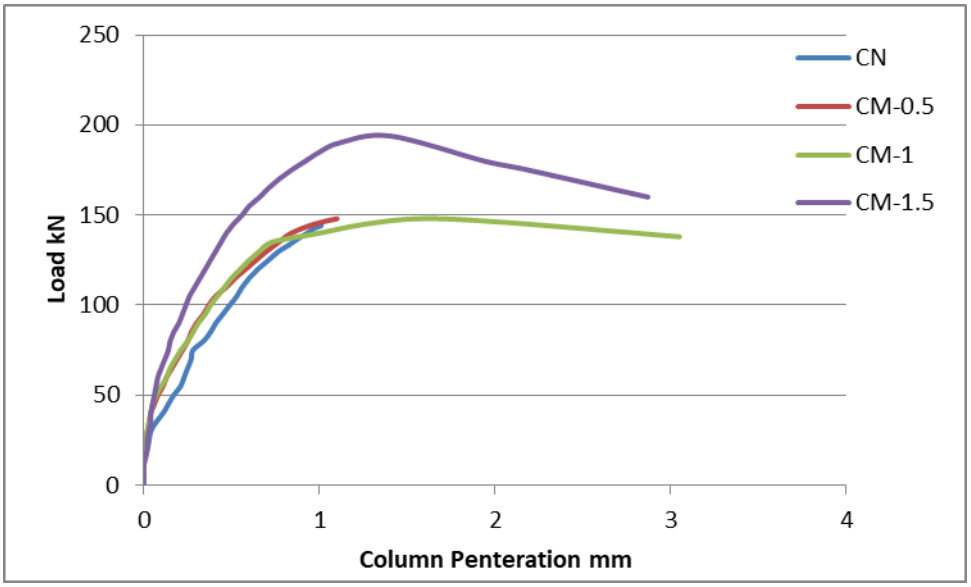

Figure (4.10): load – Column penetration slabs reinforced of straight fiber with circular column section.

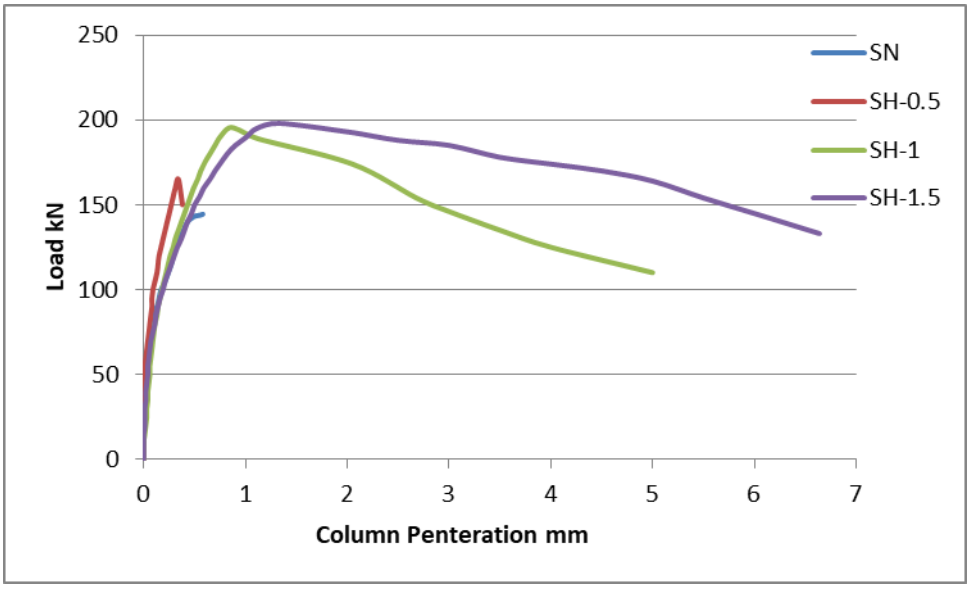

Figure (4.11): load – Column penetration slabs reinforced of hooked fiber with square column sections.

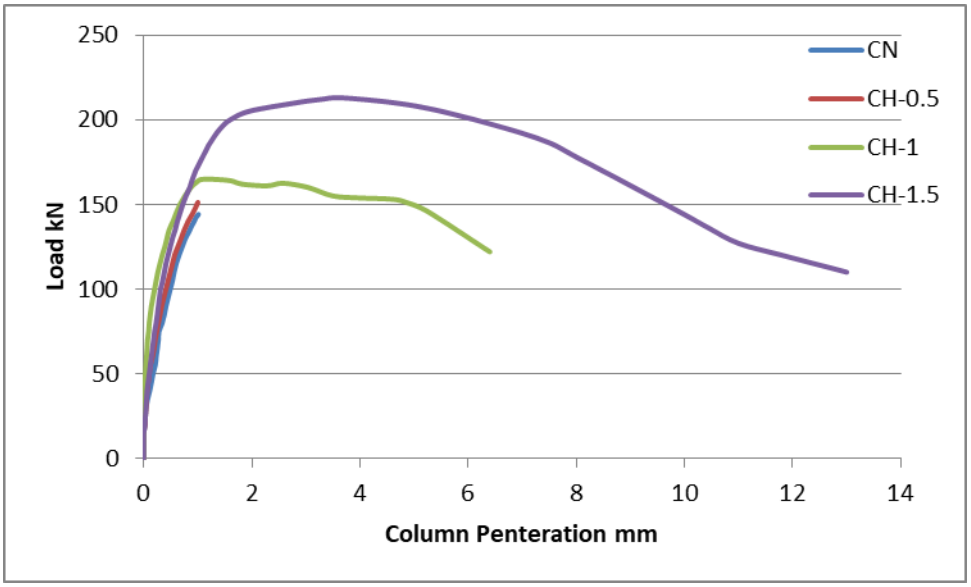

Figure (4.12): load – Column penetration slabs reinforced of hooked fiber with circular column sections.

It was found that the behavior of slab square column concrete reinforced with hook steel fibers with a ratio of 0.5% is better compared with concrete reinforced with straight fibers with the same fiber ratios. While the higher percentages of fibers gave greater penetration of the column due to the large percentage of fibers that led to random distribution in the concrete matrix and thus led to greater penetration of the column inside the slab. While using the square column, there was no effect on the column penetration. The reason may be attributed to the divergence of the angles of the square column compared to the circular column.

4.7 Influence of Considering Parameters on Ultimate Load.

The influence of the types and dosages of fibers and the column shape (circular and square) on the ultimate loading of slabs subjected to point loading Upon examination, the failure was gradual in the fiber-reinforced samples, while the failure was sudden in the non-fibrous concrete samples. In the pre-cracking stage, the behavior of the reinforced and unreinforced slabs was convergent. The non-fibrous slab showed increased behavior post-cracking, in addition to a variety of diagonal

cracks, while the reinforced slabs did not show this behavior, but the cracks stopped spreading due to the presence of fibers. The ultimate load of the reinforced circular column slab was close to the ultimate load of the unreinforced circular column slab. The ultimate load is depicted in **Table (4.4)** from the values of the tests enumerated in **Table (4.3)**.

Table (4.4) Ultimate Load of Slabs Samples

Designation of Slab	Ultimate Load (Pn)(KN)	% Increase Of Ultimate Load
CN	144.14	-
SN	144.5	-
$CM_{0.5\%}$	147.84	2.57
$CM_{1.0\%}$	148.16	2.79
$CM_{1.5\%}$	193.6	34.31
$SM_{0.5\%}$	161.32	11.64
$SM_{1.0\%}$	179.52	24.24
$SM_{1.5\%}$	191.04	32.21
$CH_{0.5\%}$	151. 2	4.89
$CH_{1.0\%}$	164.8	14.33
$CH_{1.5\%}$	212.94	47.73
$SH_{0.5\%}$	165.23	14.35
$SH_{1.0\%}$	195.33	35.18
$SH_{1.5\%}$	197.9	36.96

For hook steel-fiber for slabs with a (square and circular) column, the ultimate load greater than the slab reinforced of straight steel-fiber with a square column. When comparing the slabs made of reinforced concrete with straight fibers between the shapes of columns the square and circular , it was found that the ultimate load of the slab with a square column is higher than that of the circular column by (9.12% and 21.17%) compared to a non-fibrous concrete slab for fiber ratios (0.5% and 1.0%) respectively, while at a fiber ratio of 1.5%, the ultimate load of the slab with a circular column is slightly higher than the ultimate load of the slab with a square column by 1.34% when compared with a non-fibrous concrete slab. When comparing the slabs made of reinforced concrete with hook fibers between the shapes of the square and circular columns, it

was found that the ultimate load of the slab with a square column is higher than that of the circular column by (9.28% and 18.53%) compared to a non-fibrous concrete slab for fiber ratios (0.5% and 1.5%) respectively, while at a fiber ratio of 1.0%, the ultimate load of the slab with a circular column is slightly higher than the ultimate load of the slab with a square column by 7.59% when compared with a non-fibrous concrete slab. Perhaps due to utilization of steel fibers, this has occurred, whether straight or hooked, to make concrete a heterogeneous material, in addition to the difference in the percentage of fibers leading to a difference in their distribution, which makes the behavior of concrete during testing unstable.

4.8 Influence the shape of column on ultimate load.

Figure 4.13 shows the effect of the shape of the column used with the slab on the ultimate load, as it shows the ratio of the ultimate loads of the square-column slab to the final loads of the circular-column slab for both types of fibers (straight and hooked). It was found that the use of straight fibers was the percentage for the ultimate loads (1.091, 1.212) at the percentage of fiber 0.5% and 1.0%, respectively, while the percentage for the ultimate loads (0.987) was at the percentage of fiber 1.5% of the volume of concrete.

While using hook fibers, the ratio for ultimate loads (1.093 and 1.185) was at a fiber ratio of 0.5% and 1.0%, respectively, and the ratio for final loads (0.929) was at a fiber ratio of 1.5% of the volume of concrete.

It was found that the slab with a square column for both types of fibers (straight and hooked) is better than the slab with a circular column at a fiber ratio of 0.5% and 1.0% of the volume of concrete, while for the slab with non-fibrous concrete, the ratio for ultimate loads was (1.003).

Perhaps this is due to the fact that the presence of fiber in the concrete increases its bearing strength, especially after the cracking stage, because the fibers help prevent cracks from spreading. As well, the load distribution of the square column is better than the circular one because of its right angles that reduce the penetration of the column into the slab, but increasing the percentage of fibers to 1.5% causes an irregular distribution inside the concrete, which makes the ultimate load ratio lower. This means that the ultimate load values for the circular column are higher than the square column.

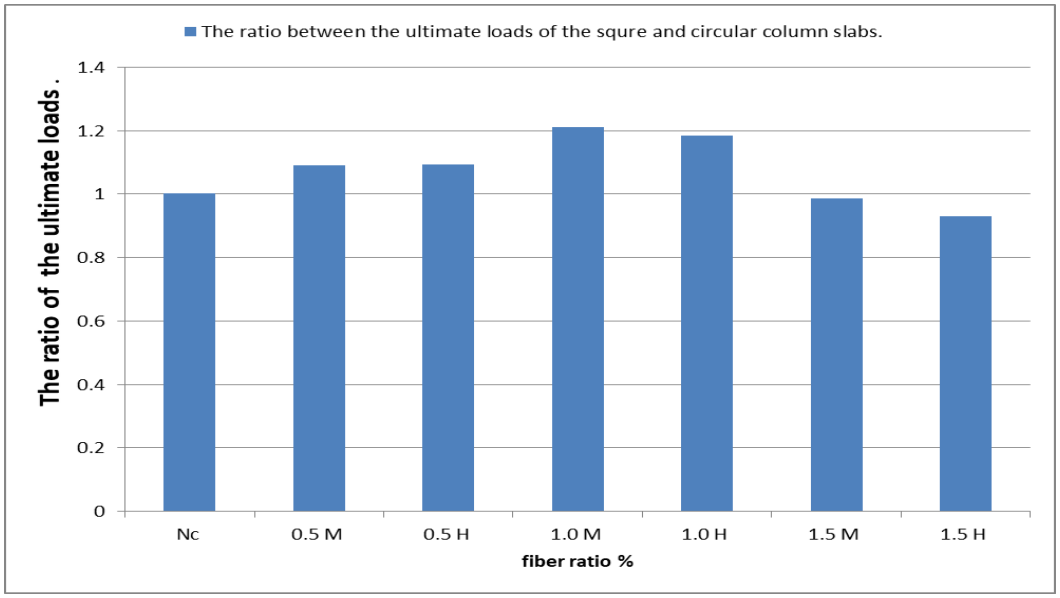

Figure (4.13): Impact of the ratio between the ultimate loads of the circular and square column slabs with the fibers ratio.

4.9 Influence types of the fibers on ultimate load.

Figure 4.14 shows the effect of the type of fibers on the strength of the slab, as measured by the ratio of the ultimate loads of the slab reinforced with straight fibers to the ultimate loads of the slab reinforced with hook fibers with the fiber ratios. It was found that the ratio of the square column slab to the ultimate loads was (0.976, 0.919, and 0.965) at the fiber ratios (0.5%, 1.0%, and 1.5%), respectively, of the concrete

volume, while in the circular column slab the percentage of ultimate loads was (0.978, 0.899, and 0.909) when the percentage of fibers was (0.5%, 1.0%, and 1.5%), respectively, of the volume of concrete.

It was noted that the use of hook fibers was more preferable and gave higher results than straight fibers. The reason for this was likely that the hook fibers in the post-cracking stage are better because they are longer, which leads to their withdrawal and non-separation of the concrete and reduces the spread of cracks in the concrete.

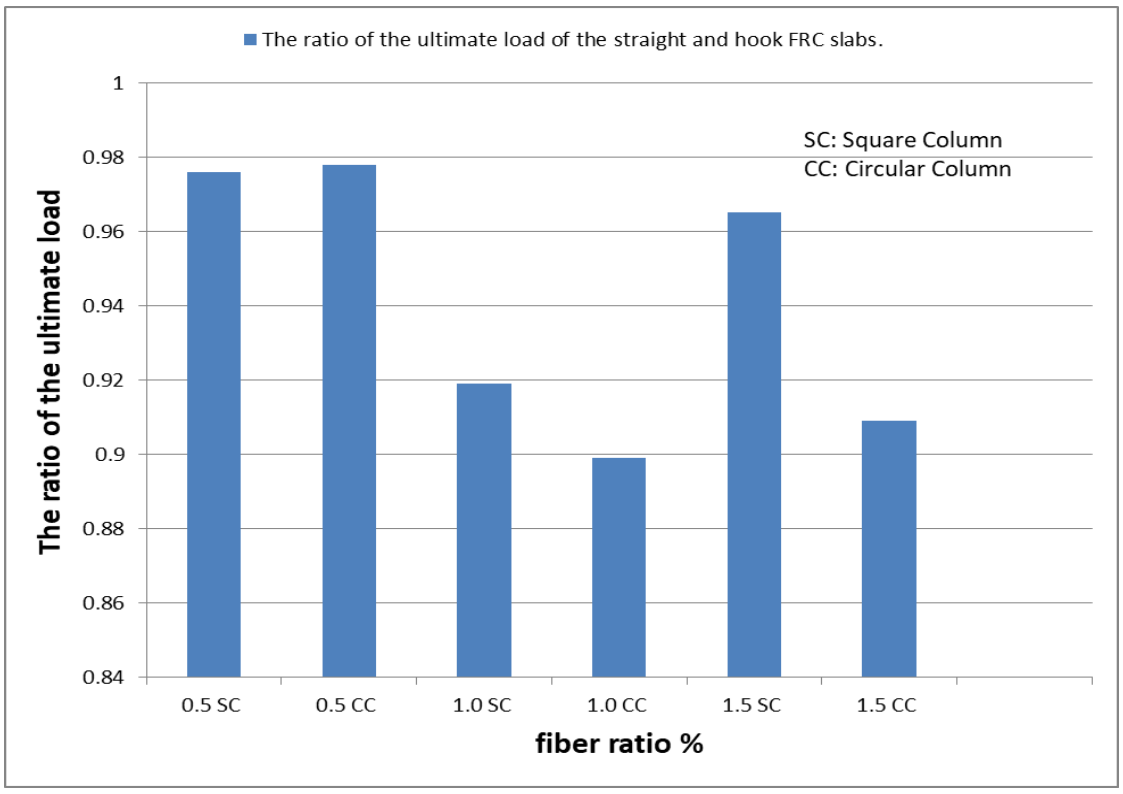

Figure (4.14): Impact of the ratio between the ultimate loads of the straight and hook FRC slabs

4.10 The punching area of samples.

As shown in **Table 4.5**, the punching area was added to each sample. Plate 4.20 depicts the punching area of a model (CN). When both types of steel fibres were added to concrete, the punching area of the samples

decreased. when straight steel fibre was used, with the greatest decrease occurring in slabs with circular column sections (70.15%, 49.05%, and 59.51%). While the rate of decrease was 69.59%, 37.09%, and 34.56% for slabs with a square column section. While hooked steel fiber was used, the punching area of the samples decreased, with the greatest decrease occurring in slabs with circular column sections (72.81%, 49.99%, and 14.29%). While the rate of decrease was 38.71%, 37.56%, and 34.56% for slabs with a square column section when using the same percentage of steel fibers (0.5%, 1.0%, and 1.5%), respectively.

Table 4.5 : Punching area for samples

Slab Symbol	Punching area(mm)	Percentage decrease by area %
CN	278254.25	-
SN	229586.16	-
$CM_{0.5\%}$	83053.27	70.15
$CM_{1.0\%}$	141772.34	49.05
$CM_{1.5\%}$	112677.56	59.51
$SM_{0.5\%}$	69828.28	69.59
$SM_{1.0\%}$	144417.39	37.09
$SM_{1.5\%}$	150236.72	34.56
$CH_{0.5\%}$	75647.29	72.81
$CH_{1.0\%}$	139127.67	49.99
$CH_{1.5\%}$	198904.15	28.52
$SH_{0.5\%}$	140714.23	38.71
$SH_{1.0\%}$	143359.87	37.56
$SH_{1.5\%}$	196788.03	14.29

Plate 4.20: Punching area of (CN) sample.

CHAPTER FIVE

THEORETICAL ANALYSIS

CHAPTER FIVE

THEORETICAL ANALYSIS

5.1 Introduction

This chapter examines the theoretical application of samples in accordance with international codes (American Code ACI 318 [66], British Code[67], EuropeanCode2[68],and *Fib* Model Code[69], providing a comprehensive overview of the interpretation, analysis, discussion, presentation, and evaluation of theoretical research in comparison to experimental research on the performance and durability of models.

5.2 ACI Code Design formula

According to **ACI318,2019** [6], the critical section of shear penetration was situated at a distance of 0.5 times the diameter (d) away from the surface of column, as depicted in **Figure 5.1.** Solid slab piercing shear capacity (V_c) is the smallest of Equation. 5.1, 5.2, and 5.3.

$$V_c=0.33\lambda_s\sqrt{f}_c\,A \qquad (5.1)$$

Where:-

$$\lambda_s=\frac{2}{\sqrt{1+(0.004d)}} \leq 1.0$$

$$V_c=\left(0.167+\frac{0.33}{\beta}\right)\sqrt{f}_c\,A \qquad (5.2)$$

$$V_c=\left(0.167+\frac{3.32d}{b_0}\right)\sqrt{f}_c\,A \qquad (5.3)$$

Where:

The parameter **λs** represents the diminished mechanical characteristics of light-weight concrete when compared to normal-weight concrete of equivalent strength of compression. In this context, **λs** is equivalent to 1.0 for normal-weight concrete. The symbol fc' denotes the specified concrete compressive cylinder strength. The variable $\mathbf{b_0}$ corresponds to perimeter of the two-way shear critical section in slabs. The symbol d represents the distance from the excessive the compression fiber to the center of the reinforcement longitudinal tension, which is commonly referred to as the depth effect. **β** denotes the ratio of the long-side to the short-side of the column. Lastly, A represents the concrete area, which is calculated as the product of $\mathbf{b_0}$ and d ($A = b_0 d$). The equation for the design piercing capacity of shear ($\mathbf{V_n}$) of the solid slab is represented by Equation 5.4, while **Φ** denotes the reduction factor of stress with a value of 0.75.

$$V_n = \Phi V_c \qquad (5.4)$$

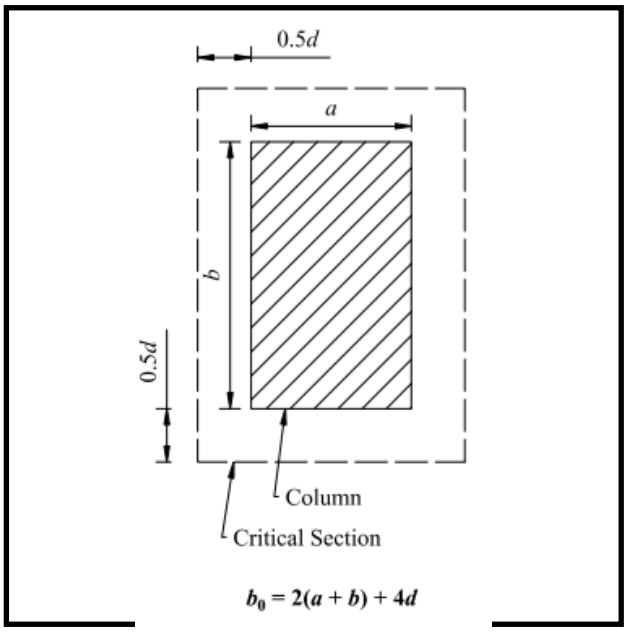

Figure 5.1: Punching shear - critical section as **ACI 318** [66]

5.3 Formula of British Standard Code

Without shear reinforcement, the critical section of concrete flat slabs is assumed to be 1.5 d from face of the column in BS 8110,1997 [67]. When tensile reinforcement is added around a structure's crucial section, its strength increases by 0.75 d. According to BS 8110 [67], the area depicted in **Figure 5.2** is of paramount importance. strength of compression , critical section, depth effect of slab, and the reinforcement of tension ratio are all calculated in Equation 5.5 to characterize the strength of shear for concrete. Shear strength is calculated by taking the cube root of the compressive strength, as specified in BS 8110[67]. Size expansion due to effective section depth and tensile reinforcement ratio is accounted for.

$$V_c=0.27k(100\rho_t)^{1/3}f_{c\,cub}\,b_o d \qquad (5.5)$$

Where:-

K is the factor according for the size and can be determined according to Equation (5.5.1)**,** $\boldsymbol{\rho_t}$ is the bending factor reinforced ratio that can be calculated as per Equation (5.5.2)

Where:-

$$K=\sqrt[4]{\frac{400}{d}} \qquad (5.5.1)$$

$$\rho_t=\frac{Abar}{Sd}\leq 0.03 \qquad (5.5.2)$$

S is the spacing from center to center of steel bar, $\mathbf{f_c}$ cub is the specified compressive cubical strength of concrete in Mpa, $\mathbf{b_0}$ is the perimeter in millimeters of the critical section of two-way shear in slabs, **d** is the distance between the high compression fiber and the centroid of a reinforcement by tension of longitudinal, i.e. the depth effect in millimeters, and **A** bar is the area of one steel bar.

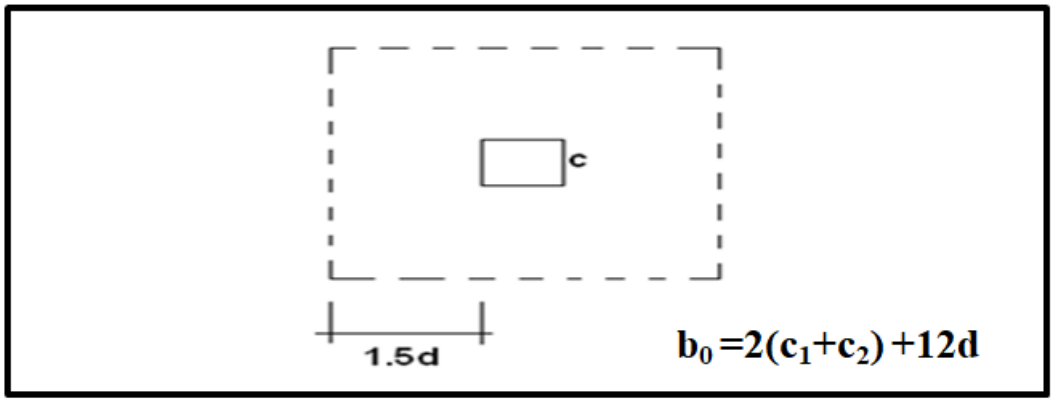

Figure 5.2: Punching shear - critical section as BS 8110 [67]

5.4 Euro code (EC2) Formula

In accordance with **Euro code EC2**[68]. The critical section for flat slabs concrete without reinforcement shear is estimated to be 2d from the column face. In flat slabs concrete with shear reinforcement, the critical section is located 1.5d from the edge of the reinforcement shear. In Euro code [68] , as opposed to ACI 318-19[66] and BS 8110[67], the critical section's extremities are divided into quadrants. The Euro code [68], critical section is illustrated in **Figure 5.3**, and suggested an equation for the shear strength. That incorporates the impact of the ratio of tension reinforcement and the strength of compression for concrete. Concrete's shear strength is described by Equation 5.6.

$$V_c = 0.18 x b_0 \, x \, d \, x \, k \, (100 \, \rho_t \, f_c)^{1/3} \qquad (5.6)$$

Where:-

K is the factor according for the effect of size and can be calculated as per Equation (5.6.1)**,** $\boldsymbol{\rho_t}$ is the bending factor reinforced ratio that can be calculated as per Equation (5.6.2)

$$K=1+\sqrt{\frac{200}{d}} \leq 2.0 \qquad (5.6.1)$$

$$\rho_t=\frac{Abar}{Sd} \leq 0.02 \qquad (5.6.2)$$

S is the spacing from center to center of steel bar, **fc'** is the specified concrete compressive cubical strength, $\mathbf{b_0}$ is the perimeter in millimeters of the critical section of two-way shear in slabs, and **d** the effective depth, is the distance between the high compression fiber and the centroid of a reinforcement by longitudinal tension. The area of one steel bar is $\mathbf{A_{bar}}$.

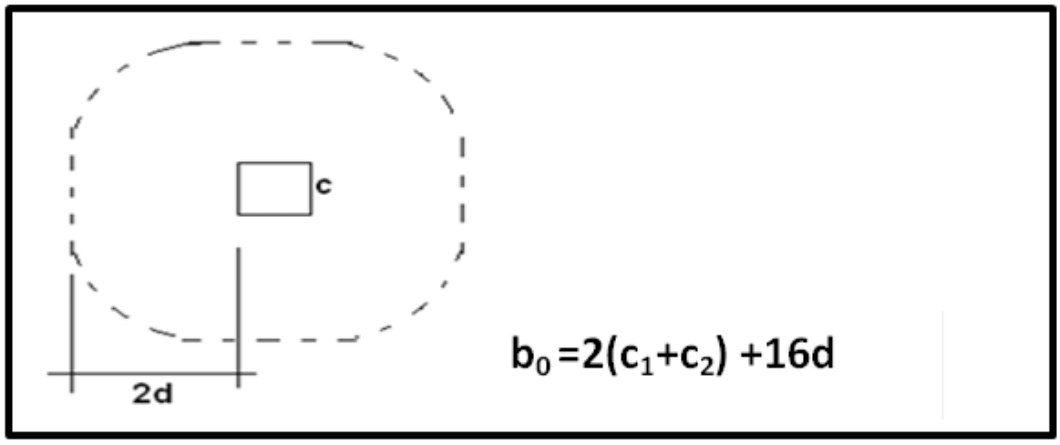

Figure 5.3: Punching shear - critical section as Euro code 2 [68]

5.5 Formula of Fib Model Code

Based on the Critical Shear Crack Theory (**CSCT**), the model code[69] developed a uniform design basis for slabs. This model's resistance of punching shear is dependent on the critical shear fracture width, that is associated with slab rotation Model Code[69],[17]**.** Strength of Punching shear ($\mathbf{V_c}$) can be determined by applying Equation 5.7 in **MC2010** [69].

$$V_c = k\psi \sqrt{f'c}\, b_0\, d \qquad (5.7)$$

Where the symbol $\mathbf{f'_c}$ represents the characteristic strength of compression for concrete, which is typically measured by cylinder. The symbol $\mathbf{b_o}$ represents the perimeter of control, which is set at half the distance among the column's face and the flexural reinforcement's centroid. The symbol dv represents the depth impact of shear resistance of the member, which is the distance among the centroid of the flexural reinforced and the concrete's surface on which the slab is supported. The

parameter **kψ** is introduced to consider the influence of the width of a shear critical crack. Its value is determined by the rotation of the slab **(ψ)** and the maximum size of the aggregate (**dg**), as described by Equation (5.7.1).

$$k\psi=\frac{1}{1.5+(0.9\psi\ d\ kdg} \leq 0.6 \qquad (5.7.1)$$

The symbol "**d**" represents the average value of the flexural depth effect, whereas "**kdg**" is a coefficient that considers the impact the size of aggregate. The calculation of **"kdg"** can be determined using Equation (5.7.2).

$$kdg=\frac{32}{16+dg} \geq 0.75 \qquad (5.7.2)$$

CSCT offers simple equations of design that facilitate the application of a level of approximation **(LoA)** strategy for analysis and design. This strategy complies with the core MC2010 principles. There is additional information available on the **LoA** method and how the selection of level impacts the value and piercing resistance of shear elsewhere **[70].** Using Equation (5.7.3) to calculate the surface rotation **(ψ).**

$$\Psi= 1.5\ r_s \frac{fy}{d\ Es} \qquad (5.7.3)$$

Where -: **Es** is the modulus of Young for the flexural reinforcing and $\mathbf{r_s}$ is the amount of distance of the centroid of the laden area to the zero-radial line moment of bending (line of contra flexure), which is commonly calculated to be 0.22L (The maximum span of adjacent slabs is denoted by the variable **L**).

5.6 Computational results for code equations

By applying the equations for the codes mentioned in the previous paragraphs to the samples used in the research, the results listed in **Table 5.1** and **Appendix C** show the calculations of the equations for one sample from the search.

Table 5.1 The Results from codes equations

Samples	ACI 318 the smallest of Equations			British Standard Code	Eurocode 2	Fib model code
	Eq.(5.1)	Eq.(5.2)	Eq.(5.3)			
CN	72.0600	108.5268	114.2069	86.6955	75.0753	83.6988
SN	86.6458	130.4938	121.5882	106.7411	92.9254	100.6404
$CM_{0.5}$	72.5678	109.2914	115.0116	87.1023	80.9801	84.2886
$CM_{1.0}$	76.0959	114.6051	120.6033	89.9031	83.5840	88.3866
$CM_{1.5}$	79.2032	119.2847	125.5279	92.3341	85.8442	91.9957
$SM_{0.5}$	87.2563	131.4133	122.4449	107.2419	100.2341	101.3495
$SM_{1.0}$	91.4986	137.8024	128.3980	110.6903	103.4572	106.2770
$SM_{1.5}$	95.2348	143.4293	133.6409	113.6834	106.2547	110.6166
$CH_{0.5}$	74.6344	112.4040	118.2870	88.7483	82.5104	86.6890
$CH_{1.0}$	78.9378	118.8851	125.1074	92.1277	85.6523	91.6875
$CH_{1.5}$	79.4016	119.5836	125.8424	92.4882	85.9875	92.2261
$SH_{0.5}$	89.7413	135.1558	125.9320	109.2684	102.1282	104.2358
$SH_{1.0}$	94.9157	142.9488	133.1932	113.4293	106.0172	110.2460
$SH_{1.5}$	95.2348	143.4293	133.6409	113.6834	106.2547	110.6166

5.6.1 Comparison of the experimental and predicted ultimate loads.

5.6.1.1 The ultimate loads (P_n) for ACI code

Table (5.2) displays the results of experiments of the ultimate load and the results of its calculation from the lowest value of the ACI code equations calculated from Equations (5.1), (5.2), and (5.3), as well as the error rates for each of them for all models.

Table (5.2). Comparison of the measured and predicted ultimate loads for ACI code[66]

Samples	$P_{n\ exp}$ (kN)	$P_{n\ ACI}$ (kN)	Error%
CN	144.14	72.0600	-50.01
SN	144.50	86.6458	-40.04
$CM_{0.5}$	147.84	72.5678	-50.91
$CM_{1.0}$	148.16	76.0959	-48.64
$CM_{1.5}$	193.60	79.2032	-59.09
$SM_{0.5}$	161.32	87.2563	-45.91
$SM_{1.0}$	179.52	91.4986	-49.03
$SM_{1.5}$	191.04	95.2348	-50.15
$CH_{0.5}$	151.20	74.6344	-50.64
$CH_{1.0}$	164.80	78.9378	-52.10
$CH_{1.5}$	212.94	79.4016	-62.71
$SH_{0.5}$	165.23	89.7413	-45.69
$SH_{1.0}$	195.33	94.9157	-51.41
$SH_{1.5}$	197.90	95.2348	-51.88

When comparing the experimental the outcomes of the models with the outcomes extracted from the equation of the ACI code (Equation 5.1) in **Table 5.2**, the value of predicted shear strengths was under estimating for all types of concrete. **Figure 5.4** shows the value of R^2 (Regression).

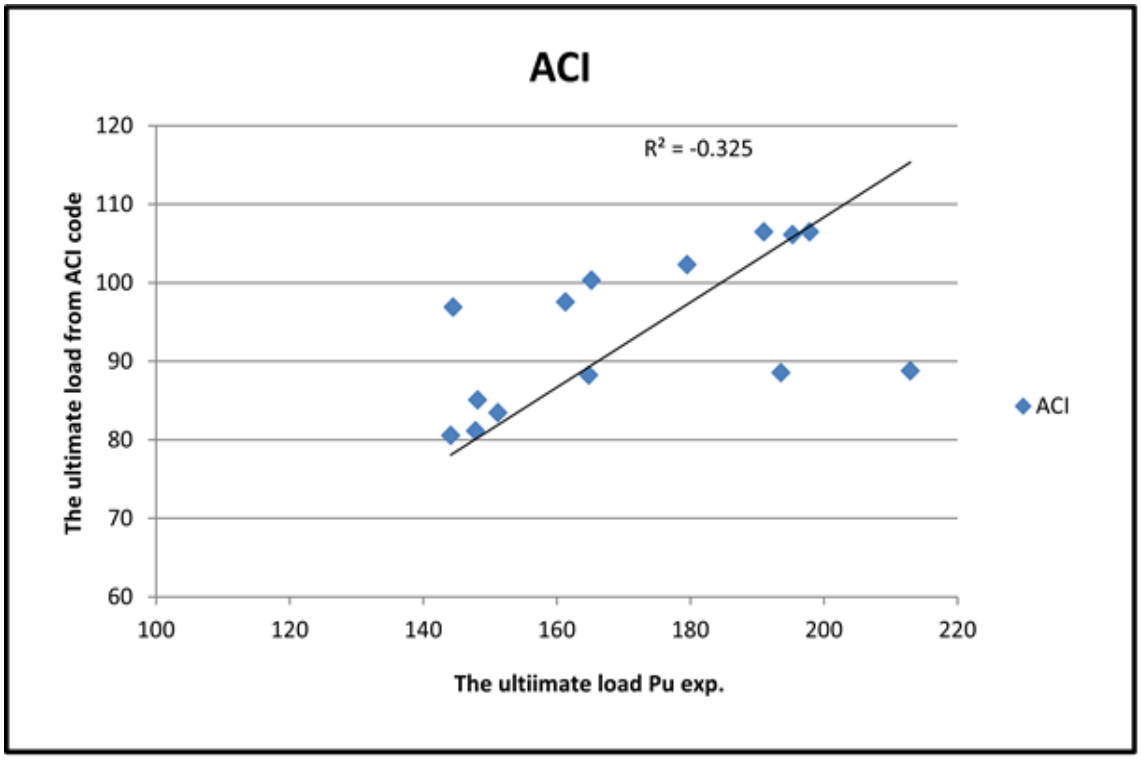

Figure 5.4: Experimental and predicted cracking ultimate load of SFRC slab According to ACI 318-19 [66]

5.6.1.2 The ultimate loads (P_n) for British Standard Code.

Table (5.3) displays the results of experiments of the ultimate load and the outcomes of its calculation from the lowest value of the British Standard code equations calculated from Equation (5.4) as well as the error rates for each of them for all models.

Table (5.3) Comparison of the measured and predicted ultimate loads for British Standard Code[67]

Samples	$P_{n\ exp}$ (kN)	$P_{n\ B.S\ code}$ (kN)	Error%
CN	144.14	86.695	-39.85
SN	144.50	106.741	-26.13
$CM_{0.5}$	147.84	87.102	-41.08
$CM_{1.0}$	148.16	89.903	-39.32
$CM_{1.5}$	193.60	92.334	-52.31
$SM_{0.5}$	161.32	107.242	-33.52
$SM_{1.0}$	179.52	110.690	-38.34
$SM_{1.5}$	191.04	113.683	-40.49
$CH_{0.5}$	151.20	88.748	-41.30
$CH_{1.0}$	164.80	92.128	-43.05
$CH_{1.5}$	212.94	92.488	-56.57
$SH_{0.5}$	165.23	109.268	-33.87
$SH_{1.0}$	195.33	113.429	-41.93
$SH_{1.5}$	197.90	113.683	-42.56

When comparing the experimental outcomes of the models with the outcomes extracted from the equation of the British Standard Code **[67]** (Equation 5.4) in **Table 5.3**, the value of predicted shear strengths was under estimating for all types of concrete. **Figure 5.5** shows the value of R^2 (Regression).

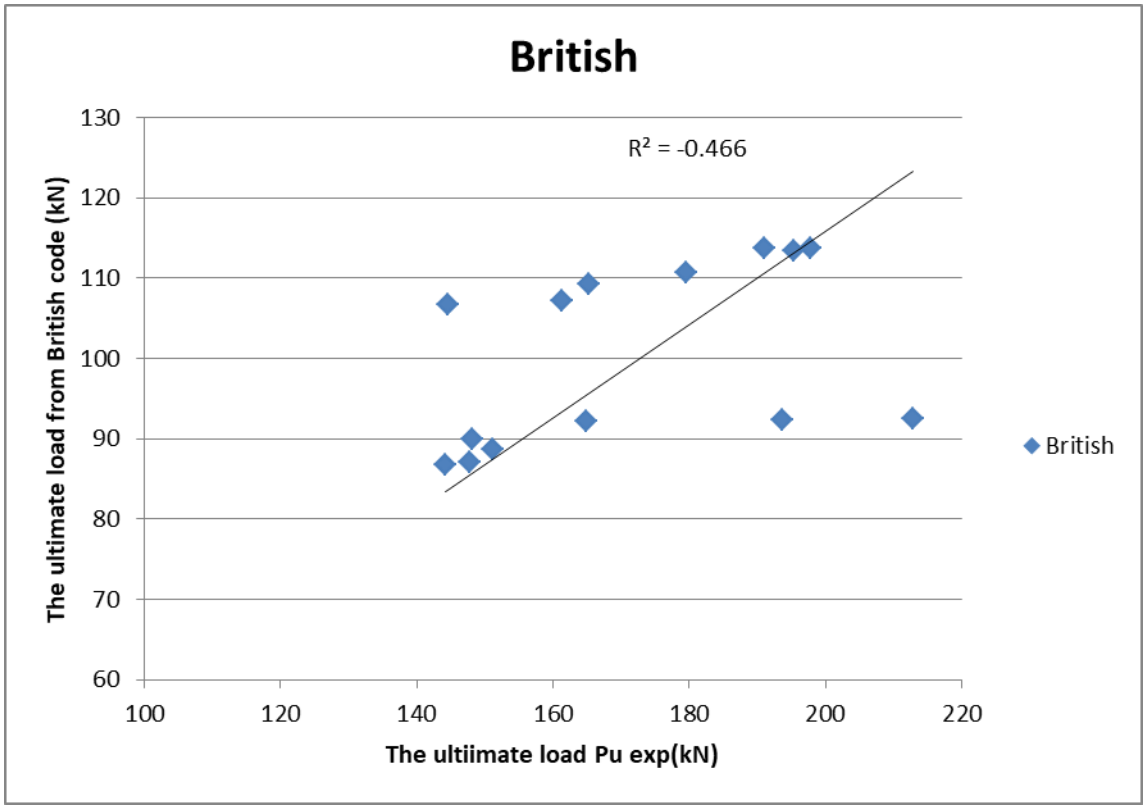

Figure 5.5: Experimental and predicted cracking ultimate load of SFRC slab for BS 8110 [67]

5.6.1.3 The ultimate loads (P_n) for Eurocode2Code.

Table (5.4) displays the results of experiments of the ultimate load and the outcomes of its calculation from the lowest value of the Eurocode2 code equations calculated from Equation (5.5) as well as the error rates for each of them for all models.

Table (5.4). Comparison of the measured and predicted ultimate loads for Eurocode2 Code[68]

Samples	$P_{n\ exp}$ (kN)	$P_{n\ Eurocode2}$ (kN)	Error%
CN	144.14	75.0753	-47.92
SN	144.50	92.9254	-35.69
$CM_{0.5}$	147.84	80.9801	-45.22
$CM_{1.0}$	148.16	83.5840	-43.59
$CM_{1.5}$	193.60	85.8442	-55.66
$SM_{0.5}$	161.32	100.2341	-37.87
$SM_{1.0}$	179.52	103.4572	-38.51
$SM_{1.5}$	191.04	106.2547	-44.38
$CH_{0.5}$	151.20	82.5104	-45.43
$CH_{1.0}$	164.80	85.6523	-48.03
$CH_{1.5}$	212.94	85.9875	-59.62
$SH_{0.5}$	165.23	102.1282	-38.19
$SH_{1.0}$	195.33	106.0172	-45.72
$SH_{1.5}$	197.90	106.2547	-46.31

When comparing the results of experimental of the models with the outcomes extracted from the equation of the Eurocode2 **[68]** (Equation 5.5) in **Table 5.4**, the value of predicted shear strengths was under estimating for all types of concrete. **Figure 5.6** show the value of R^2 (Regression).

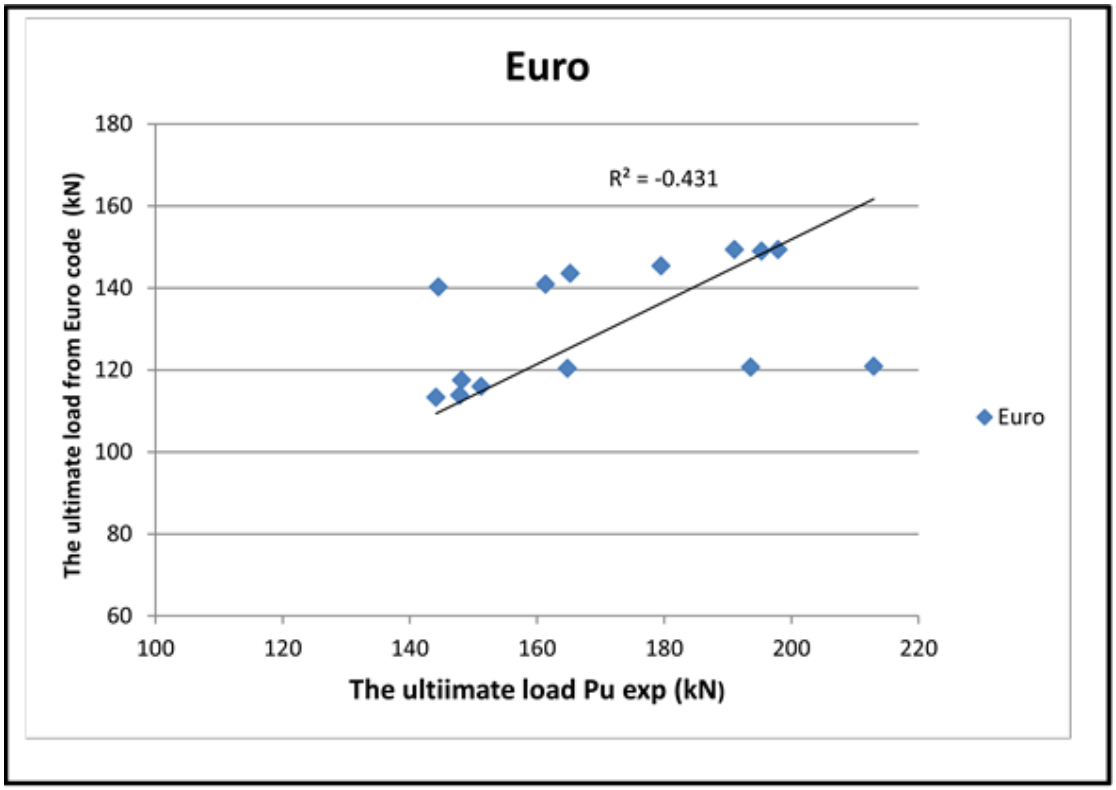

Figure 5.6: Experimental and predicted cracking ultimate load of SFRC slab according to Euro code (EC2) [68]

5.6.1.4 The ultimate loads (P_n) for Fib model code.

Table (5.5) displays the results of experimental of the ultimate load and the outcomes of its calculation from the lowest value of the Fib model [69] code equations calculated from Equation (5.6) as well as the error rates for each of them for all models.

Table (5.5). Comparison of the measured and predicted ultimate loads for Fib model Code[69]

Samples	$P_{n\ exp}$ (kN)	$P_{n\ Fib\ model}$ (kN)	Error%
CN	144.14	83.699	-41.93
SN	144.50	100.640	-30.35
$CM_{0.5}$	147.84	84.289	-42.69
$CM_{1.0}$	148.16	88.387	-40.34
$CM_{1.5}$	193.60	91.996	-52.48
$SM_{0.5}$	161.32	101.349	-37.18
$SM_{1.0}$	179.52	106.277	-40.79
$SM_{1.5}$	191.04	110.617	-42.09
$CH_{0.5}$	151.20	86.689	-42.67
$CH_{1.0}$	164.80	91.688	-44.36
$CH_{1.5}$	212.94	92.226	-56.69
$SH_{0.5}$	165.23	104.236	-36.91
$SH_{1.0}$	195.33	110.246	-43.56
$SH_{1.5}$	197.90	110.617	-44.10

When comparing the experimental results of the models with the results extracted from the equation of the Fib model **[69]** code Equation 5.6 in **Table 5.5**, the value of predicted shear strengths was under estimating for all types of concrete. **Figure 5.4** show the value of R^2 (Regression).

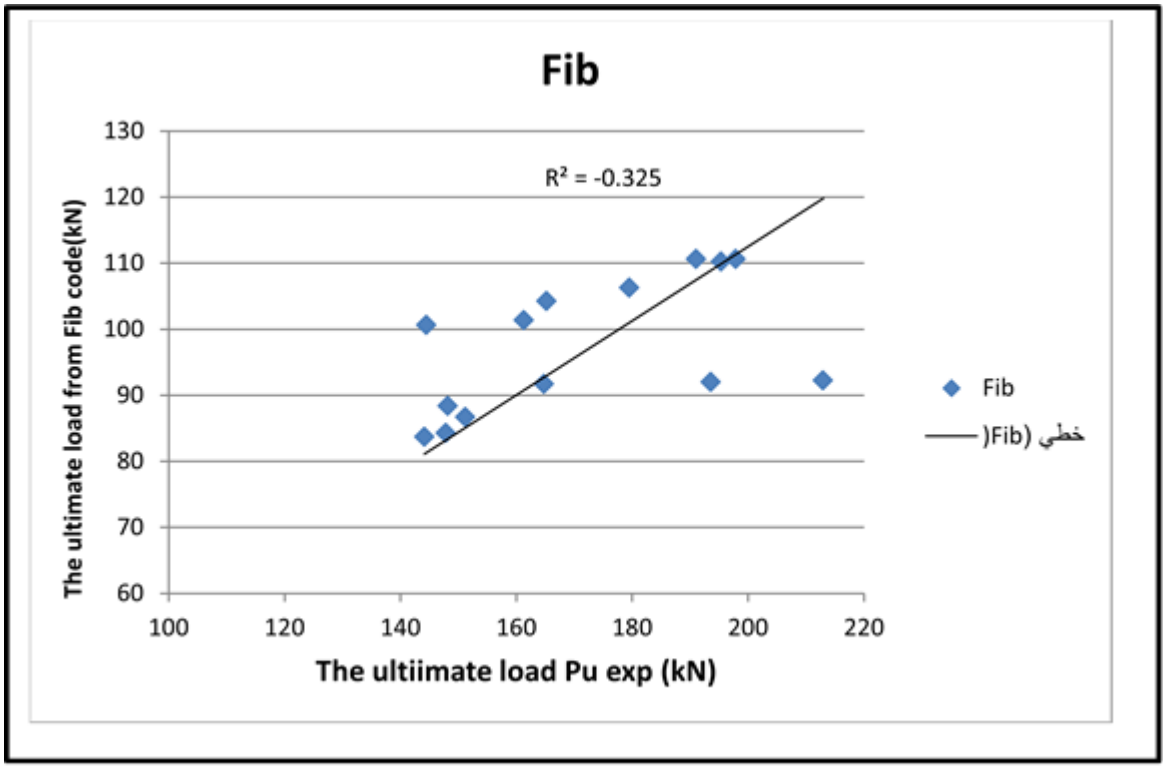

Figure 5.7: Experimental and predicted cracking ultimate load of SFRC slab according to Fib model [69]

5.7 proposed equations

From previous studies, it can be concluded that all proposed Equations were under estimating so the new Equations were proposed in this work. The first Equation proposed equations from ACI code **[66]** equation. The equation is proposed depending on the compressive strength of the concrete.

$$Pu_{Sug1} = V_{ACI} * f_{Vf} * f_{Lf} \qquad (5.7)$$

Where: f_{Vf} is increase factor for fiber dosage (V_f)and f_{Lf} is increase factor for fiber length(L_f in mm).

Where: -

$$f_{Vf} = \left(1.2 + \left(\frac{V_f}{2.5}\right)\right) \qquad (5.7.1)$$

$$f_{Lf} = \left(1 + \frac{L_f}{300}\right) \qquad (5.7.2)$$

For example: for $CM_{0.5}$

Fiber: Type= Straight steel fiber , Fiber length= 13mm, v_f = 0.5%.

Pu $_{ACI}$ = 72.5678kN

$$f_{Vf} = \left(1.2 + \left(\frac{V_f}{2.5}\right)\right) = \left(1.2 + \left(\frac{0.5}{2.5}\right)\right) = 1.4$$

$$f_{Lf} = \left(1 + \frac{L_f}{300}\right) = \left(1 + \frac{13}{300}\right) = 1.0433$$

$$P_{n_{Sug1}} = V_{ACI}\, f_{Vf}\, f_{Lf} = 72.5678\, x1.4\, x1.0433 = 105.994\text{kN}$$

Table (5.6) ACI mode field

Samples	$P_{n\ exp}$ (kN)	Sug-1	Sug-1/Exp.
CN	144.14	-	-
SN	144.50	-	-
$CM_{0.5}$	147.84	**105.9973**	**0.7170**
$CM_{1.0}$	148.16	**127.0295**	**0.8574**
$CM_{1.5}$	193.60	**148.7435**	**0.7683**
$SM_{0.5}$	161.32	**127.4523**	**0.7901**
$SM_{1.0}$	179.52	**152.7416**	**0.8508**
$SM_{1.5}$	191.04	**178.8509**	**0.9362**
$CH_{0.5}$	151.20	**116.6785**	**0.7717**
$CH_{1.0}$	164.80	**141.0356**	**0.8558**
$CH_{1.5}$	212.94	**159.5972**	**0.7495**
$SH_{0.5}$	165.23	**140.2955**	**0.8491**
$SH_{1.0}$	195.33	**169.5827**	**0.8682**
$SH_{1.5}$	197.90	**191.4219**	**0.9673**

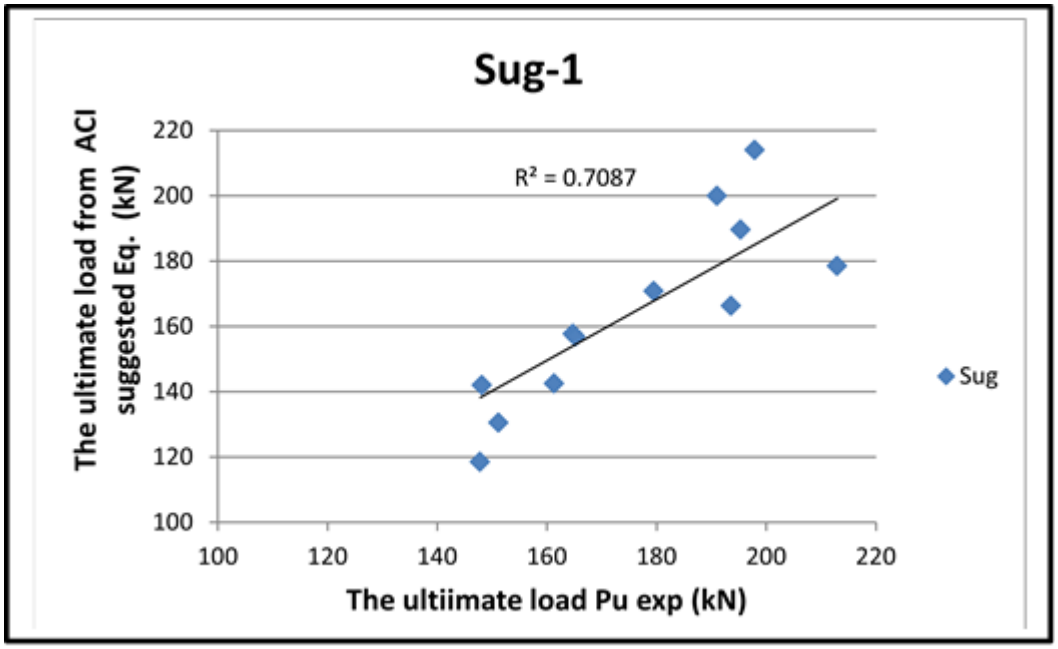

Figure 5.8: Experimental and predicted cracking ultimate load of SFRC slab for ACI suggested Eq.

Table (5.7): Compare the experimental results with the proposed equation of ACI code

Samples ID	L_f *mm*	V_f *%*	f_{vf}	f_{lf}	P_n sug1	P_n Experimental
CN	-	-	-	-	-	144.14
SN	-	-	-	-	-	144.50
$CM_{0.5}$	13	0.5	1.4	1.0433	105.9973	147.84
$CM_{1.0}$	13	1.0	1.6	1.043	127.0295	148.16
$CM_{1.5}$	13	1.5	1.8	1.0433	148.7435	193.60
$SM_{0.5}$	13	0.5	1.4	1.0433	127.4523	161.32
$SM_{1.0}$	13	1.0	1.6	1.0433	152.7416	179.52
$SM_{1.5}$	13	1.5	1.8	1.0433	178.8509	191.04
$SH_{0.5}$	35	0.5	1.4	1.1167	140.2955	165.23
$CH_{0.5}$	35	0.5	1.4	1.1167	116.6785	151.20
$CH_{1.0}$	35	1.0	1.6	1.1167	141.0356	164.80
$CH_{1.5}$	35	1.5	1.8	1.1167	159.5972	212.94

$SH_{1.0}$		35	1.0	1.6	1.1167	169.5827	195.33
$SH_{1.5}$		35	1.5	1.8	1.1167	191.4219	197.90
[71] Cheng MY and Parra-Montesinos GJ,2010	S1	-	-	-	105.9973	-	433
	S2	-	-	-	116.6785	-	379
	S3	30.0	1.000	1.600	127.0295	414.869	386
	S4	30.0	1.000	1.600	141.0356	414.869	389
	S5	35.0	1.500	1.800	148.7435	723.944	530[1]
	S6	35.0	1.500	1.800	159.5972	712.347	444[1]
	S7	30.0	1.500	1.800	127.4523	515.618	522
	S8	30.0	1.500	1.800	152.7416	515.618	472
	S9	30.0	1.500	1.800	178.8509	628.779	530
	S10	30.0	1.500	1.800	140.2955	711.935	503[1]
[35] L. NGUYEN-MINH,et.al, 2011	A_0	-	-	-	-	-	284
	A_1	60	0.4	1.36	1.2	272.5026	330
	A_2	60	0.6	1.44	1.2	295.1777	345
	A_3	60	0.8	1.52	1.2	324.1282	397
	B_0	-	-	-	-	-	301
	B_1	60	0.4	1.36	1.2	272.5026	328
	B_2	60	0.6	1.44	1.2	295.1777	337
	B_3	60	0.8	1.52	1.2	324.1282	347
	C_0	-	-	-	-	-	264
	C_1	60	0.4	1.36	1.2	272.5026	307
	C_2	60	0.6	1.44	1.2	295.1777	310
	C_3	60	0.8	1.52	1.2	324.1282	326
[18] I. Siva Kishore and Ch.Mallika Chowdary, 2015	PN/30/100/0	-	-	-	-	-	8.8
	PN/30/200/0	-	-	-	-	-	34.2
	PN/30/400/0	-	-	-	-	-	101.6
	PN/30/100/2	50	2	2.000	1.167	5.246	20.6
	PN/30/200/2	50	2	2.000	1.167	37.360	57.8
	PN/30/400/2	50	2	2.000	1.167	142.974	165.6[2]
	PN/30/100/4	50	4	2.800	1.167	7.344	13.4
	PN/30/200/4	50	4	2.800	1.167	52.304	40.22[2]

	PN/30/400/4	50	4	2.800	1.167	200.164	113.42[2]
[42] Dr. Layth Al-Jaberi,et.al, 2016	S1 (NSC)	-	-	-	-	-	85
	S2 (LWC)	-	-	-	-	-	60
	S3 (RPC)	13	0.5	1.4	1.043	302.805	145[3]
	S4 (RPC)	13	1.0	1.6	1.043	348.714	165[4]
	S5 (RPC)	13	2.0	2.0	1.043	440.818	175[5]
[41] Tamara Adnan Qasim Al-Shaikhli,2016	S0.0	-	-	-	-	-	47.5
	S0.5	13	0.5	1.400	1.043	45.019	65.0
	S1.0	13	1	1.600	1.043	54.016	85.0
	G0.0	-	-	-	-	-	425
	G0.5	13	0.5	1.400	1.043	45.019	65.0
	G1.0	13	1	1.600	1.043	54.016	95.0

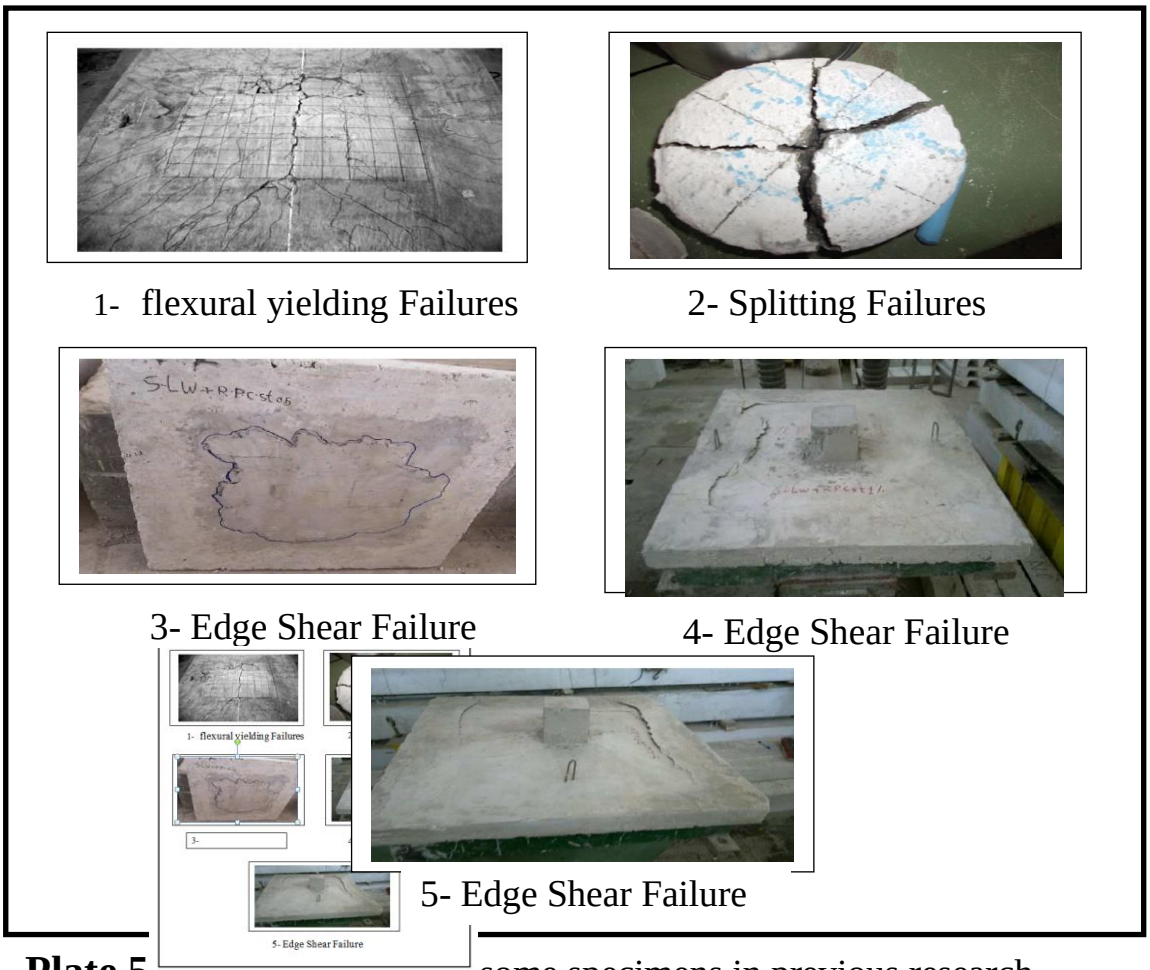

Plate 5.1 : Failure modes of some specimens in previous research

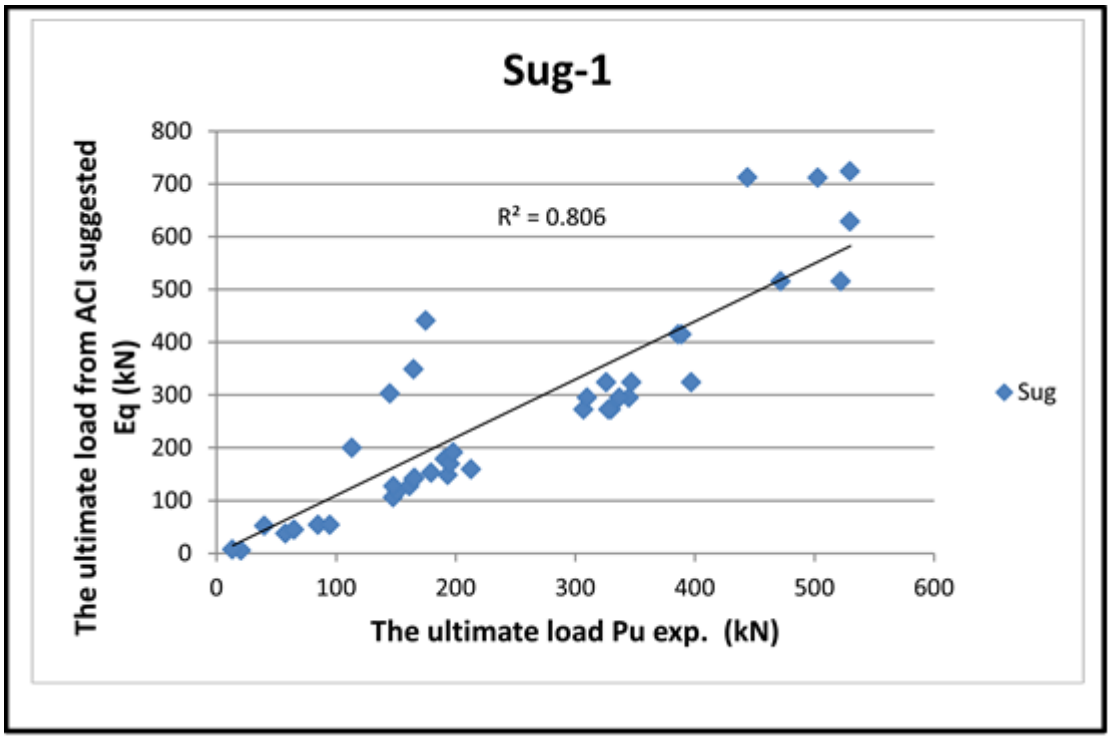

Figure 5.9: Experimental and predicted cracking ultimate load of SFRC slab of suggested Eq. based on ACI code[66]for the previous studies and the present study.

The second proposed equation is proposed depending on the splitting strength of concrete

$$P_{n\,Sug2} = 0.95 f_t \; b_0 \; \frac{d}{f_{Lf}} \qquad (5.8)$$

Where : f_t is splitting strength and L_f is fiber length (L_f in mm).

$$f_{Lf} = (1.5 - \frac{Lf}{100}) \qquad (5.8.1)$$

f_{Lf}=1 for non-fibrous concrete beams.

For example: for $CM_{0.5}$

Fiber: Type= Straight steel fiber , Fiber length= 13mm, f_t = 5.5Mpa , Slab : d= 61mm , b_0=568.857mm.

$$f_{Lf} = (1.5 - \frac{Lf}{100}) \; = (1.5 - \frac{13}{100}) = 1.37$$

$$P_{n\,Sug2} = 0.95 f_t \; b_0 \; \frac{d}{f_{Lf}}$$

$$P_{n\,Sug2} = \frac{0.95x5.5x568.857x\frac{61}{1.37}}{1000} = 132.342\,kN$$

Table (5.8) Suggested equation based on f_t field

Samples	$P_{n\,exp}$ (kN)	Sug-2	Sug-2/Exp.
CN	144.14	118.6749	0.8233
SN	144.50	142.6961	0.9875
$CM_{0.5}$	147.84	132.3423	0.8952
$CM_{1.0}$	148.16	146.7796	0.9907
$CM_{1.5}$	193.60	192.4979	0.9943
$SM_{0.5}$	161.32	159.1299	0.9864
$SM_{1.0}$	179.52	176.4895	0.9831
$SM_{1.5}$	191.04	231.4616	1.2116
$CH_{0.5}$	151.20	149.0603	0.9858
$CH_{1.0}$	164.80	169.1261	1.0263
$CH_{1.5}$	212.94	200.6581	0.9423
$SH_{0.5}$	165.23	179.2318	1.0847
$SH_{1.0}$	195.33	203.3591	1.0411
$SH_{1.5}$	197.90	241.2736	1.2192

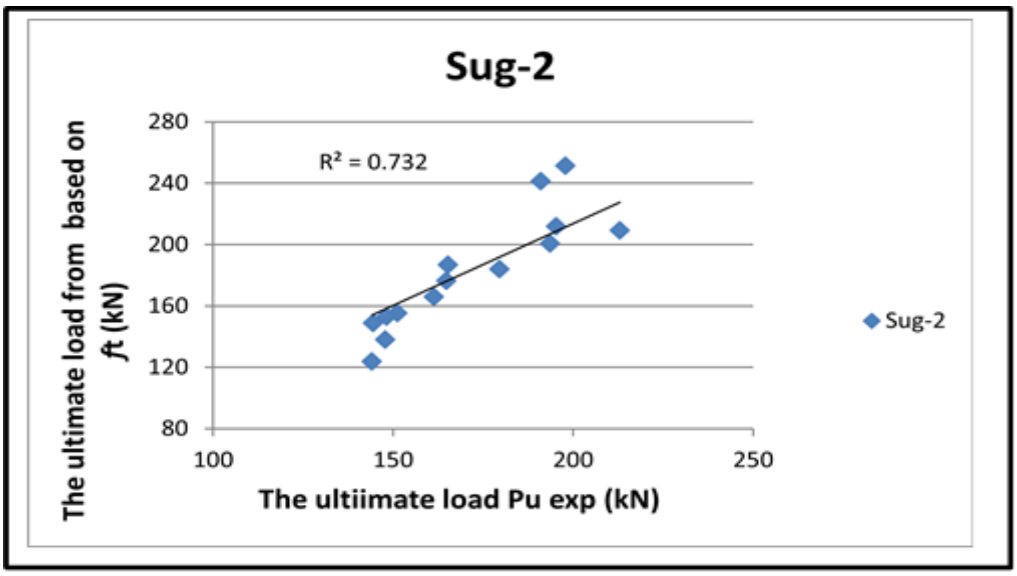

Figure 5.10: Experimental and predicted cracking ultimate load of SFRC slab from the equation based on f_t

Table (5.9): Compare the experimental results with the proposed equation of sug.2 based on f_t

Samples ID		L_f *mm*	$F_{L.f}$	f_t Mpa	*d* *mm*	b_0 *mm*	P_n Sug2	P_n Experimental
CN		-	1		61	568.857	118.6749	144.14
SN		-	1	3.6	61	684	142.6961	144.50
$CM_{0.5}$		13	1.0433	5.5	61	568.857	132.3423	147.84
$CM_{1.0}$		13	1.0433	6.1	61	568.857	146.7796	148.16
$CM_{1.5}$		13	1.0433	8.0	61	568.857	192.4979	193.60
$SM_{0.5}$		13	1.0433	5.5	61	684	159.1299	161.32
$SM_{1.0}$		13	1.0433	6.1	61	684	176.4895	179.52
$SM_{1.5}$		13	1.0433	8.0	61	684	231.4616	191.04
$CH_{0.5}$		35	1.1167	5.2	61	568.857	149.0603	151.20
$CH_{1.0}$		35	1.1167	5.9	61	568.857	169.1261	164.80
$CH_{1.5}$		35	1.1167	7.0	61	568.857	200.6581	212.94
$SH_{0.5}$		35	1.1167	5.2	61	684	179.2318	165.23
$SH_{1.0}$		35	1.1167	5.9	61	684	203.3591	195.33
$SH_{1.5}$		35	1.1167	7.0	61	684	241.2736	197.90
[35] L. NGUYEN-MINH,et .al,2011	A_0	-	1	1.95	105	1020	198.4028	284
	A_1	60	1.2	2.23	105	1020	189.0761	330
	A_2	60	1.2	2.42	105	1020	205.1858	345
	A_3	60	1.2	2.57	105	1020	217.9039	397
	B_0	-	1	1.95	105	1020	198.4028	301
	B_1	60	1.2	2.23	105	1020	189.0761	328
	B_2	60	1.2	2.42	105	1020	205.1858	337
	B_3	60	1.2	2.57	105	1020	217.9039	347
	C_0	-	1	1.95	105	1020	198.4028	264
	C_1	60	1.2	2.23	105	1020	189.0761	307
	C_2	60	1.2	2.42	105	1020	205.1858	310

	C_3	60	1.2	2.57	105	1020	217.9039	326
[18] I. Siva Kishore and Ch.Mallika Chowdary, 2015	PN/30/100/0	-	1	1.845	7.0	188.0	2.307	8.8
	PN/30/200/0	-	1	1.845	32.0	332.0	18.621	34.2
	PN/30/400/0	-	1	1.845	82.0	532.0	76.462	101.6
	PN/30/100/2	50	1.167	2.3092	7.0	232.0	3.054	20.2
	PN/30/200/2	50	1.167	2.3092	32.0	332.0	19.977	57.8
	PN/30/400/2	50	1.167	2.3092	82.0	532.0	82.028	165.6
	PN/30/100/4	50	1.167	2.0110	7.0	232.0	2.659	13.4
	PN/30/200/4	50	1.167	2.0110	32.0	332.0	17.397	40.22
	PN/30/400/4	50	1.167	2.0110	82.0	532.0	71.436	113.42

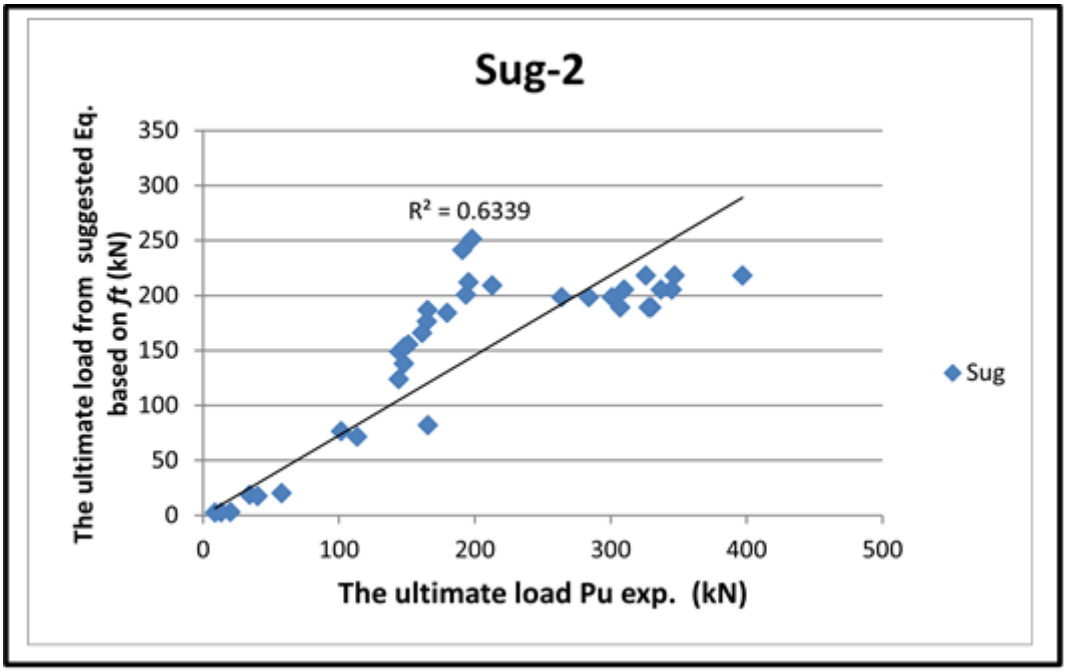

Figure 5.11: Experimental and predicted ultimate load of SFRC slab of suggested Eq. based on *f*t for the previous and these studies.

The equations have been developed to estimate the shear strength of FRC slabs. The accuracy of these equations was confirmed by comparing the results from the equations with data from past research experiments. The comparison showed that the proposed equations provide accurate predictions for the shear strength of FRC slabs.

CHAPTER SIX

CONCLUSIONS AND RECOMMENDATIONS

CHAPTER SIX

CONCLUSIONS AND RECOMMENDATIONS

6.1 Introduction

Experimental work was conducted to determine the punching shear strength of (straight and hook) steel fiber-reinforced concrete slabs under concentrated load. The investigations included studies of the mechanical properties of fibrous concrete, the ultimate load, and the corresponding deflection and column penetration. A study is conducted for column shape, types of steel fibers, and different percentages of steel fiber, as well as a comparison of the practical results with the different types of codes.

In this chapter, the results of experimental and theoretical research are presented, along with some recommendations for future researchers.

6.2 Conclusions

The following are inferences that can be drawn from the outcomes of this experimental and theoretical study:

1. Straight fibers showed more pronounced effect on compressive strength as compared with hook steel fibre especially for fiber dosage 0.5 and 1 %. The compression strength increases of straight and hook fibers with respect to control concrete sample by (1.41%, 11.52%, and 20.81%) and (7.27%,20%, and 21.41%), respectively, when the percentage of fibres used is 0.5%, 1.0%, and 1.5%. This phenomena was resulted of number of fibres per volume.

2. When using two different types of fibres (straight and hook), the splitting tensile strength increases the control concrete sample by (52.78, 69.44, and 122.22%) and (44.44, 62.82%, and (94.44%), respectively, when the percentage of fibres used is 0.5%, 1.0%, and 1.5%.

3. Micro straight steel fibers increase the direct tensile strength of a control concrete sample by (54.17, 87.5%, and 162.5%) whereas hook fibers increase the strength by (45.83, 75%, and 150%) when the percentage of fibres used is 0.5%, 1.0%, and 1.5%.

4. When compared to the non-fibrous sample, the flexural strength of straight steel fibers increased by (44.23%, 61.54%, 86.54%) and the flexural strength of hook steel fibers increased by (11.54%, 28.85%, 55.77%), when the percentage of fibres used is 0.5%, 1.0%, and 1.5%.

5. The deflection of slabs was decreased by 10.48% when using straight steel fibre with a circular column for fiber dosage 0.5% and decreased by 5.24% , 6.89% when using straight steel fibre with a circular column for fiber dosage 0.5% and 1.0% respectively..

6. The behaviour of concrete slab reinforced with hook steel fibres with a ratio of 0.5% is better compared with concrete reinforced with straight fibres with the same fibre ratios. While the higher percentages of fibres gave greater penetration of the

column due to the large percentage of fibres that led to random distribution in the concrete matrix and thus led to greater penetration of the column inside the slab. While using the square column, there was no effect on the column penetration. The reason may be attributed to the divergence of the angles of the square column compared to the circular column.

7. The ultimate load of the slab reinforced with straight steel fibre with a square column section is higher than that of the circular column by 9.12% and 21.17%, respectively, compared to a non-fibrous concrete slab for fibre ratios of 0.5% and 1.0%, while at a fibre ratio of 1.5%, the ultimate load of the slab with a circular column is slightly higher than the ultimate load of the slab with a square column by 1.34% when compared with a normal concrete slab.

8. When compression the ultimate load of the slabs made of reinforced concrete with hook fibres between the shapes of the square and circular columns, it was found that the ultimate load of the slab with a square column is higher than that of the circular column by (9.28% and 18.53%) compared to a non-fibrous concrete slab for fibre ratios of 0.5% and 1.0%, respectively, while at a fibre ratio of 1.5%, the ultimate load of the slab with a circular column is slightly higher than the ultimate load of the slab with a square column by 7.59% when compared with a normal concrete slab.

9. Using of steel fibers, whether straight or hooked, to make concrete a heterogeneous material. The presence of fiber in the concrete increases its bearing strength, especially after the cracking stage, because the fibers help prevent cracks from spreading.

10. Adding of steel fibers in the concrete mix led to a reduction in the penetration area of the slabs, as the use of straight fibers at the ratios of 0.5%, 1.0% and 1.5% of the reduction was 59.51%, 49.05% and 70.15% for the circular column, while for the square column the percentage of reduction was 69.5%, 37.09% and 34.56%, respectively. When using hook fibers at ratios of 0%, 1.0%, and 1.5%, the percentage of decrease was 72.81%, 49.99%, and 28.52% for the circular column, while for the square column, the percentage of decrease was 38.71%, 37.56% and 14.29%, respectively. This phenomena as the result of enhancing tensile strength that was changed failure mode from shear to compound shear and flexural.

11. On the tension surface, flexural crack are nearly invisible. The slab develops fractures, appearing more in the center as the stress level rises.

12. When comparing the experimental shear strength and the value obtained from the ACI cod coefficients, it gave varying and inaccurate percentages, as the error rate ranged from 40.04% to 62.71%, while when comparing the experimental shear strength and the value obtained from the proposed equations, the

proposed equations gave acceptable predictions. The first proposed equation gave an error rate ranging from 3.38% to 39.48%, and the second proposed equation gave an error rate ranging from 0.57% to 17.97%. The comparison showed that the proposed equations provide accurate predictions for the ultimate strength of FRC slabs as compared with the existing formula of different design code

5.3 Recommendations For Future Work

1. Investigating the performance of UHPC concrete slabs with circular and square column section reinforced.
2. Investigating the performance of reinforcement concrete slabs with inclined columns.
3. Investigating the behavior of punching shear under eccentric load.
4. Researching of the size effect of reinforced concrete (slabs) with various thicknesses with the same fibers and subject to influence from punching shear.
5. An analytical study of the behavior of SFRC slabs reinforced with all types of the fiber under punching shear.

REFERENCES

1. Raid Jameel Barjas Al-Ani “Effect of Line Load on Moments in Two-way Slab Systems.”, M.sc Thesis, University of Baghdad, Dec.1991.

2. Nilson A. H., D. Darwin, and Dolan C. W.,” Design of Concrete Structures” McGraw-Hill book Company, 13th Edition, 2004.

3. Jones A. E. K. and Morrison J. "Flat Slab Design: Past, Present and Future”, Proceedings of the Institution of Civil Engineers Structures & Buildings 15, April 2005 Issue SB2, pp. 133–140.

4. Muttoni A et al. Security of parking garages (in French: Securite Structurale des parking couverts) Documentation D 0226 SIA. Zurich (Switzerland): Societe Suisse des ingenieurs et des architects ;2008.

5. Schousboe I. Bailley’s Crossroads Collapse Reviewed J. Eng Mech Div 1976;102 (co2): 365-78. SFRC slabs. Int J Concr Struct Mater 2011;5(1):35–42.

6. Kaminetzky D. Design and construction failures, lessons from forensic investigations New Yourk: Mc Graw- Hill 1991.

7. Kings, Delatte NJ. Collapse of 2000 common weath avenue: punching shear case study. J pref constr facil 20al; 18(1): L54-61.2004.

8. M. K. Jawad, “Experimental study on shear heads in reinforced concrete flat plates,” Ph.D. thesis, Civil Engineering Department, College of Engineering, Al-Mustansiriya University, Baghdad-Iraq, September 2005.

9. Harris, D. K., "Characterization of Punching Shear Capacity of Thin UHPC Plates", M.Sc. Thesis, Virginia Polytechnic Institute and State University, Blacksburg, Virginia, December, 2004, pp. 1 -20.

10. F. A. Ahmed “Punching shear strength and time – dependent deflection of high- strength reinforced concrete panels “Ph. D thesis , University of Baghdad, November , 2005, P; 118.

11. Ibrahim, J. K., "Punching Shear Strength of Steel Fiber Reinforced Concrete Slabs", M.Sc. Thesis, Baghdad University, January, 1984, pp. 1-169.

12. Oehlers, D.J. and Seracino R., ―Design of FRP and Steel Plated RC Structures: Retrofitting Beams and Slabs for Strength, Stiffness and Ductility, Elsevier Ltd., pp. 228, 2004.

13. Hong, G. and Yew-Chang, L., "Failure Analysis of Column-slab Connections with Stud Shear Reinforcement", Canadian Journal of Civil Engineering, Vol.30, pp.934-944. (2003).

14. Mc. Cormac, J.C "Design of Reinforced Concrete", 5th Edition, John Wiley & Sons, Inc., pp.738, (2001).

15. ACI Committee 318. Building code requirements for structural concrete (ACI 318-02). 87(3), pp. 350-361. (2002).

16. Feretzakis A. Flat slabs and punching shear: reinforcement systems. Msc. Thesis, University of Dundee, UK. (2005).

17. Muttoni A. Punching shear strength of reinforced concrete slabs without transverse reinforcement. ACI Struct J 2008; 4:440–50.

18. I.Siva Kishore, Ch.Mallika Chowdary;" PUNCHING SHEAR STRENGTH OF THE FIBER REINFORCED CONCRETE SLABS", Department of Civil Engineering, K L E F University, Vaddeswaram, Guntur, Andhra Pradesh, India-522 502. (2015).

19. Nguyen- Minih .L, Rovnak M, Tran-Quoc T. punching shear capacity of interior SFRC slab-column connections. J Struct Eng 2012;138(5):613-624.

20. Vanderbilt, M. D., "Shear Strength of Continuous Plates," Journal of the Structural Division, ASCE, V. 98, 1972, pp. 961-973.

21. Sagaseta, J.; Tassinari, L.; Fernández Ruiz, M.; and Muttoni, A., "Punching of Flat Slabs Supported on Rectangular Columns," Engineering Structures, V. 77, 2014, pp. 17-33.

22. Vaz Rodrigues, R.; Fernández Ruiz, M.; and Muttoni, A., "Shear Strength of R/C Bridge Cantilever Slabs," Engineering Structures, V. 30, No. 11, 2008, pp. 3024-3033.

23. Kasper, T., Tvede, B., Stang, H., Mjoernell, P., Slot, H., Vitt, G., Thrane, L., N., Reimer, L., “Design Guideline for Structural Applications of Steel Fiber Reinforced Concrete”, 2014.

24. The European Guidelines for Self Compacting Concrete should be submitted to the EPG Secretary at: www.efca.info or www.efnarc.org, May 2005.

25. Nguyen Van CHANH, "STEEL FIBER REINFORCED CONCRETE", Vietnam Joint Seminar, Ho Chi Minh City University of Technology.

26. M. S. Pawar and M.M Patil, “prediction of shear strength of steel fiber reinforced concrete beams without web reinforcement" International Journal of Engineering Research & Technology, Vol.4, no. 4, April 2015.

27. Einpaul J., Bujnak J., Fernández Ruiz M., Muttoni A., Study on Influence of Column Size and Slab Slenderness on Punching Strength, ACI Structural Journal V. 113, Farmington Hills, USA, 2016, pp. 135-145.

28. João T. Simões, Jan Bujnak, Miguel Fernández Ruiz, and Aurelio Muttoni, "Punching shear tests on compact footings with uniform soil pressure", Technical Paper, 2016.

29. Jaroslav HALVONÍK, Lucia MAJTANOVÁ, “EXPERIMENTAL INVESTIGATION OF THE MAXIMUM PUNCHING RESISTANCE OF SLAB-COLUMN CONNECTIONS”, Slovak Journal of Civil Engineering, Vol. 26, 2018, No. 3, 22 – 28.

30. Zoran Brujić, Danijel Kukaras, Radomir Folić, Sohela Ali, Arpad Čeh, “Punching shear strength of eccentrically loaded RC flat slabs without transverse reinforcement”, DOI: https://doi.org/10.14256/JCE.240.2018.,GRAĐEVINAR 70 9, 757-770. (2018).

31. João Tiago RAMOS BERNARDO DE SANTA RITA SIMÕES, “The mechanics of punching in reinforced concrete slabs and footings without shear reinforcement”, THÈSE NO 8387 (2018) ÉCOLE POLYTECHNIQUE FÉDÉRALE DE LAUSANNE PRÉSENTÉE LE 12 MARS 2018.

32. Einpaul J.; Fernández Ruiz M.; Muttoni A.: Measurements of internal cracking in punching test slabs without shear reinforcement “. Magazine of Concrete Research. (2017).

33. Clément T.: „Influence de la précontrainte sur la résistance au poinçonnement de dalles en béton armé“. PhD thesis. Lausanne, Switzerland: EPFL, p. 224.Committee for Standardization; 2010, 225p. (2012).

34. Abdulhameed Abdullah Yaseen, “PUNCHING SHEAR STRENGTH OF STEEL FIBER HIGH STRENGTH REINFORCED CONCRETE SLABS”, Thesis • December 2006.

35. L. NGUYEN-MINH, M. ROVNÁK, T. TRAN-QUOC, and K. NGUYENKIM, “Punching Shear Resistance of Steel Fiber Reinforced Concrete Flat Slabs”, The Twelfth East Asia-Pacific Conference on Structural Engineering and Construction; Procedia Engineering 14 1830–1837. (2011).

36. L.F. Maya, M. Fernández Ruiz, A. Muttoni, S.J. Foster,” Punching shear strength of steel fibre reinforced concrete slabs”, Engineering Structures 40 83–94. (2012).

37. A.M.T. Hassan, G.H. Mahmud, S.W. Jones, C. Whiteford,” A new test method for investigating punching shear strength in Ultra High-Performance Fiber Reinforced Concrete (UHPFRC) slabs”, Composite Structures 131 (2015) 832–841.

38. BS EN 1992-1-1, Euro code 2: design of concrete structures-Part 1–1: general rules and rules for buildings. British Standards Institution; p. 230, 2004.

39. Mosley WH, Hulse R, Bungey JH. Reinforced concrete design to Euro code 2. 7th ed. Palgrave MacMillan; 2012.

40. Mahmud GH, Yang Z, Hassan AMT. Experimental and numerical studies of size effects of ultra-high performance steel fibre reinforced concrete (UHPFRC) beams. Constr Build Mater; 48:1027–34,2013.

41. Tamara Adnan Qasim Al-Shaikhli; “Effect of Steel Fiber on Punching Shear Strength of Non-Rectangular Reactive Powder Concrete Slabs”, Hayway and Transportation Department, Faculty of Engineering, Al-

Mustansiriyah University, Baghdad, Iraq, International Journal of Structural and Civil Engineering Research Vol. 5, No. 2, May 2016.

42. Dr. Layth Al-Jaberi, Zinah Waleed Abbas, Esraa Kamal Jaffar," EFFECT OF VOLUME OF STEEL FIBERS ON THE PUNCHING SHEAR BEHAVIOR OFHYBRID REINFORCED CONCRETE FLAT SLAB", Vol. 20, No.02, March 2016 ISSN 1813-7822.

43. Jae Ho Lee, Busan (KR)," TRUSS-TYPE SHEAR REINFORCEMENT MATERAL HAVING DOUBLE ANCHORAGE FUNCTIONS AT BOTH TOP AND BOTTOM THEREOF", United States, Pub. No.: US 2012/0023858 A1.

44. Gerd Ginther, Bad Orb (DE)," REINFORCED CONCRETE COMPONENT REINFORCED WITH L-SHAPEID SHEET METAL PIECES", United States Patent, Patent No.: US 8,815,366 B2,2014.

45. Majid M.A. Kadhim, Abdul Ridah Saleh, Lee S. Cunningham, Ali A. Semendary," Numerical investigation of non-shear-reinforced UHPC hybrid flat slabs subject to punching shear", Engineering Structures 241 (2021) 112444.

46. Minkwan Ju, Jiann-wen Woody Ju, and Jongsung Sim. A new formula of punching shear strength for fiber reinforced polymer (FRP) or steel reinforced two-way concrete slabs. Composite Structures 259 (2021) 113471.

47. Hadi N. G. Al-Maliki, Ali Al-Balhawi, Asma M. Ali," Punching Shear Resistance of Reinforced Concrete Flat Slabs Strengthened by CFRP and GFRP: A Review of Literature", Engineering and Technology Journal 39 (08) (2021) 1281-1290.

48. Iraqi Specification, No.5, " Portland Cement ",1984.

49. Iraqi Specification, No.5, " fine aggregate ",1984.

50. Iraqi Specification, No.5, " Coarse aggregate ",1984.

51. ASTM A615, "Standard specification for deformed and plain billet-steel bars for concrete reinforcement", Annual book of American society for testing and material standards, vol. 4, no. 1, 1986.

52. ASTM C496-04, "Standard test method for splitting tensile strength for cylindrical concrete specimens", American society for testing and materials, 2010.

53. ACI Committee 211.1-95, Standard Practice for Selection Proportions for Normal, Heavy Weight and Mass Concrete, ACI Manual of Concrete Practice, Part 1-1995.

54. American Society for Testing and Materials, ASTM C1437-01. Standard test method for flow of hydraulic cement mortar.

55. Okamura H. Self-consolidating high-performance concrete. ConcrInt J 1997:50–4, 1989.

56. Ozawa K. Development of high-performance concrete based on the durability design of concrete structures. EASEC-2; 1:445–50.

57. Kaszynska M. .Self-consolidating concrete for repair of bridges. Transportation Research Record: Journal of the Transportation Research Board, TRB, vol. 11- S. Washington (DC): National Research Council; p. 429–34, 2005.

58. Takada K., Influence of chemical admixtures on the mix proportion of self-consolidating concrete. In: Presented at international conference on concretes, Dundee, Scotland, 1999.

59. Ramachandran VS. Concrete admixtures handbook: properties, science, and technology. Noyes Publications, 1984.

60. The European Guidelines for Self Compacting Concrete should be submitted to the EPG Secretary at: www.efca.info or www.efnarc.org, May 2005.

61. British Standard Institution (B.S.I) 1881, Part 116, Method for Determination of Compressive Strength of Concrete Cubes,pp.3. 1989.

62. ASTM C496-04, "Standard test method for splitting tensile strength for cylindrical concrete specimens", American society for testing and materials, 2010.

63. ASTM D2936-08: Standard Test Method for Direct Tensile Strength of Intact Rock Core Specimens, Annual Book of ASTM Standards, ASTM International, West Conshohocken, PA, 2008a

64. ASTM C293-02, “Standard Test Method for Flexural Strength of Concrete (Using Simple Beam with Center-Point Loading),” Annu. B. ASTM Stand., pp. 1–3, (2002).

65. British Standard Institution (B.S.I) 1881, Part 116, Method for Determination of Compressive Strength of Concrete Cubes, pp.3. 1989.

66. ACI 318-19. Building Code Requirements for Structural Concrete and Commentary, ACI 318 (2019), American Concrete Institute, Farmington Hills, MI.

67. BS 8110, Structural use of concrete, 1997.

68. CEN. EN 1992-1-1:2004 + AC:2010: Eurocode 2: design of concrete structures—Part 1–1: General rules and rules for buildings. Brussels, Belgium: CEN European.

69. F´ed´eration Internationale du B´eton (fib): Model Code 2010 – Final Draft, vol. 1 und 2, Bulletin 65 und 66, Lausanne, Switzerland; 2012.

70. Muttoni A, Fern´andez Ruiz M. The levels-of-approximation approach in MC 2010: applications to punching shear provisions. Structural Concrete, Ernst & Sohn, Germany 2012;13(1):32–41.

71. Cheng MY and Parra-Montesinos GJ (2010a). Evaluation steel fibers reinforcement for punching shear resistance in slab-column connections-part1: Monotonically increased load. ACI Structural Journal. 107(1), pp. 101–109.

CHECK OF REINFORCED CONCRETE SLAB

1- Check the Ultimate Punching Shear from ACI 318-19 Code Equations

The smallest of the three equations:

- $V_c=0.33\lambda_s\sqrt{f}_c\ A$ ……(1)
- $V_c=\left(0.167+\frac{0.33}{\beta}\right)\sqrt{f}_c\ A$ ……. (2)
- $V_c=\left(0.167+\frac{3.32d}{b_0}\right)\sqrt{f}_c\ A$ …… (3)

Where:-

- λ_s is reflects the reduced mechanical properties of light-weight concrete in comparison to normal-weight concrete with the same compressive strength and is equal to 1.0 for normal-weight concrete.
- **fc'** is the specified compressive cylinder strength of concrete.
- b_0 is the perimeter of the critical section for two-way shear in slabs.
- **d** is the distance from the extreme compression fiber to the centroid of the longitudinal tension reinforcement, i.e. the effective depth.
- **β** is the ratio of the long side to the short side of the column.
- **A** is the concrete area (**A= b_0d**).

For non-fibrous concrete with circular column section :

d= 61mm , f_c= 45Mpa , b_0= 568.857mm for (d/2).

- $V_c=0.33\lambda_s\sqrt{f}_c\ A$ ……(1)

$\lambda_s = \frac{2}{1+(0.004d)} \leq 1.0$

$\lambda_s = \frac{2}{1+(0.004*61)}$ = 1.608 ≥ 1.0 use λ_s=1

A= $b_0$xd= 568.857x61= 34700.277mm^2

V_c=0.33x1 x$\sqrt{45x0.8}$ x34700.277= 68706.548N= 68.707kN

- $V_c = \left(0.167 + \frac{0.33}{\beta}\right)\sqrt{f_c}$ A …… (2)
  $\beta = 1$

$V_c = \left(0.167 + \frac{0.33}{1}\right) * \sqrt{45x0.8}$ **x** 34700.277 = 103476.226N = 103.476kN

- $V_c = \left(0.167 + \frac{3.32d}{b0}\right)\sqrt{f_c}$ A …… (3)

$V_c = \left(0.167 + \frac{3.32*61}{568.857}\right)\sqrt{45x0.8}$ x 34700.277=108891.997N=108.892**kN**

∴ use V_c= 68.707kN

2- Check the Ultimate Bending load from Yield Line for square slab.

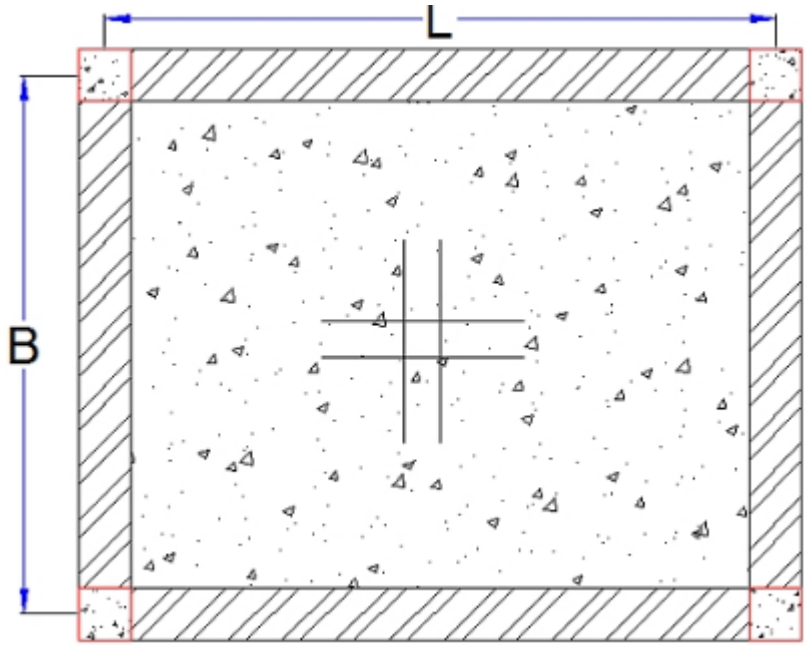

Figure A.1 : Simply- support slab.

$M_n = \rho b d^2 f_y (1-0.59 \frac{fc'}{fy})$

ρ=0.00834 , d= 61mm, b=1000mm, fy= 440Mpa.

fc=36Mpa, As=50.265mm^2

$M_n = 0.00834 \times 1000 \times 61^2 \times 440 \times (1-0.59 \frac{36}{440}) \times 10^{-6}$

M_n=12.984kN.m

From Yield Line:-

$M_n = \frac{P}{8}$

P= M_nx8 = 12.984x8 = 103.873kN

Compared with V_c= 68.707kN from ACI code.
P > V_c Shear Control.

Table (B.1): Chemical analysis for cement.

Compound composition	Chemical composition	Percentage by weight	Limits (IQS NO.5/1984)
Lime	CaO	63.66	----
Silica	SiO2	21.86	----
Alumina	Al2O3	3.96	----
Iron oxide	Fe2O3	4.72	----
Magnesia	MgO	2.24	<5.00
Sulfate	SO_3	2.21	<2.50
Loss on ignition	L.O.I	1.20	<4.00
Insoluble residue	I.R	1.46	<1.5
Lime saturation factor	L.S.F	0.89	0.66-1.02
Main compounds (Bogue's equs.)		Percent by weight of cement	
Tricalcium silicate (C_3S)		51.00	
Dicalcium silicate (C_2S)		23.28	
Tricalcium aluminate (C_3A)		2.51	
Tetracalcium aluminoferrite (C_4AF)		14.36	

Table (B.2): Physical properties for cement.

Physical properties	Test results	Iraqi specifications limits (I.O.S.5/1984)
Setting time (Vicat s method) Initial setting, hr: min Final setting, hr: min	 4:24 5:32	 ≥00:45 ≤10:00
Fineness (Blaine Method), m^2/Kg	314	≥250
Compressive strength, MPa 3days 7days	 25.7 29.68	 ≥15:00 ≥23:00
Soundness (Autoclave) method %	0.15	≤0.8

Table(B.3): Grading of fine aggregate.

Sieve size	Passing (%)	
	Fine aggregate	Limits of Iraqi specification No. 45/1984 for Zone
10 mm	100	100
4.75 mm	92	90-100
2.36 mm	81	75- 100
1.18 mm	73	55-90
600 mm	55	35 - 59
300mm	24	8 - 30
150 mm	7	0-10

Table (B.4): Physical properties of fine aggregate.

Physical properties	Test results	Limits of Iraqi specification No.45/1984 for zone (2)
Specific gravity	2.67	_
Sulfate content SO_3	0.09%	≤0.5
Absorption	0.76%	_

Table (B.5): Grading of coarse aggregate.

Sieve size	Passing %	
	Coarse aggregate	Limits of Iraqi Specification No. 45/1984
14 mm	100	100

Table (B.6): Physical properties of coarse aggregate.

Physical Properties	Test Results	Limits of Iraqi specification No.45/1984 for Zone (2)
Specific gravity	2.66	_
Sulfate content SO_3	0.6%	_
Absorption	0.043%	0.1%

Calculate Ultimate Punching Shear from Codes Equations

1- Calculate Ultimate Punching Shear from ACI 318-19 Codes Equations.

For example $CM_{0.5\%}$

d= 61mm , f_c= 50.2Mpa , b_0= 568.857mm for (d/2).

The smallest of the three equations:

- $\mathbf{V_c = 0.33\lambda_s\sqrt{f_c}\,A}$ ……**(1)**

$\lambda_s = \frac{2}{1+(0.004d)} \leq 1.0$

$\lambda_s = \frac{2}{1+(0.004*61)} = 1.608 \geq 1.0$ use λ_s=1

A= $b_0$xd= 568.857x61= 34700.277mm^2

V_c=0.33x1 x$\sqrt{50.2x0.8}$ x34700.277= 72567.763N**= 72.568kN**

- $\mathbf{V_c = \left(0.167 + \frac{0.33}{\beta}\right)\sqrt{f_c}\,A}$ …… **(2)**

$\boldsymbol{\beta = 1}$

$V_c = \left(0.167 + \frac{0.33}{1}\right) * \sqrt{50.2x0.8}$ **x** 34700.277 = 109291.449N= **109.291kN**

- $\mathbf{V_c = \left(0.167 + \frac{3.32d}{b0}\right)\sqrt{f_c}\,A}$ …… **(3)**

$V_c = \left(0.167 + \frac{3.32*61}{568.857}\right)\sqrt{50.2}$ x 34700.277= 115039.113N= **115.0391kN**

∴ use V_c= 72.568kN

2- Calculate Ultimate Punching Shear from British Standard Code Equation BS 8110.

For example $CM_{0.5\%}$

d= 61mm , f_c= 50.2Mpa , b_0= 951.903mm for (1.5d), D_{bar}=8mm,

$V_c = 0.27k(100\rho_t)^{1/3} f_{c\,cub}\, b_o d$ …….(BS 8110)

$K = \sqrt[4]{400/d}$

$K = \sqrt[4]{400/61} = 1.6$

$\rho_t = \frac{Abar}{Sd} \leq 0.03$

$A_{bar} = \frac{\pi}{4} D_{bar}^{\,2} = \frac{\pi}{4} * (8)^2 = 50.286 mm^2$

S= 98.889mm

$\rho_t = \frac{50.286}{98.889 * 61} = 0.00834 \leq 0.03$ ∴OK

V_c= 0.27x1.6 x$(100x0.00834)^{1/3}$50.2x951.903x61/1000= 87.102282kN

3- Calculate Ultimate Punching Shear from Euro code (EC2)Equation.

For example $CM_{0.5\%}$

d= 61mm , f_c= 50.2Mpa , b_0= 1144mm for (2d),

D_{bar}=8mm, S= 98.889mm.

$$\mathbf{V_c = 0.18\, b_0\, d\, K\, (100\, \rho_t\, f_c)^{1/3}}$$

$$\mathbf{K=1+\sqrt{\frac{200}{d}} = 1+\sqrt{\frac{200}{61}} = 2.811 \leq 2.0 \quad \therefore \text{ use } K= 2}$$

$$\mathbf{\rho_t=\frac{Abar}{Sd} \leq 0.02}$$

$$A_{bar}= \frac{\pi}{4} D_{bar}^{\,2} = \frac{\pi}{4} x\ (8)^2 = 50.286mm^2$$

S= 98.889mm

$$\rho_t= \frac{50.286}{98.889x61} = 0.00834 \leq 0.02 \ \therefore OK$$

$$V_c= 0.18x1144\ x61x2\ (100\ x0.00834\ x50.2x0.8)^{1/3}/1000$$

V_c= 80.98kN

4- Calculate Ultimate Punching Shear Fib model code Equation.

For example $CM_{0.5\%}$

d= 61mm , f_c= 50.2Mpa , b_0= 568.857mm for (0.5d), fy = 440Mpa, r_s= 350mm, Es= 200000Mpa, dg=14mm.

$V_c = k\psi \sqrt{f'c}\, b_0\, d$ ……(Fib code)

$k\psi = \frac{1}{1.5+(0.9\psi\, d\, kdg}$ ≤ 0.6

$\Psi = 1.5\, r_s \frac{fy}{d\, Es} = 1.5 \times 350 \times \frac{440}{61x200000} = 0.01893$

$kdg = \frac{32}{16+dg}$ ≥ 0.75

$kdg = \frac{32}{16+14} = 1.0667 \geq 0.75$ ∴OK

$k\psi = \frac{1}{1.5+(0.9x0.01893x61x1.0667} = 0.3833 \leq 0.6$ ∴OK

V_c = 0.3833x $\sqrt{50.2x0.8}$ x568.857 x61/1000= **84.288kN**

الخلاصة

ابدى الباحثون والمهندسون اهتمامًا باستخدام الخرسانة المسلحة بالألياف الفولاذية (SFRC) لتحسين أداء الهياكل الخرسانية في مجموعة متنوعة من التطبيقات الإنشائية. ومع ذلك ، هناك عدد قليل من نتائج الاختبارات التجريبية فيما يتعلق بتأثير المتغيرات (المقطع العرضي للعمود ، ونسبة محتوى الألياف ، وهيئة الالياف على سلوك قص الاختراق للسقوف الخرسانية.

يتضمن هذا البحث دراسة عملية و نظرية لتأثير استخدام نوعين من الألياف (ألياف فولاذية مستقيمة وألياف فولاذية خطافية) وجرعاتها تحت تأثير قص الاختراق للسقوف الخرسانة المسلحة بالألياف. كانت هناك ثلاث نسب مختلفة من الألياف ألمستخدمة ٠,٥٪ و ١٪ و ١,٥٪ من حجم النموذج. تم تسليط احمال مركزة على أربعة عشر سقفا مصبوبًا ابعاد السقف ٩٢٠ x٩٢٠x ٨٠ مم (اثنان من الخرسانة الاعتيادية مع مقاطع العمود الدائرية و المربعة المكافئة بينما تم صب الألواح ألاثني عشر الأخرى من الخرسانة المصنوعة من ألياف الصلب).

أظهرت اختبارات الخواص الميكانيكية للخلطات الخرسانية (مقاومة الانضغاط وقوة الشد وقوة الانحناء وقوة الشد المباشر) إلى أن ألياف الصلب المستقيمة أكثر فاعلية من ألياف الصلب الخطافية .على العكس من ذلك، تُظهر السقوف المصبوبة بألياف فولاذية خطافية مقاومة تحميل أعلى من السقف المصبوب بألياف فولاذية مستقيمة. قد يكون هذا السلوك نتيجة لمرحلة ما بعد التشقق حيث يعطي طول الألياف طولً تثبيت أفضل لزيادة القوة الرابطة. بشكل عام ، كان الفشل تدريجيًا في السقوف المعززة بالألياف ، بينما كان الفشل مفاجئًا في السقوف غير المعززة بالألياف. كان تأثير أشكال الأعمدة (المربعة والدائرية) يتأرجح اعتمادًا على آلية الفشل التي تباينت من القص إلى القص المركب والانثناء. لذلك ، كان من غير الدقيق اعتماد المساحة المكافئة للأعمدة الدائرية كأعمدة مربعة في سقوف الخرسانة المسلحة بالألياف المعززة بالألياف.

أدت إضافة الألياف الفولاذية في الخلطة الخرسانية إلى تقليل مساحة الاختراق للسقوف، إذ بلغ استخدام الألياف المستقيمة بنسب ٠.٥% و١.٠% و١.٥% من التخفيض ٥٩.٥١% و٤٩.٠٥% و٧٠.١٥ % للعمود الدائري، بينما للعمود المربع بلغت نسبة التخفيض ٦٩.٥%، ٣٧.٠٩%، ٣٤.٥٦% على التوالي. وعند استخدام ألياف الخطاف بنسب ٠.٥%، ١.٠%، ١.٥%، بلغت نسبة الانخفاض ٧٢.٨١%، ٤٩.٩٩%، ٢٨.٥٢% للعمود الدائري، أما للعمود المربع فقد بلغت نسبة النقصان ٣٨.٧١%، ٣٧.٥٦% و١٤.٢٩% على التوالي. تأتي هذه الحقيقة نتيجة لزيادة قوة الشد التي تم تغيير وضع الفشل من القص إلى القص المركب والانثناء. عند المقارنة بين قوة القص التجريبية والقيمة التي تم الحصول من معاملات ACI cod اعطت نسب متفاوتة وغير دقيقة حيث كانت نسبة الخطأ تتراوح بين ٤٠.٠٤% الى ٦٢.٧١% بينما عند مقارنة قوة القص التجريبية والقيمة التي تم الحصول عليها من المعادلات المقترحة ان المعادلات المقترحة اعطت تنبؤات مقبولة حيث اعطت المعادلة المقترحة الاولى نسبة الخطأ تتراوح من ٣,٣٨% الى ٣٩,٤٨% والمعادلة المقترحة الثانية اعطت نسبة خطأ تتراوح من ٠,٥٧% الى ١٧,٩٧%. أظهرت المقارنة بين قوة القص التجريبية والقيمة التي تم الحصول عليها من المعادلات المقترحة أن المعادلات المقترحة توفر تنبؤات مقبولة لقوة القص لألواح FRC.

جمهورية العراق
وزارة التعليم العالي و البحث العلمي
جامعة بابل
كلية الهندسة
قسم الهندسة المدنية

التحقيق التجريبي والتحليلي لسلوك القص ثنائي الاتجاه لسقوف الخرسانة المسلحة بالألياف

بـحث

مقدم الى كليَّةِ الهندسة / جامعةِ بابل وهي جزء مِنْ متطلبات نيل درجةِ الماجستير في الهندسة / الهندسة المدنيةِ / الإنشاءات

من قبل

بان علاء سلمان علي

أشراف

أ. د : رافع فليح حسن

كانون الثاني
٢٠٢٤

رجب
١٤٤٥